Search for Charged Higgs Bosons Decaying via $H^+ \to \tau_{lep.} + \nu$ in $t\bar{t}$ Events at $\sqrt{s} = 7$ TeV in ATLAS

William Dmitri Morgan Breaden Madden

University of Glasgow

A thesis submitted for the degree of

Master of Science by Research

at the University of Glasgow

School of Physics and Astronomy

University of Glasgow

June 2012

Abstract

This thesis for the degree of Master of Science by Research presents the theory, methodology and results of a search for charged Higgs bosons decaying via $H^+ \to \tau_{lep.} + \nu$ using single lepton and two lepton channels in t quark pair ($t\bar{t}$) events with a leptonically decaying τ in the final state based on 1.03 fb^{-1} of proton-proton collision data at centre of mass energy $\sqrt{s} = 7$ TeV from ATLAS, an experiment of the LHC, with special attention given to the statistical analysis and calculation involved in the limit setting process.

For the single lepton channel, the expected number of Standard Model-like $t\bar{t} \to b\bar{b}W^+W^-$ background events lies between 0.99 and 1.03 times the Standard Model prediction, with uncertainties in the range 2% – 3%. For the two lepton channel, the expected number of Standard Model-like background events lies between 0.99 and 1.03 times the Standard Model prediction, with uncertainties in the range 5% – 25%. Assuming the branching fraction $\mathcal{B}(H^+ \to \tau\mu) = 1$, the upper limits on the branching fraction $\mathcal{B}(t \to bH^+)$ at the 95% confidence level are between 5.2% and 14.1% for charged Higgs boson masses in the range 90 GeV $\leq m_{H^+} \leq$ 160 GeV. In the context of the $m_h^{\text{max.}}$ scenario of the MSSM, values of $\tan\beta$ greater than 30–56 are excluded in the mass range 90 GeV $\leq m_{H^+} \leq$ 140 GeV.

The compatibility with background of the combination of the single lepton and two lepton channels ranges between 26% and 50%, as measured by p_0 values. Hence, no indication of a H^+-like excess is found.

Acknowledgements

I thank my supervisors, Prof. Tony Doyle and Dr. Chris Collins-Tooth, for their advice, assistance, patience and guidance through this thesis.

I thank members of the group involved in the charged Higgs boson search described in this thesis, specifically, Liron Barak, Elliott Cheu, Arnaud Ferrari, Martin Flechl, Eilam Gross, Jacob Groth-Jensen, Silje Hattrem Raddum, Alexander Madsen, Prolay Mal, Koji Nakamura, Daniel Pelikan, Donnchadha Quilty, Alex Read and, in particular, Michael Wright for programming assistance in limit setting.

I also thank Sarah Allwood-Spiers, Aaron Armbruster, Craig Buttar, Brian Colquhoun, Umar Gul, Lars Eklund, Kate Elliott, Samir Ferrag, James Ferrando, Danilo Ferreira de Lima, Valerie Flood, Alistair Gemmell, Nicolas Gutierrez, Gavin Kirby, Aaron Mac Raighne, Alex Martyniuk, David J. Miller, António Morais, Stephen Ogilvy, Cristina Oropeza Barrera, Andrew Pickford, Thomas Ravenscroft, Peter Alexander Smith, Richard St. Denis, Genevieve Steele, Hiu Fung Wong, Kenneth Wraight and everyone in the Glasgow Particle Physics Experiment research group for various things ranging from assistance in physics, to assistance in typesetting, to whisky, to philosophical discussion and argument.

Thanks go to CERN for the very successful operation of the LHC and to everyone involved in the ATLAS Collaboration.

I dedicate this thesis to my immediate family for love and support.

The television show *Lexx* (1997 – 2002) is also acknowledged for introducing the author to the term *Higgs boson*.

"My name is Dr. Ernst W. Longbore. Till recently, I was associated with a team of researchers divided between this planet's two most powerful nuclear particle accelerators. My team has been building ever more powerful particle accelerators to try to determine the mass, if any, of the Higgs boson in order to complete our picture of the basic building blocks of this universe... but I, alone, realised that the experiment that we were doing was extremely dangerous; it will trigger a chain reaction that will cause the entire planet to instantly collapse into an ultradense particle about the size of a pea. We were drowning in the sea of our own insanity. I tried to stop the project, but, in their blind rush to be the first to measure the Higgs boson, no one would listen. I warned the government and, for my efforts to save the human race, I was fired, dismissed from WAARP, the World Association for Applied Research Physicists, and stripped of all seven of my Ph.D.s."

— Dr. Ernst W. Longbore, in the television show *Lexx*

Declaration

This thesis represents work completed from August 2011 to November 2011 in the Experimental Particle Physics research group in the School of Physics and Astronomy at the University of Glasgow. I contributed to work in the Higgs subgroup "H to Complex Final States" (HSG5) of the ATLAS Collaboration. The work presented in chapter 6 on limit setting is my own, except where stated in the text. This work has not been submitted for any other degree at the University of Glasgow or any other institution.

Contents

Abstract **ii**

Acknowledgements **iii**

Declaration **v**

List of Tables **xii**

List of Figures **xiv**

1 Introduction **1**

1.1 Introduction and Motivation 1

1.2 Structure of Thesis 2

2 Theory **3**

2.1 Introduction 3

2.2 Fundamental Particles and Interactions 4

2.2.1 Polarisation and Spin 4

2.2.2 Fundamental Particles 5

2.2.3 Interactions 10

2.3 Quantum Field Theory 10
2.3.1 Symmetry 10
2.3.2 Quantum Field Theory 12
2.4 Quantum Electrodynamics 16
2.5 Quantum Chromodynamics 18
2.6 The Standard Model 19
2.6.1 Description of Nature 19
2.6.2 The Standard Model 21
2.7 Englert-Braut-Higgs Mechanism 23
2.7.1 Before the Englert-Braut-Higgs Mechanism 23
2.7.2 1964 PRL Symmetry Breaking Papers 24
2.7.3 Electroweak Theory 25
2.7.4 Spontaneous Symmetry Breaking 25
2.8 Supersymmetry 34
2.8.1 Hierarchy Problem 34
2.8.2 Supersymmetry 34
2.8.3 Minimal Supersymmetric Standard Model 35
2.9 Searches for Higgs Bosons 37
2.9.1 Early Searches for Higgs bosons 37
2.9.2 Searches for Higgs bosons at the Large Electron-Positron Collider 37
2.9.3 Searches for Higgs bosons at the Tevatron 38
2.9.4 Searches for Higgs bosons at the Large Hadron Collider 39
2.9.5 Search for Charged Higgs Bosons Decaying via $H^+ \to \tau_{lep.} + \nu$ in $t\bar{t}$ Events 40

2.9.5.1 Single Lepton Events 44
2.9.5.2 Two Lepton Events 46

3 Statistical Methodology **48**

3.1 Introduction 48
3.2 A Search as a Statistical Test 48
3.3 Profile Likelihood Ratio 52
3.4 Modified Frequentist Confidence Level CL_s 55
3.4.1 Significance Level $1 - CL_b$ 55
3.4.2 Discovery Potential $1 - CL_{s+b}$ 56
3.4.3 Approximate Confidence CL_s 56
3.5 ATLAS Statistical Methods 57
3.6 Bayes' Theorem 59
3.6.1 Some Formulae from Probability Calculus 59
3.6.2 Bayes' Theorem 61
3.6.3 Discovery 62
3.7 Software 63
3.7.1 ROOT 63
3.7.2 RooFit and RooStats 64

4 Large Hadron Collider **66**

4.1 Large Hadron Collider 66
4.1.1 General Description of LHC operation 68
4.1.2 Luminosity 69
4.1.3 LHC Experiments 75

4.1.3.1 A Large Ion Collider Experiment (ALICE) 76
4.1.3.2 A Large Toroidal LHC Apparatus (ATLAS) 76
4.1.3.3 Compact Muon Solenoid (CMS) 76
4.1.3.4 Large Hadron Collider Beauty (LHCb) 76

5 A Large Toroidal LHC Apparatus 77

5.1 ATLAS 77
5.1.1 General Description of ATLAS Operation 77
5.1.2 ATLAS Detector 81
5.1.2.1 ATLAS Coördinate System 81
5.1.2.2 Inner Detector 83
5.1.2.3 Pixel Detector 86
5.1.2.4 Semiconductor Tracker 86
5.1.2.5 Transition Radiation Tracker 86
5.1.2.6 Calorimetry 87
5.1.2.7 Electromagnetic Calorimeter 88
5.1.2.8 Hadronic Calorimeter 88
5.1.2.9 Muon Spectrometer 90
5.1.2.10 Magnet System 92
5.1.2.11 Forward Detectors 93
5.1.2.12 Triggers and Data Acquisition 94
5.1.2.13 Resolution 94

6 Search for Charged Higgs Bosons Decaying via $H^+ \to \tau_{lep.} + \nu$ in $t\bar{t}$ Events 96

6.1 Introduction 96
6.2 Monte Carlo and Data Samples 97
6.3 Object Reconstruction 99
6.3.1 Electron and Muon Triggers 99
6.3.2 Event Cleaning 99
6.3.3 Electron Reconstruction 100
6.3.4 Muon Reconstruction 100
6.3.5 Jet Reconstruction 101
6.3.6 Missing Transverse Energy Reconstruction 101
6.4 Data Driven Estimation of Backgrounds with Misidentified Leptons . 102
6.5 Search with Single Lepton Events 105
6.5.1 Event Selection 105
6.5.2 Jet Identification 106
6.5.3 Control Region 106
6.5.4 Reconstruction of Discriminating Variables 108
6.6 Search with Two Lepton Events 108
6.6.1 Event Selection 108
6.6.2 Jet Identification 110
6.6.3 Control Region 111
6.6.4 Reconstruction of Discriminating Variables 112
6.7 Limits on the Branching Fraction of $t \to bH^+$ 113
6.7.1 Systematic Uncertainties 113
6.7.2 Methodology 116
6.7.3 Expected Events in the Control Region 117

6.7.4 Expected Events in the Signal Region 117
6.7.5 Observed Events in the Control and Signal Regions 117
6.7.6 Profile Likelihood Statistical Analysis 118
6.8 Results 119
6.8.1 Single Lepton Analysis 119
6.8.2 Two Lepton Analysis 120
6.8.3 Combination 122
6.8.4 Results in the Context of the MSSM 124
6.9 Conclusions 124
6.9.1 Discussion on Results 124
6.9.1.1 Comparison with Previous Results 127
6.9.2 Recent Developments and Future Searches 131

7 Epilogue **132**

7.1 Discovery of a Neutral Boson 132
7.2 Consideration of the Mass of the Neutral Boson in the Context of Asymptotic Safety of Gravity 133
7.3 Current Studies and the Future 134

References **135**

List of Tables

2.1 Standard Model fundamental particles 6

2.2 Known interactions 11

2.3 Fermion fields of the Standard Model 22

2.4 Degrees of freedom in the Minimal Supersymmetric Standard Model . 36

2.5 Early searches for Higgs bosons 37

4.1 LHC nominal beam parameters 75

5.1 ATLAS subdetector performance goals 95

6.1 Standard Model background Monte Carlo samples 98

6.2 Events for simulated processes in the single lepton channel 107

6.3 Events for simulated processes in the two lepton channel 111

6.4 Main systematic uncertainties considered in this analysis 115

6.5 Observed and expected upper limits on $\mathcal{B}(t \to bH^+)$ at the 95% confidence level for the single lepton channel, the two lepton channel and the combination of both channels 123

6.6 Relative uncertainties on $\mathcal{B}(t \to bH^+)$ in the context of the $m_h^{\text{max.}}$ scenario of the MSSM 126

6.7 Observed and expected upper limits on $\mathcal{B}(t \to bH^+)$ at the 95% confidence level for the single lepton channel, the two lepton channel and the combination of both channels of the search of this thesis and for recent CMS results 128

List of Figures

2.1 Potential $V(\phi)$ for a complex scalar field ϕ for the case of $\lambda > 0$ and $\mu^2 > 0$ 27

2.2 Potential $V(\phi)$ for a complex scalar field ϕ for the case of $\lambda < 0$ and $\mu^2 < 0$ 27

2.3 Potential $V(\phi)$ for many fields for the case of $\lambda > 0$ and $\mu^2 < 0$ . . . 28

2.4 LEP Higgs boson exclusion (shown with LHC 2011 exclusion) 38

2.5 Tevatron Higgs boson exclusion (shown with LHC early 2012 exclusion) 39

2.6 100 GeV $\leq m_H \leq$ 600 GeV ATLAS Higgs boson combined upper limits for 2011 data 40

2.7 110 GeV $\leq m_H \leq$ 150 GeV ATLAS Higgs boson combined upper limits for 2011 data 41

2.8 Leading order Feynman diagram for the production of $t\bar{t}$ events arising from gluon fusion, where a t quark decays to a charged Higgs boson, followed by the decay $H^+ \to \tau\nu$ 42

4.1 CERN accelerator complex 67

4.2 Cross section of LHC superconducting cryodipole 70

4.3 Three dimensional representation of LHC superconducting cryodipole 71

5.1 ATLAS detector 78
5.2 ATLAS Inner Detector 84
5.3 Cross section of ATLAS Inner Detector 85
5.4 Calorimetry in ATLAS 89
5.5 ATLAS liquid argon Electromagnetic Calorimeter 90
5.6 Muon Spectrometer 91

6.1 Reconstruction of $\cos\theta_l^*$ on the leptonic side of the single lepton events 109
6.2 Reconstruction of m_T^H on the leptonic side of the single lepton events 109
6.3 Reconstruction of $\cos\theta_l^*$ on the leptonic side of the two lepton events 112
6.4 Reconstruction of m_T^H on the leptonic side of the two lepton events . 113
6.5 Upper limits on $\mathcal{B}(t \to bH^+)$ at the 95% confidence level in the single lepton channel, as a function of charged Higgs boson mass, with the assumption of $\mathcal{B}(H^+ \to \tau\mu) = 1$ 119
6.6 Upper limits on $\mathcal{B}(t \to bH^+)$ at the 95% confidence level in the two lepton channel, as a function of charged Higgs boson mass, with the assumption of $\mathcal{B}(H^+ \to \tau\mu) = 1$ 121
6.7 Upper limits on $\mathcal{B}(t \to bH^+)$ at the 95% confidence level in the combination of the single lepton channel and the two lepton channel, as a function of charged Higgs boson mass, with the assumption of $\mathcal{B}(H^+ \to \tau\mu) = 1$ 122
6.8 Limits for charged Higgs boson production from t quark decays in the context of the $m_h^{\text{max.}}$ scenario of the MSSM, with the assumption of $\mathcal{B}(H^+ \to \tau\mu) = 1$ 125

6.9 Exclusion limits on $\mathcal{B}(t \to H^+b) \times \mathcal{B}(H^+ \to \tau^+\nu)$ at the 95% confidence level as a function of charged Higgs boson mass in recent ATLAS results, shown with the best limit provided by the Tevatron experiments 129

6.10 Limits for charged Higgs boson production from t quark decays in the context of the $m_h^{\text{max.}}$ scenario of the MSSM in recent ATLAS results . 130

Chapter 1

Introduction

1.1 Introduction and Motivation

Perhaps the most pressing open question in fundamental particle physics is why the $W^{\pm}$ and Z gauge bosons, the mediator particles associated with the weak interaction, are massive. The fact that these bosons have mass is associated with a phenomenon called electroweak symmetry breaking. The mechanism for this electroweak symmetry breaking has not been established. The Englert-Braut-Higgs mechanism provides a general framework to describe electroweak symmetry breaking and the observed masses of the $W^{\pm}$ and Z bosons. Higgs bosons are observable particles that result from this mechanism and, thus, the search for Higgs bosons and the study of their properties has a high priority for both theoretical and experimental activities in high energy physics. One of the primary goals of the Large Hadron Collider (LHC) and A Large Toroidal LHC Apparatus (ATLAS) is the exploration of the Higgs sector in the Standard Model and beyond it [1].

Charged Higgs bosons, H^+ and H^-, are predicted by several non-minimal Higgs scenarios. The observation of charged Higgs bosons would indicate physics beyond the Standard Model. The analysis presented in this thesis considers the type II 2HDM (2 Higgs doublet model) [2], which is also the Higgs sector of the Minimal Supersymmetric Standard Model. For charged Higgs bosons with masses less than the t quark mass, the dominant production mode at the LHC is through the t quark decay $t \to bH^+$. The dominant source of t quarks at the LHC is through $t\bar{t}$ production. For $\tan\beta > 3$ (see section 2.8.3), charged Higgs bosons decay primarily via $H^+ \to \tau\nu$. Investigation of this channel is the focus of this thesis.

1.2 Structure of Thesis

Initially, the theoretical basis for the charged Higgs boson search of this thesis is presented. This includes an outline of the known fundamental particles and interactions and general descriptions of quantum field theory, the Standard Model, the Englert-Braut-Higgs mechanism, supersymmetry and a summary of Higgs boson searches. Next, the statistical theory and methodology, together with the software used in the statistical analysis, is described. The experimental apparatus used in the search is then described, including general descriptions of the LHC and LHC experiments, with special attention given to ATLAS. A description of the analysis involved in the charged Higgs boson search is then given. Finally, the results of the search are presented, together with conclusions drawn.

Chapter 2

Theory

2.1 Introduction

This chapter offers a brief description of the theoretical basis for the $H^+ \rightarrow \tau_{lep.} + \nu$ charged Higgs boson search that is the main subject of this thesis. Initially, a general description of fundamental particles and interactions, together with particle classifications, is presented. Next, the framework of *quantum field theory* is described briefly. The theories of *quantum electrodynamics* and *quantum chromodynamics* are described. The framework of quantum field theory is used then in characterising the general approach to describing nature in terms of Lagrangians. The *Standard Model* is given as an example of such a description and is outlined. Following this, the theory concerning the *Englert-Braut-Higgs mechanism* is presented. The theory of *supersymmetry* is described briefly, with consequences for the Englert-Braut-Higgs mechanism. Finally, past and present searches for Higgs bosons are outlined, with special attention given to the theory concerning the $H^+ \rightarrow \tau_{lep.} + \nu$ charged Higgs

boson search. For the purposes of brevity, charged Higgs bosons are often denoted in this thesis as H^+, with the charge conjugate H^- implied.

Discussion on theory will generally involve units of the $\hbar = c = 1$ convention. This is because the physical constants $\hbar$ and c are so deeply embedded in the formulation of relativistic quantum field theory that they are taken generally as the units of action and velocity, respectively. With this convention, all physical quantities of interest have units that are powers of mass. As examples, the dimension of momentum is $(\text{mass})^1$, or simply 1, because mass $\times\, c$ is a momentum and the dimension of length is $(\text{mass})^{-1}$, or simply -1, because $\frac{\hbar c}{\text{mass}}$ is a length.

2.2 Fundamental Particles and Interactions

2.2.1 Polarisation and Spin

Fundamental particles can be classified by polarisation, or *spin*. Spin may be described as an intrinsic angular momentum of particles. *Photons*, for example, exist in four conditions, called polarisations, that are geometrically related to the dimensions of space and time. That is, photons are polarised in the three dimensions of space and the dimension of time. At large scales (i.e., for *real* photons, as opposed to *virtual* photons), the probability amplitudes for the polarisation in the direction of propagation and the polarisation in time effectively cancel, leaving two polarisations of *real* photons observable. In a similar manner, *electrons* exist in four conditions that are also related to geometry, but there are more subtleties involved.

Polarisation naturally implies a large number of different possible *couplings*. In

the electromagnetic interaction between photons and electrons, all possible combinations of polarised electrons and photons do not couple, but those that do, do so with the same probability amplitude (*charge*), with some phase considerations. The possibilities for the various different polarisations and the nature of couplings arise from the principles of *quantum electrodynamics*, symmetries of physical laws and the principle of relativity.

Every particle must be in one class of possible polarisations, called *spin 0*, *spin* $\frac{1}{2}$, *spin 1*, *spin* $\frac{3}{2}$, *spin 2* etc. The different classes of polarisations have various different attributes. Spin 0 particles feature one component and, effectively, are not polarised. So far, no fundamental spin 0 (scalar) particles have been found. The electron is an example of a spin $\frac{1}{2}$ particle and the *real* photon is an example of a spin 1 particle. The spin $\frac{1}{2}$ and spin 1 particles each have four components, corresponding to the probability amplitude to absorb each of the different polarisations (for the three space dimensions and the time dimension) a photon may be in. These are called the vector and scalar electromagnetic potentials. From combinations of these, the convenient components of classical physics called the electric and magnetic fields are derived.

2.2.2 Fundamental Particles

The number of possible particles seems to be open ended, depending on the energies involved in the production of the particles. Table 2.1 depicts some fundamental particles as they appear today.

Table 2.1: Standard Model fundamental particles

	spin $\frac{1}{2}$ particles			spin 1 particles		
				photon	gluon	W, Z
leptons	tau τ 1776.82	muon μ 105.658	electron e 0.511	-1	0	↩
	tau neutrino ν_τ < 0.02	muon neutrino ν_μ < 0.0002	electron neutrino ν_e < 0.00000001	0	0	↩
quarks	b quark b ~ 4.19	s quark s ~ 101	d quark d $4.1 - 5.8$	$-\frac{1}{3}$	g	↩
	t quark t 173,000	c quark c 1270	u quark u $1.7 - 3.3$	$+\frac{2}{3}$	g	↩
				couplings		

At the start are listed the spin $\frac{1}{2}$ particles. The first of these is the electron. Then, two *flavours* of quark (the particles featuring in the theory of strong interactions, quantum chromodynamics) are listed, d and u. Electrons and quarks have a *charge*, meaning that they couple with photons.[1]. They couple with photons in the following amounts: -1, $-\frac{1}{3}$ and $+\frac{2}{3}$ (negative multiples of the *charge* of the electron, consistent with the convention started by Franklin [4]). These numbers are called *coupling constants*. The coupling constants are listed alongside the particles. For the d quark, the probability amplitude to couple with a photon is $-\frac{1}{3}$ and for the u quark, the coupling is $+\frac{2}{3}$ and so on. The arrows indicate the particles that couple with the W and Z. The approximate masses of the particles are also shown, given in units of MeV/c^2, together with the various observed *generations* of particles. There are three known generations of fundamental particles. Between generations, particles differ by

[1]The name *photon* was coined by Gilbert N. Lewis in 1926. It was originally intended to refer to "the carrier of radiant" as made distinct by Lewis from "a corpuscle of light" [3].

flavour and mass, but their interactions appear to be identical. There are three known generations; further generations have not been observed [5].

There are two main classifications of known fundamental particles: particles that are described by *Bose-Einstein statistics* (called *bosons*) and particles that are described by *Fermi-Dirac* statistics (called *fermions*). *Leptons* are particles that are not subject to *strong interactions* and are subject to gravitation, electromagnetism and *weak interactions*.

For every particle, there is a corresponding *antiparticle*, often denoted by a bar over the particle symbol (exceptions are often when an electric charge symbol is shown). In the Feynman-Stückelberg interpretation of antiparticles, antiparticles may be considered as particles moving backward in time [6, 7, 8, 9].

Particles made of quarks are called *hadrons*. All particles made of quarks come in one of two known possible classes: those made of a quark and an antiquark (*mesons*) and those made of three quarks (*baryons*), of which the proton and neutron are common examples. The charges of the d and u quarks combine to make $+1$ for the proton and 0 for the neutron. The fact that the proton and neutron are composed of charged particles moving inside them helps explain why the proton has a magnetic moment greater than 1 and the neutral neutron has a magnetic moment.

The photons are an example of spin 1 particles. *Gluons* are another type of spin 1 particle. Quarks couple to gluon particles (in what is called the *strong interaction*) and this coupling enables quarks to bind together (the electromagnetic interaction is far too weak to do this). The wave amplitude for gluons is similar to the wave amplitude for the photons, except the coupling for gluons is much larger than the coupling for photons. Gluons indirectly account for how protons and neutrons are

held together in nuclei.

The quarks have an additional type of polarisation, called *colour*. At a particular time, a quark can be in one of three conditions, or *colours*: R, G or B (respectively referred to as "red", "green" and "blue"). The colour state of a quark can be changed when the quark emits or absorbs a gluon. For example, if a red quark changes to green, it emits a red-antigreen gluon. The gluons come in eight different types, according to the colours they can couple with. There is red-antired, red-antigreen, red-antiblue and so on. Essentially, the gluon theory, quantum chromodynamics, differs from the photon theory, quantum electrodynamics, in that gluons couple with things that have *colour*, in one of three possible conditions, R, G or B. Thus, it follows that gluons can couple with other gluons. The groups of three quarks (*baryons*) contain one quark of each colour and the quark-antiquark pairs (*mesons*) contain quarks that are red-antired, green-antigreen or blue-antiblue. Linear superpositions of the nine possible combinations of gluon colours form a special unitarity group (see section 2.3.1) $SU(3)$ octet of eight physical gluon types. This may seem to imply nine different colour gluons, but one combination of gluons, the colour $SU(3)$ singlet, which responds equally to all charges is different from the rest. It must be removed in order to have a perfectly colour symmetric theory. What is left is eight physical gluon states forming a colour $SU(3)$ octet. This is indicated by experiment.[2]

Quarks are not observed as individual particles (because of *asymptotic freedom*;

[2]In attempting to describe reality, one is seeking an internal symmetry having a three dimensional representation that can give rise to a neutral combination of three particles. The simplest such representation has a linear combination of each type of charge being neutral. The gluons are postulated to occur in colour anticolour units (that is, nine of them), however, $r + b + g$ is neutral, which means that the linear combination $r\bar{r} + b\bar{b} + g\bar{g}$ must be noninteracting because, otherwise, the colourless baryons would be able to emit these gluons and interact with each other via the strong interaction. This is contrary to observations. Essentially, the hypothetical ninth gluon that cannot interact with anything (and, therefore, cannot be detected) is assumed not to exist.

see section 2.5). As nuclei are bombarded with protons of higher and higher energy, jets of mesons and baryons are observed instead of isolated quarks coming out of the collisions.

A form of radioactivity called *beta decay* involves a neutron changing to a proton. Specifically, one of the d quarks of the neutron changes flavour to a u quark. In this process, the d quark emits a particle called a W (similar in many respects to the photon), which has a coupling with an electron and a particle called an *antineutrino*. The *neutrino* is another example of a spin $\frac{1}{2}$ particle. It does not couple to photons (and, thus, has no electric charge) and does not interact with gluons. A neutrino can be described as being in one of a number of flavour states, labelled by the type of lepton associated with its production.

The W is a spin 1 particle (similar to the photon and the gluon) that changes the flavour and electric charge of quarks. Specifically, the W^- takes away a charge of -1 while its antiparticle, the W^+, takes away a charge of $+1$. As the W changes the electric charge, it can couple with a photon. The W has a mass of $80,385 \pm 15$ MeV/c^2 [10].

There is another particle, which may be thought of as a neutral W, called Z^0. The Z^0 does not change the electric charge or flavour of a quark, but does couple with a d quark, a u quark, an electron or a neutrino in interactions referred to as "*weak neutral current interactions*". The Z can couple to any *Standard Model* (see section 2.6.2) particle except the photon and the gluon. The Z has a mass of $91,187.6 \pm 2.1$ MeV/c^2 [11].

There are quantum theories of gravity that involve *gravitons* (which would appear under a new category of polarisations called *spin* 2) and some other fundamental particles (some with spin $\frac{3}{2}$). There are currently no experiments with which to test

a quantum theory of gravity.

One particularly unsatisfactory feature in the description of fundamental particles and interactions is the observed masses of the particles. There is no theory that adequately explains these numbers.

2.2.3 Interactions

The strengths of the known interactions relative to the strength of the electromagnetic interaction for two u quarks separated by specified distances are shown in table 2.2.

2.3 Quantum Field Theory

2.3.1 Symmetry

Symmetry plays a central, unifying role in physics. Symmetry implies invariance. All of the physical conservation laws are principles of invariance. For example, the conservation of linear momentum and the conservation of angular momentum derive respectively from translational and rotational invariance. Symmetry, such as that related to translational and rotational invariance, can be described by a set of transformation rules that constitute a mathematical group. Groups such as these can also describe transformations of internal symmetries such as the interchange of colour and flavour of quarks. Three dimensional *special unitarity* groups, $SU(3)$, are used to describe the symmetry based on three-quark flavours as well as three-quark colours. Similarly, two dimensional *special unitarity* groups, $SU(2)$, can be used to describe isospin doublets that interact via weak interactions. The simplest of these kinds of group is the

Table 2.2: Known interactions

	interactions			
property	gravitation	weak	electromagnetic	strong
concerns property:	mass, energy	flavour	electric charge	colour charge
couples with:	all known particles	quarks, leptons	electrically charged particles	quarks, gluons
mediator particles:	graviton (not observed)	W^+, W^-, Z^0	γ	gluons
strength at 10^{-18} m :	10^{-41}	0.8	1	25
strength at 3×10^{-17} m :	10^{-41}	10^{-4}	1	60
		electroweak interaction		

one dimensional unitary group $U(1)$. This is the symmetry group associated with quantum electrodynamics. It involves one gauge boson, the photon, and a conserved quantity, the electric charge. In *group theory*, $SU(3) \times SU(2) \times U(1)$ represents the underlying symmetry of the Standard Model. Specifically, the Standard Model incorporates the symmetries representing the electroweak theory, $SU(2) \times U(1)$, and the symmetries representing quantum chromodynamics, $SU(3)$.

2.3.2 Quantum Field Theory

Quantum field theory provides a framework for describing quantum mechanical models of systems that would be represented classically by an infinite number of degrees of freedom using fields and many body systems. The Standard Model is formulated as a relativistic quantum field theory using the theories of the electroweak and strong interactions. Quantum field theory also provides powerful tools for condensed matter physics, especially concerning the quantum many body problem as it arises in the theory of metals, the theory of superconductivity, the behaviour of quantum fluids at low temperature and the quantum Hall effect. The continuing exchange of ideas between the theory of condensed matter physics and the theory of high energy physics is significant. Spontaneous symmetry breaking, the renormalisation group, effective field theory, solitons, instantons and fractional charge and statistics have all arisen out of this exchange.

Quantum field theory occupies a central position in the description of nature. It provides the best known description of the fundamental physical laws and is useful for investigation of the behaviour of complex systems. The central ideas of quantum field

theory are twofold. First, the basic dynamical degrees of freedom are operator functions of space and time (quantum fields, obeying appropriate commutation relations). Second, the interactions of these quantum fields are local. That is, the equations of motion and the commutation relations governing the evolution of a quantum field at a point in space-time depend only on the behaviour of fields and their derivatives at that point. Other variables, whose equations are not local, may be used, but there must always be some underlying fundamental, local variables.

The most profound fact about nature that quantum field theory describes uniquely is the existence of different, yet indistinguishable, copies of elementary particles. Two electrons, for example, are observed to have exactly the same properties despite their respective origins. This is understood as a consequence of the fact that both are excitations of the electron field. The same description applies to other particles (including composite objects such as nuclei, atoms and molecules).

The existence of classes of indistinguishable particles is the necessary logical prerequisite to the assignment of unique quantum statistics to each class. Given the indistinguishability of a class of elementary particles, and the invariance of their behaviour under interchange, the general principles of quantum mechanics explain that solutions forming any representation of the permutation symmetry group retain that property in time, but do not constrain which representations are realised. Quantum field theory not only describes the existence of indistinguishable particles and the invariance of their interactions under interchange, but also constrains the symmetry of the solutions. For bosons, only the identity representation is physical (described by symmetric wave functions); for fermions, only the one dimensional odd representation is physical (described by antisymmetric wave functions). There is also the

spin statistics theorem, according to which objects with integer spin are bosons and objects with half odd integer spin are fermions. The fermion character of electrons underlies the stability of matter and the structure of the periodic table.

Quantum field theory also gives insight into the existence of antiparticles. A general consequence of quantum field theory is the CPT theorem, which states that any local and Lorentz-covariant quantum field theory is invariant under the CPT operation, which is a combination of the three discrete transformations of charge conjugation, parity transformation and time reversal. At present, CPT is observed as an exact symmetry of nature, though each separate transformation can be violated. Antiparticles are the CPT conjugates of their corresponding particles.

The considerations so far (the existence of indistinguishable particles, the phenomenon of quantum statistics and the existence of antiparticles) are all consequences of *free* quantum field theory. Two further considerations emerge when interactions are incorporated into quantum field theory: the first is the ubiquity of particle creation and destruction processes and the second is the association of interactions with particle exchange.

In *perturbative* quantum field theory, the forces between particles are mediated by particles. The electromagnetic interaction is described as the exchange of photons. Intermediate vector bosons mediate the weak interactions and gluons mediate the strong interactions. There is no complete quantum theory of the gravitational interaction. Prominent proposed quantum theories of gravity postulate the existence of a *graviton* particle as a mediator. These interaction particles are virtual particles and are not detected (detection would imply that the interaction is not being mediated).

The virtual particles obey all of the usual physical laws, such as conservation of

energy and conservation of momentum, with the precept that the virtual particle mass can differ from that of the corresponding real particle. In general, the more massive the virtual particle, the shorter the lifetime of that particle.

The gravitational field and the electromagnetic field are the only two fundamental fields in nature that have infinite range and a corresponding classical low energy limit, which greatly diminishes and hides their "particle-like" excitations. Einstein attributed "particle-like" and discrete exchanges of momenta and energy, characteristic of "*field quanta*", to the electromagnetic field. Originally, his principal motivation was to explain the thermodynamics of radiation. It is often claimed that the photoelectric and Compton effects require a quantum description of the electromagnetic field, but the quantum nature of radiation is now understood in quantum optics as the *antibunching effect* [12].

The most common approach to the formulation of a quantum field theory involves the use of a Lagrangian ($\mathcal{L}$), which is a scalar function that represents the dynamics of a given system. The equations of motion can then be derived using the *least action principle*. Feynman generalised the least action principle to the *path integral formulation* of quantum mechanics and Feynman diagrams [13, 14]. The path integral formulation of quantum mechanics is a description of quantum theory that generalises the least action principle of classical mechanics. It generalises the classical notion of a single, unique trajectory for a system with a sum (functional integral) over an infinity of possible trajectories to calculate a probability amplitude. A Feynman diagram represents a class of particle paths, which join and split as described by the diagram. The Feynman diagrams provide a visualisation of the calculations involved in the interactions of particles: particles interact in all allowed possible ways; the

probability for each final state is the sum over all such possibilities.

Both quantum chromodynamics and the electroweak theory are formulated as *Yang-Mills theories* [15]. As such, they are gauge quantum field theories based on certain symmetry groups ($SU(N)$). Through *gauge invariance*, symmetry gauging gives rise to classical force fields. The physical observables are invariant in a chosen gauge. This invariance is caused by a continuous symmetry, which implies a conservation law (Noether's theorem). For the case of classical electrodynamics, many electromagnetic potentials describe the same electromagnetic field. In quantum electrodynamics, the requirement of local gauge invariance under the $U(1)_{\mathrm{EM}}$ symmetry group leads to the introduction of a gauge field. This field transforms just as Maxwell's equations. Indeed, it describes the massless spin 1 photon field.

In summary, quantum theory has three main types of interaction: the *strong interactions* of quarks and gluons, the *weak interactions* of the W and Z bosons and the *electromagnetic interactions* of photons.

2.4 Quantum Electrodynamics

Quantum electrodynamics [14, 16] is a relativistic quantum field theory of the electromagnetic interactions. In classical terms, it describes the interaction of the charged Dirac field with the electromagnetic field. In more modern terms, it can be described as a *perturbation theory* of the electromagnetic quantum vacuum. It provides a complete foundation for atomic physics and chemistry.

The general approach in quantum electrodynamics has proven to be very highly quantitatively accurate, though at high energies, it must be combined with the theory

of the weak interaction. The calculation of quantities in quantum electrodynamics involves the use of perturbation theory. Greater than first order perturbation calculations directly produces infinite results and the *renormalisation* approach is used to address this. Briefly, this involves the redefinition of parameters, such as particle masses and coupling constants, of the theory in such a way that calculations of any order give finite results. Renormalisability is now considered to be an essential property of any theory of fundamental particles and interactions.

The simplest calculations ignore virtual particles; they have no closed loops and are called *tree diagrams* (a simple diagram may be the repulsion of two electrons by the exchange of a photon). Progressively more complicated diagrams add loops one by one. This additive procedure is called *"perturbation"*, meaning that an initial estimate (represented by tree diagrams) is gradually perturbed by adding refinements (loops). In the example of a photon exchange between two electrons, the photon can spontaneously split into a virtual electron and a virtual antielectron (positron), which live for a short time before annihilating, producing a photon, which resumes the 'journey' the original photon was taking. In the next level of complexity, the electron and antielectron may themselves split temporarily. With increasing numbers of virtual particles, the diagrams describe quantum effects with increasing precision. In principle, the sum of the various possibilities represented by the Feynman diagrams is unity. This principle of *unitarity* is implicit in the perturbation technique. In practice, it is not possible to sum all possible terms and there are various approaches to approximating the sum [17].

2.5 Quantum Chromodynamics

By analogy with quantum electrodynamics, quantum chromodynamics is a quantum field theory of strong interactions between fundamental particles (including the interaction that binds protons and neutrons in the nucleus); it features the assumption that strongly interacting particles (hadrons) are made of quarks and that gluons bind the quarks together. As for quantum electrodynamics, quantum chromodynamics is also governed by a coupling, but as the word *"strong"* suggests, its value is higher than that of the electromagnetic coupling. In general, a greater coupling increases the number of Feynman diagrams that must be included in calculations for a certain precision.

Quantum chromodynamics is a non-abelian[3] gauge theory consisting of a colour field mediated by a set of exchange particles. The theory features *confinement*, which is the phenomenon in which particles with colour charge can not be isolated singularly (hence, a quark is not observed in isolation). The theory also features *asymptotic freedom* [18, 19, 20], which is a property of some gauge theories that causes bonds between particles to become weaker asymptotically with increase in energy and decrease in distance between the particles, hence, quarks and gluons interact very weakly in very high energy reactions (though still more strongly than the other interactions). Confinement is dominant at low energies and asymptotic freedom is dominant at high energies.

[3]If the symmetry group of gauge transformations for a gauge theory is non-commutative, the gauge theory is referred to as *non-abelian* and if the symmetry group is commutative, the gauge theory is referred to as *abelian*. *Quantum electrodynamics* is an abelian gauge theory while *quantum chromodynamics* and the *Standard Model* (see section 2.6) are non-abelian gauge theories.

2.6 The Standard Model

2.6.1 Description of Nature

The overall goal of high energy physics is to determine the Lagrangian of nature and to determine its parameters experimentally. In order to design a Lagrangian for this purpose, three principal components are needed:

1. the gauge group of the model;
2. the representations of the fields under this gauge group;
3. the pattern of spontaneous symmetry breaking.

The pattern of spontaneous symmetry breaking is represented typically by a sign, for example, the sign of the Higgs squared mass parameter at the unstable vacuum ($\mu^2 < 0$) (see section 2.7.4).

With these components, the *most general renormalisable Lagrangian* that is invariant under the gauge symmetry and provides the required spontaneous symmetry breaking pattern must be determined. The statement "most general" implies that all terms that satisfy the above conditions must be present in the Lagrangian, even terms that may be phenomenologically problematic, for example, a term that includes proton decay cannot be omitted without some symmetry principle forbidding it. However, renormalisability strongly constrains the form of the Lagrangian and limits the number of terms to a finite number.

A few rules for designing models are as follows:

- Poincaré invariance[4] is imposed (the 'gauge group' with respect to gravity).
- The terminology of quantum field theory is used.
- Global symmetries are not imposed (global symmetries may be broken by gravity, for example).
- The fermion representation is two-component chiral (Weyl) spinors.
- Until the physical parameters (finite in number) associated with the model are experimentally measured, the model is not considered a description of nature; if a Lagrangian features n physical parameters, n measurements must be performed first before predictions of further measurements are made.

Regarding the last point, the number of parameters required to define a theory is independent of how they are parameterised. In practice, if $m > n$ measurements of a theory are performed, it is not the case that n 'parameter measurements' are made, followed by $m - n$ observations of the theory; instead, all m measurements are used to make a statistical fit (e.g., χ^2) for the n parameters in order to check for self-consistency. Essentially, a model (a Lagrangian) by itself does not make predictions; it must come with measurements of its parameters.

At this time, the most successful model of nature is the *Standard Model*.

[4]Poincaré invariance is covered by the generalisation of Lorentz covariance.

2.6.2 The Standard Model

The Standard Model, currently the most successful model of nature, describes all atomic, nuclear and subnuclear phenomena using a dozen fermions and a dozen bosons[5]. It unifies the strong interactions of quantum chromodynamics and the electroweak interactions. It serves as an effective example of the aforementioned principles (see section 2.6.1) because it works and is familiar.

The three principal components of the Standard Model are as follows:

1. Gauge group: $SU(3)_c \times SU(2)_L \times U(1)_Y$.

2. Representations of matter: The fermion fields of the Standard Model are the left handed quark doublet Q, the right handed U, the right handed D, the left handed lepton doublet L and the right-handed charged lepton E. Using the convention in which all fields are written in terms of left handed Weyl spinors, taking CP conjugations as necessary, the gauge representations can be shown using the $(c, L)_Y$ notation[6] (see table 2.3, in which i is the generation index, $i = 1, 2, 3$). In addition to the fermions, there is also a complex scalar Higgs field, ϕ, with the representation $(1, 2)_{1/2}$.

3. Spontaneous symmetry breaking: $SU(2)_L \times U(1)_Y \to U(1)_{EM}$. This can be seen from the sign of the Higgs mass term, $\mathcal{L} \supset \mu^2|\phi|^2$, so that the potential contains the term $-\mu^2|\phi|^2$.

[5] In a sentence, the Standard Model may be described as the simplest four dimensional low energy quantum effective field theory description consistent with the known degrees of freedom and their interactions (except gravity) and all experimental data.

[6] The Standard Model gauge group is $SU(3)_C$, $SU(2)_L$, $U(1)_Y$.

Table 2.3: Fermion fields of the Standard Model

Q_i	$(3,2)_{1/6}$
U_i^c	$(\bar{3},1)_{-2/3}$
D_i^c	$(\bar{3},1)_{1/3}$
L_i	$(1,2)_{-1/2}$
E_i	$(1,1)_1$

The most general renormalisable Lagrangian is composed of three parts: the kinetic Lagrangian, $\mathcal{L}_{\text{kin.}}$, the Higgs Lagrangian, $\mathcal{L}_{\text{Higgs}}$, and the Yukawa Lagrangian, $\mathcal{L}_{\text{Yuk.}}$:

$$\mathcal{L}_{SM} = \mathcal{L}_{\text{kin.}} + \mathcal{L}_{\text{Higgs}} + \mathcal{L}_{\text{Yuk.}}. \tag{2.1}$$

The kinetic Lagrangian, $\mathcal{L}_{\text{kin.}}$, includes the gauge interactions through the covariant derivative and non-abelian field strength. The Higgs Lagrangian, $\mathcal{L}_{\text{Higgs}}$, gives the sombrero potential[7]:

$$\mathcal{L}_{\text{Higgs}} = \mu^2|\phi|^2 - \lambda|\phi|^2, \tag{2.2}$$

where λ is the self interaction coupling constant of the scalar field and μ^2 defines the shape of the potential.

[7]The sombrero function is the two dimensional polar coördinate analogue of the sinc function.

The Yukawa Lagrangian, $\mathcal{L}_{\text{Yuk.}}$, is

$$\mathcal{L}_{\text{Yuk.}} = y^e_{ij}\bar{L}^i\phi E^j + y^d_{ij}\bar{Q}^i\phi D^j + y^u_{ij}\bar{Q}^j\tilde{\phi}U^j + \text{Hermitian conjugate.} \tag{2.3}$$

In the Standard Model, fermions acquire masses only through these terms. In a general model, it is possible to have bare masses when gauge and spacetime symmetries allow it.

2.7 Englert-Braut-Higgs Mechanism

2.7.1 Before the Englert-Braut-Higgs Mechanism

Before the Englert-Braut-Higgs (EBH) mechanism was described, the prominent view was that gauge theories were largely irrelevant. There was progress towards quantisation of unbroken gauge theories, but these theories required massless gauge bosons which were considered unrealistic. There was also progress in demonstrating the breaking of global symmetries [21, 22], but this also required massless bosons. It was shown later that these theories are renormalisable; breaking a symmetry spontaneously in these theories did not affect the renormalisability properties [23]. So the considerations of the time involved two different sets of massless bosons: the massless gauge bosons and the massless Goldstone bosons.

It was suggested (by Anderson [24]) that this division could be addressed by the theory of superconductivity (though this was not a relativistic theory). It was speculated that the Goldstone and Yang-Mills zero mass problems could effectively

cancel [25]. An argument against this Anderson mechanism concerned the idea that a relativistic theory required a time-like vector [26].

2.7.2 1964 PRL Symmetry Breaking Papers

In 1964, three teams proposed related but different approaches to describe how mass may arise in local gauge theories. A series of papers, known as the *1964 PRL (Physical Review Letters) symmetry breaking papers*, emerged, effectively predicting the Englert-Braut-Higgs mechanism, the means by which gauge bosons may acquire nonzero masses in the process of spontaneous symmetry breaking. The mechanism is a key element in electroweak theory.

The first paper was by Englert and Brout [27]. The second and third papers were by Higgs [28, 29] and the fourth was by Guralnik, Hagen and Kibble [30]. In the first of Higgs' papers, essentially it is suggested that the Anderson mechanism could be made to work in a relativistic theory. In the second, a specific example using the Englert-Brout-Higgs mechanism is described. The Higgs boson is so called because Higgs was the first to explicitly express that the Englert-Braut-Higgs mechanism necessitated a massive scalar particle [29]: *"... an essential feature of [this] type of theory ... is the prediction of incomplete multiplets of scalar and vector bosons."* Higgs was the one to discuss the quantum degree of freedom corresponding to oscillations out of the bottom of the Higgs potential (see section 2.7.4).

The Higgs boson particles represent the key experimental test of the Englert-Braut-Higgs mechanism.

2.7.3 Electroweak Theory

The Englert-Braut-Higgs mechanism was incorporated into the electroweak theory by Weinberg and Salam [31, 32]. This work became consensus following the demonstration by 't Hooft and Veltman that the theory is renormalisable [33, 34].

The electroweak interaction is the united description of the electromagnetic interaction and the weak interaction. The standard Glashow-Weinberg-Salam [35] model of electroweak interactions has been successful at predicting low energy phenomena. With the discovery of the W and Z gauge bosons, the only particle of the theory remaining to be discovered is the Higgs boson. The Higgs boson is required for the spontaneous symmetry breaking which gives rise to masses in the theory. Although the couplings of the Higgs boson to quarks and leptons are predicted, the Higgs boson mass is not.

An early, detailed discussion of the phenomenological profile of the Higgs boson, is given by Ellis, Gaillard and Nanopoulos[8] [36].

2.7.4 Spontaneous Symmetry Breaking

The Standard Model in its early form was a theory of massless particles. The mechanism of spontanous symmetry breaking proposed by Englert, Braut, Higgs and others enabled the generation of massive gauge bosons in the theory while retaining local gauge invariance.

To demonstrate the principle of spontaneous symmetry breaking in terms of a gauge theory, consider the case of a complex scalar field $\phi = \frac{1}{\sqrt{2}}(\phi_1 + i\phi_2)$ described

[8] This paper [36] features the comment "... we do not want to encourage big experimental searches for the Higgs boson ...".

by the following Lagrangian:

$$\mathcal{L} = \underbrace{(\partial_\mu \phi)^* (\partial_\mu \phi)}_{\text{kinetic } T(\phi)} - \underbrace{\left(\mu^2 \phi^* \phi + \lambda (\phi^* \phi)^2\right)}_{\text{potential } V(\phi)}. \tag{2.4}$$

In order to make this Lagrangian invariant under the $U(1)$ local gauge transformation $\phi \to e^{-i\alpha(x)}\phi$, ∂_μ is replaced by the covariant derivative $D^\mu = \partial_\mu - ieA_\mu$ where the gauge field transforms as $A_\mu \to A_\mu + \frac{1}{e}\partial_\mu \alpha$.

Thus, the gauge invariant Lagrangian is as follows:

$$\mathcal{L} = (D_\mu \phi)^* (D_\mu \phi) - \mu^2 \phi^* \phi - \lambda (\phi^* \phi)^2 - \frac{1}{4} F_{\mu\nu} F^{\mu\nu}, \tag{2.5}$$

where $F_{\mu\nu} = \partial_\mu A_\nu - \partial_\nu A_\mu$.

The potential of this field $V(\phi)$, assuming $\lambda > 0$, is shown in figure 2.1 for the case in which $\mu^2 > 0$. The potential, assuming $\lambda < 0$, is shown in figure 2.2 for the case in which $\mu^2 < 0$.

In the case of $\mu^2 > 0$, the potential has a minimum at $\phi = 0$, whereas in the case of $\mu^2 < 0$, the potential has a *maximum* at $\phi = 0$ and a *minimum* at a circle of radius ν in the plane of ϕ values (e.g., ϕ_1, ϕ_2 etc.), such that

$$\phi_1^2 + \phi_2^2 = \nu^2 \text{ with } \nu^2 = -\frac{\mu^2}{\lambda}. \tag{2.6}$$

Thus, there are an infinite number of states with the same lowest energy, as shown in figure 2.3.

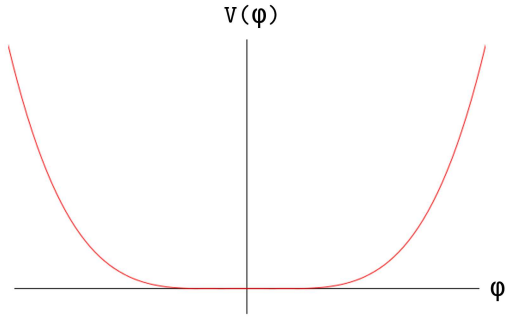

Figure 2.1: Potential $V(\phi)$ for a complex scalar field ϕ for the case of $\lambda > 0$ and $\mu^2 > 0$

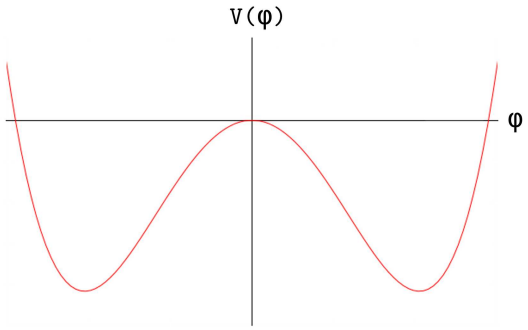

Figure 2.2: Potential $V(\phi)$ for a complex scalar field ϕ for the case of $\lambda < 0$ and $\mu^2 < 0$

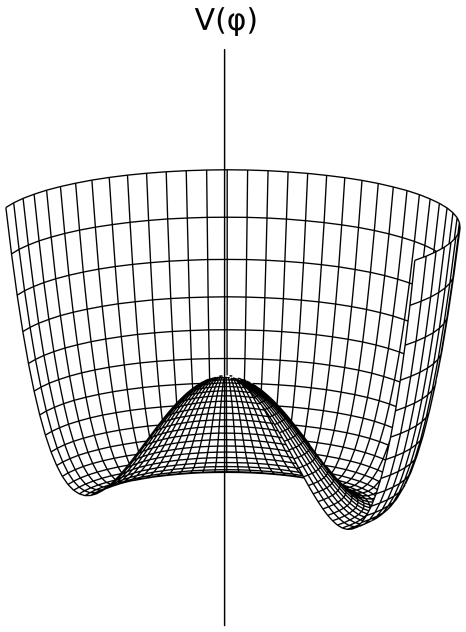

Figure 2.3: Potential $V(\phi)$ for many fields for the case of $\lambda > 0$ and $\mu^2 < 0$

If the field ϕ is translated to a minimum energy position at $\phi_1 = \mu, \phi_2 = 0$, then a new set of fields η and ξ can be defined:

$$\phi(x) = \frac{1}{\sqrt{2}}(\nu + \eta(x) + i\xi(x)), \tag{2.7}$$

where $\phi_1(x) \equiv \nu + \eta(x)$ and $\phi_2(x) \equiv \xi(x)$. The Lagrangian can now be expanded about the vacuum in terms of these fields through the substitution of the translated field $\phi(x)$ (equation 2.7) into the gauge invariant Lagrangian (equation 2.5):

$$\mathcal{L}' = \frac{1}{2}(\partial_\mu \xi)^2 + \frac{1}{2}(\partial_\mu \eta)^2 - \nu^2\lambda\eta^2 + \frac{1}{2}e^2\nu^2 A_\mu A^\mu - e\nu A_\mu \partial^\mu \eta - \frac{1}{4}F_{\mu\nu}F^{\mu\nu} + \text{interaction terms.} \tag{2.8}$$

The Lagrangian now contains terms representing the desired massive vector boson A_μ, a massive scalar η and also what appears to be a massless boson η (known as a Goldstone boson). By giving a mass to the A_μ boson, the particle's polarisation degrees of freedom have been increased from two to three. Since simply translating variables should not create a new degree of freedom, the fields in the gauge invariant Lagrangian expanded about the vacuum (equation 2.8) are not distinct physical particles. Since the difficulties in the Lagrangian involve the $\xi \equiv \phi(x)$ field, a suitable gauge transformation can be chosen to eliminate $\phi_2(x)$. By writing the $U(1)$ transformation in terms of its real and imaginary parts,

$$\phi \to \phi' = e^{-i\theta(x)}\phi \tag{2.9}$$

and

$$\begin{aligned}\phi \to \phi' &= (\cos\theta(x) + i\sin\theta(x))(\phi_1 + i\phi_2) \\ &= (\phi_1\cos\theta(x) - \phi_2\sin\theta(x)) + i(\phi_1\sin\theta - \phi_2\cos\theta(x)),\end{aligned} \tag{2.10}$$

respectively, the suitable gauge transformation is identified as $\theta = -\tan^{-1}\left(\frac{\phi_2}{\phi_1}\right)$. This transformation, combined with the approximation

$$\phi = \frac{1}{\sqrt{2}}(\nu + \eta + i\eta) \approx \frac{1}{\sqrt{2}}(\nu + \eta)\, e^{i\frac{\xi}{\nu}}, \tag{2.11}$$

to the lowest order in η, points to a different set of real fields h, θ and A_μ, that are substituted into the gauge invariant Lagrangian (equation 2.5):

$$\phi \to \frac{1}{\sqrt{2}}(\nu + h(x))\, e^{i\theta(x)\nu}; \tag{2.12}$$

$$A_\mu \to +\frac{1}{e\nu}\partial_\mu\theta. \tag{2.13}$$

Thus, a Lagrangian is obtained that describes just two interacting massive particles, a vector gauge boson, A_μ, with a mass $m_A = e\nu$, and a massive scalar boson, h, with a mass $m_h = \sqrt{2\lambda\nu^2}$. The massless Goldstone boson has been turned into the extra degree of freedom for the original gauge boson, allowing the gauge boson

to become massive. This is the Englert-Braut-Higgs mechanism. By introducing a complex scalar Higgs field with two additional degrees of freedom, one of the degrees of freedom is provided to the A_μ boson, allowing it to become massive, and the other becomes a massive scalar boson, known as the Higgs boson:

$$\begin{aligned}\mathcal{L}'' &= \frac{1}{2}\left(\partial_\mu h\right)^2 - \lambda\nu^2 h^2 + \frac{1}{2}e^2\nu^2 A_\mu^2 \\ &= \lambda\nu h^3 - \frac{1}{4}\lambda h^4 + \frac{1}{2}e^2 A_\mu^2 h^2 + \nu e^2 A_\mu^2 h - \frac{1}{4}F_{\mu\nu}F^{\mu\nu}.\end{aligned} \tag{2.14}$$

The Lagrangians 2.4 and 2.14 describe exactly the same physical system; it is in just the ground state that the $U\left(1\right)$ symmetry becomes 'hidden'.

For the case of the electroweak Lagrangian, the $SU\left(2\right)$ group has three generators which correspond to the gauge bosons $\left\{W_\mu^1, W_\mu^2, W_\mu^3\right\}$ and a coupling constant g. The $U\left(1\right)$ group has one boson B_μ (of weak hypercharge) and a coupling g'. The relative strength of these interactions is determined according to $g' = g\tan\theta_W$, where θ_W is the *weak mixing angle*.

The physical electroweak bosons, $W^\pm$, Z and γ correspond to linear superpositions of the following gauge fields:

$$\begin{aligned}W^\pm &\equiv \frac{1}{\sqrt{2}}\left(W_\mu^1 \mp iW_\mu^2\right), \\ Z_\mu &\equiv \cos\theta_W W_\mu^3 - \sin\theta_W B_\mu \text{ and} \\ A_\mu &\equiv \cos\theta_W B_\mu + \sin\theta_W W_\mu^3.\end{aligned} \tag{2.15}$$

Only the Z and W acquire mass through the Englert-Braut-Higgs mechanism. In order to break the $SU\left(2\right)_L \times U\left(1\right)_Y$ symmetry, a doublet of complex fields is

introduced, providing four extra degrees of freedom:

$$\phi = \begin{pmatrix} \phi^+ \\ \\ \phi^- \end{pmatrix} = \frac{1}{\sqrt{2}} \begin{pmatrix} \phi_1 + i\phi_2 \\ \\ \phi_3 + i\phi_4 \end{pmatrix}. \tag{2.16}$$

During spontaneous symmetry breaking, three of the extra degrees of freedom are given to the $W^{\pm}$ and Z bosons, allowing the bosons to become massive and the other degree of freedom corresponds, as before, to a massive scalar Higgs boson. The photon remains massless because the electroweak Lagrangian is invariant under local $U(1)_{EM}$ transformations with generator Q.

An explicit mass term for the fermions is not present in the Lagrangian because this would mix the right handed and left handed states that must be treated separately for the weak interaction. However, it is possible to have an interaction between the left handed fermion doublet, the right handed fermion singlet and the scalar doublet (Higgs field), Φ. These interactions are known as Yukawa interactions and have the following form:

$$\mathcal{L}_{\text{Yuk.}} = G_f \left(\bar{\psi}_L \Phi \psi_R + \bar{\psi}_R \Phi \psi_L \right), \tag{2.17}$$

where G_f is the coupling constant of the interaction.

The Yukawa interaction for the electron in the unitary gauge is given by the following:

$$\mathcal{L}_{\text{Yuk.}} = -\frac{G_e}{\sqrt{2}} \begin{pmatrix} \bar{\nu}_L \\ \\ \bar{e}_L \end{pmatrix}^T \begin{pmatrix} 0 \\ \\ \nu + H \end{pmatrix} e_R + \text{Hermitian conjugate.} \tag{2.18}$$

This results in two terms:

$$\frac{G_e \upsilon}{\sqrt{2}} \bar{e}e - \frac{G_e}{\sqrt{2}} \bar{e}He. \tag{2.19}$$

The first term is a mass term for the electron, which is proportional to the vacuum expectation of the scalar field. From this term is obtained a relation for the Yukawa coupling in terms of the electron mass, m_e, and the W boson mass, m_W:

$$G_e = g \frac{m_e}{\sqrt{2} M_W}. \tag{2.20}$$

The second term gives the coupling between the electron and the scalar Higgs field, which is proportional to the electron mass. In a similar way, quarks also acquire mass through their respective couplings with the Higgs field, with the respective couplings being proportional to the respective masses.

In summary, the introduction of the Englert-Braut-Higgs mechanism of electroweak symmetry breaking is the simplest way to give masses to elementary particles. In the Standard Model, a single Higgs doublet gives rise to one observable

Higgs boson. In the *Minimal Supersymmetric Standard Model*, two Higgs doublets spawn two charged and three neutral Higgs bosons.

2.8 Supersymmetry

2.8.1 Hierarchy Problem

A problem with a light Higgs boson in the Standard Model is that quantum corrections to the Higgs boson mass have a quadratic divergence. Assuming the Standard Model to be valid up to the Planck scale, this correction is very large compared to the physical Higgs boson mass. This problem is known as the *hierarchy problem* [37, 38, 39, 40]. Since divergences are removed by renormalisation, this may not be considered a problem technically, however, conceptually, it may be considered an important problem because it implies that the theory is not stable under small variations of the fundamental parameters. *Supersymmetry* can solve the hierarchy problem.

2.8.2 Supersymmetry

Supersymmetry [41, 42] (often abbreviated as "*SUSY*") is a symmetry that relates elementary particles to particles called *superpartners* that differ from the regular particle by half a unit of spin. It is a proposed extension to the Standard Model and is the only so far 'unused' symmetry of the Poincaré group. One prominent property of this theory (assuming unbroken symmetry) is that every fermion has a supersymmetric boson partner and vice versa. So quarks have *squarks* which are integer spin quarks. Photons have half integer spin particles called *photinos*. The naming conventions are

straightforward: the partner of a fermion is named by adding the prefix "s" to the regular fermion's name (electron becomes *selectron*, neutrino becomes *sneutrino* and so on), while the partner of a boson is found by adding the suffix "ino" to the regular boson's name (gluon becomes gluino, graviton becomes gravitino and so on). The theory has predictive power, can include gravitational interactions and offers solutions to certain cosmological problems (such as the hypothetical "dark matter" [43, 44, 45]). Supersymmetric particles have not been observed. If supersymmetry exists (as superpartners of Standard Model particles), it must be a broken symmetry, allowing superparticles to be more massive than the corresponding particles.

No meaningful indications of the superpartners have been observed.

2.8.3 Minimal Supersymmetric Standard Model

The Minimal Supersymmetric Standard Model (MSSM) [46, 47, 48] is a prominent candidate for physics beyond the Standard Model. In effect, it doubles the Standard Model particle content. Two complex doublets in the MSSM contain a total of eight degrees of freedom, as shown in table 2.4.

Electroweak symmetry breaking through two complex Higgs doublets leads to five physical states, two of which are charged (H^+ and H^-). *A priori*, the mass of the charged Higgs bosons is not predicted by theory. At the tree level, the MSSM Higgs sector is determined fully by two parameters: the charged Higgs boson mass $m_{H^\pm}$ and the ratio of the vacuum expectation values of the two Higgs fields, commonly denoted as

$$\tan\beta = \frac{v_2}{v_1}. \tag{2.21}$$

It characterises the relative fraction that the two Higgs doublets contribute to the electroweak symmetry breaking $v^2 = v_1^2 + v_2^2$, where $v \simeq 246$ GeV [49].

Table 2.4: Degrees of freedom in the Minimal Supersymmetric Standard Model

G^0	neutral Goldstone boson (used by Z)
$G^\pm$	charged Goldstone boson (used by W)
h^0	light CP even Higgs boson
H^0	heavy CP even Higgs boson
A^0	CP odd
$H^\pm$	charged Higgs boson pair

2.9 Searches for Higgs Bosons

2.9.1 Early Searches for Higgs bosons

Some of the early searches for Higgs bosons and their respective results are shown in table 2.5.

Table 2.5: Early searches for Higgs bosons

year	search	result	references
1975	emission from stars	$m_H > 0.7 m_e$	[50, 51]
1974	neutron-electron scattering	$m_H > 0.7$ MeV	[52, 53]
1975	neutron-nucleus scattering	$m_H > 13$ MeV	[54]
1974	nuclear $0^+ - 0^+$ transitions	$m_H > 18$ MeV	[55]

2.9.2 Searches for Higgs bosons at the Large Electron-Positron Collider

The CERN Yellow Report *Physics with Very High-Energy e^+ e^- Colliding Beams* [56] offers a detailed description of searches for Higgs bosons at the Large Electron-Positron Collider (LEP).

In brief, at the LEP collider, the principal processes used to constrain the mass of the Higgs boson were $e^+e^- \to Z + H$ [36, 57] (associated production) and $Z \to H + \mu^+\mu^-$ [58]. The first modern experimental estimations of the mass of the Higgs boson were made on the basis of electroweak radiative corrections (which are sensitive to massive particles) measured at the LEP collider [59]. After the discovery of the t quark, the uncertainties were reduced significantly. The LEP Higgs boson exclusion is shown in figure 2.4. The LEP searches did not show any conclusive evidence

for the production of a Standard Model Higgs boson.

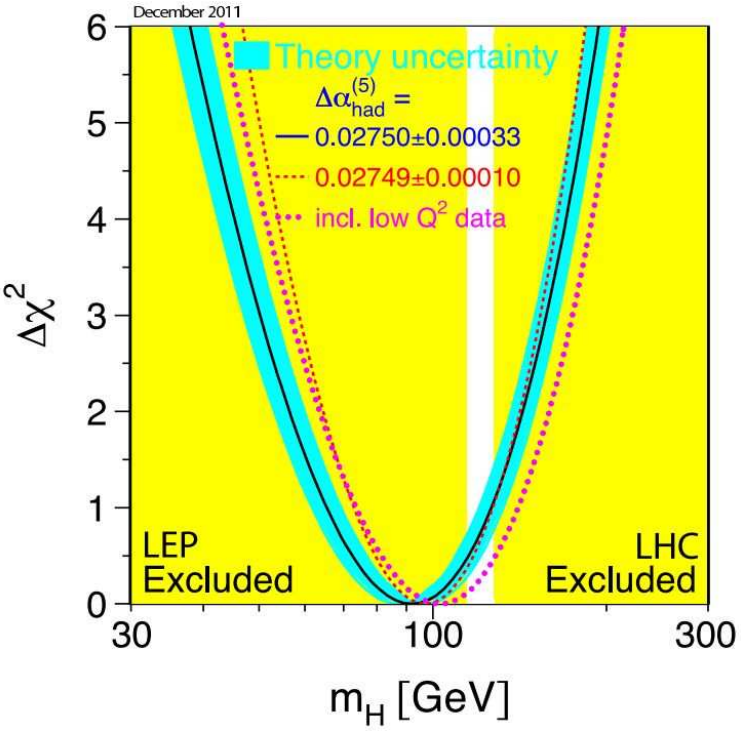

Figure 2.4: LEP Higgs boson exclusion (shown with LHC 2011 exclusion)

2.9.3 Searches for Higgs bosons at the Tevatron

In brief, at the Tevatron, the principal processes used to constrain the mass of the Higgs boson were gluon fusion ($gg \to H$) and Higgs boson production in association with a vector boson ($W^{\pm}H$ or ZH). The Tevatron Higgs boson exclusion is shown in figure 2.5.

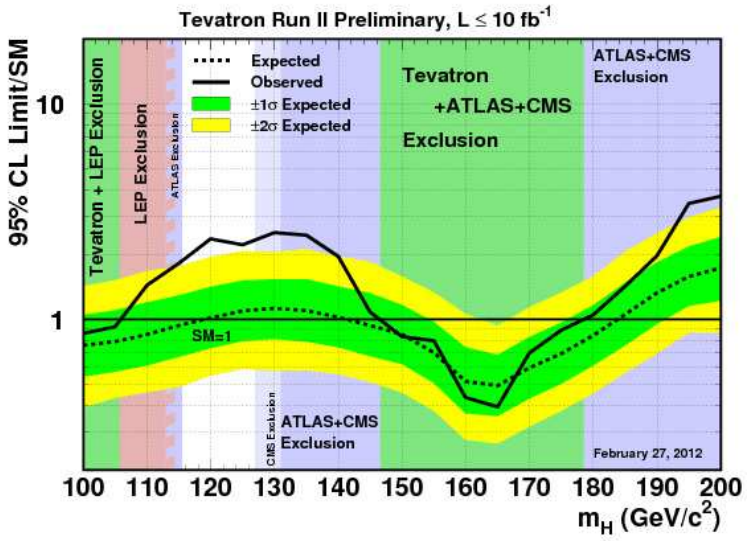

Figure 2.5: Tevatron Higgs boson exclusion (shown with LHC early 2012 exclusion)

2.9.4 Searches for Higgs bosons at the Large Hadron Collider

At the time of submission, the most stringent constraints on the mass of the Standard Model Higgs boson are a lower limit of 114.4 GeV at the 95% confidence level, set using the combined results of the four LEP experiments [60], and an excluded band of 156 GeV to 177 GeV, from the combined results of the Tevatron experiments [61].

At the LHC, the principal processes used to constrain the mass of the Higgs boson are gluon fusion ($gg \to H$) [62, 63], Higgs boson production in association with a vector boson ($W^{\pm}H$ or ZH) [64] or Higgs boson production with a t quark pair ($t\bar{t}H$) and the vector boson fusion process (qqH or $q\bar{q}H$).

ATLAS combined upper limits on the Standard Model Higgs boson at the 95% confidence level are shown in figure 2.6 for 100 GeV $\leq m_H \leq$ 600 GeV [65]. The combined upper limits are also shown for 110 GeV $\leq m_H \leq$ 150 GeV in figure 2.7. An excess of events is observed around $m_H \sim 126$ GeV with a local significance of

2.5σ, where the expected significance in the presence of a Standard Model Higgs boson for that mass hypothesis is 2.9σ.[9]

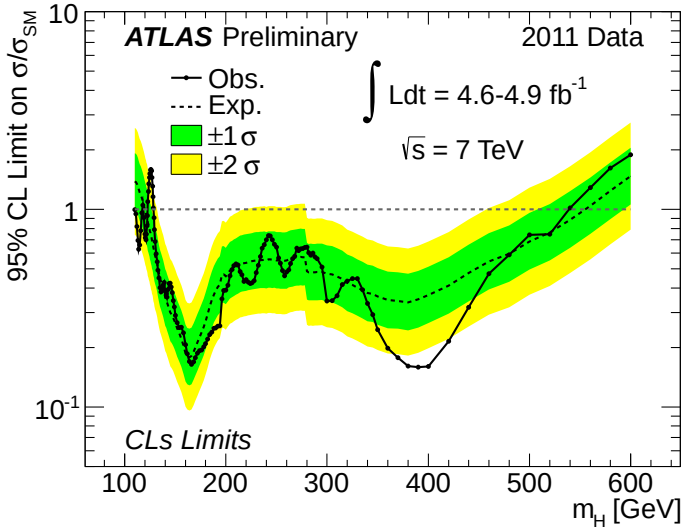

Figure 2.6: 100 GeV $\leq m_H \leq$ 600 GeV ATLAS Higgs boson combined upper limits for 2011 data

2.9.5 Search for Charged Higgs Bosons Decaying via $H^+ \to \tau_{lep.} + \nu$ in $t\bar{t}$ Events

The search for charged Higgs bosons presented in this thesis considers the type-II 2HDM. For charged Higgs bosons with masses less than the t quark mass, the dominant production mode for H^+ at the LHC is through the t quark decay $t \to bH^+$, due to the large Yukawa coupling of the t. The dominant source of t quarks at the

[9]ATLAS and CMS have reported on the results of Higgs searches based on 5 fb^{-1} of 2011 LHC data in several channels [66, 67, 68, 69, 70, 71]. The results give hints of the existence of a Higgs boson with a mass of approximately 126 GeV manifesting in the diphoton $h \to \gamma\gamma$ and 4 lepton $h \to ZZ^*$ final states.

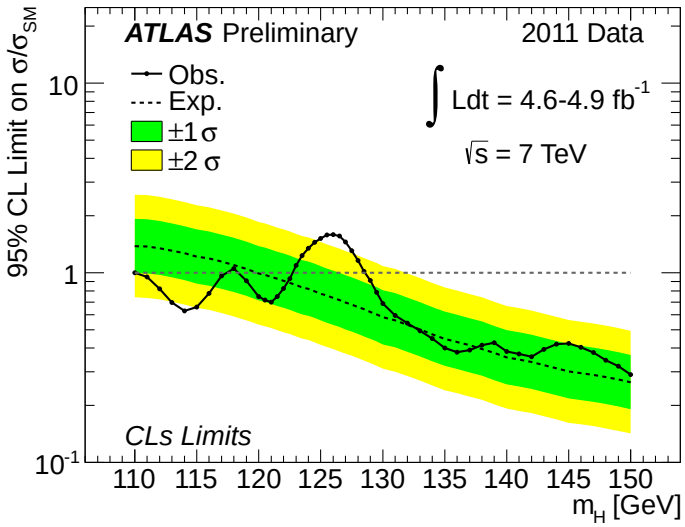

Figure 2.7: 110 GeV $\leq m_H \leq$ 150 GeV ATLAS Higgs boson combined upper limits for 2011 data

LHC is through $t\bar{t}$ production. The cross section for charged Higgs boson production from single t quark events is much smaller and is not considered in this analysis. For $\tan\beta > 3$, charged Higgs bosons decay primarily via $H^+ \to \tau\nu$[10] [72]. Experimental limits tend to rule out lower values of $\tan\beta$ (at least for relatively light supersymmetric partners). For the purposes of the analyses of this thesis, the assumption of $\mathcal{B}(H^+ \to \tau\nu) = 1$ is made.

In the search of this thesis, the charged Higgs bosons are searched for in $t\bar{t}$ events with one or two light charged leptons (electrons or muons, here represented by l) in the final state (see figure 2.8). So, specifically, $t\bar{t}$ events arising from gluon fusion decay as $t \to H^+b \to \tau^+\nu_\tau b$ and $\bar{t} \to W^-b \to l^-\bar{\nu}_l\bar{b}$.

[10]In this thesis, the charged Higgs bosons are denoted as H^+ and the decay of a charged Higgs boson to a tau and a tau neutrino is denoted as $H^+ \to \tau\nu$ (as opposed to $H^+ \to \tau^+\nu_\tau$) for reasons of brevity. Charge conjugated processes are implicitly included.

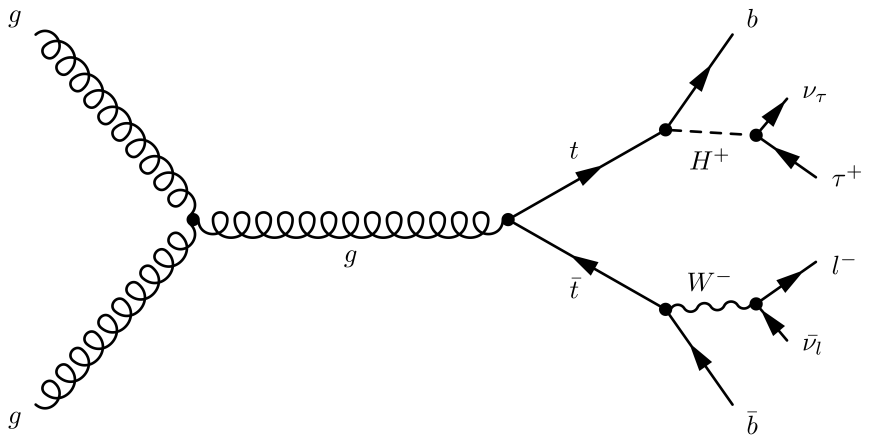

Figure 2.8: Leading order Feynman diagram for the production of $t\bar{t}$ events arising from gluon fusion, where a t quark decays to a charged Higgs boson, followed by the decay $H^+ \to \tau\nu$

If the charged Higgs boson arising from $t \to bH^+$ decays solely to $\tau\nu$, a small increase in the branching fraction for single lepton and two lepton decays of $t\bar{t}$ pairs occurs, as the t decays leptonically more often than the W boson: $\mathcal{B}(H^+ \to \tau\nu \to l + N\nu) \simeq 35\%$ while $\mathcal{B}(W \to l + N\nu) \simeq 25\%$ (where N indicates the number of neutrinos). It is useful to identify discriminating variables that allow a distinction between leptons produced in $\tau \to l\nu_l\nu_\tau$ (e.g., in decays of W or charged Higgs bosons) and leptons arising directly from W boson decays, rather than relying only on the presence or absence of an excess of single lepton and two lepton $t\bar{t}$ events.

One discriminating variable is the invariant mass m_{bl} of a b quark and a lepton l coming from the same t quark, which can be described using $\cos\theta_l^*$:

$$\cos\theta_l^* = \frac{2m_{bl}^2}{m_t^2 - m_W^2} - 1 \simeq \frac{4p^b \cdot p^l}{m_t^2 - m_W^2} - 1, \\ \text{with } p^b \cdot p^l = 2E_b E_l \left(1 - \cos\theta_{bl}\right) = 4E_b E_l \sin^2\left(\frac{\theta_{bl}}{2}\right), \tag{2.22}$$

where p^b and p^l are the four-momenta of the b quark and of the lepton l (which can be chosen in any reference frame because $\cos\theta_l^*$ contains the invariant product $p^b \cdot p^l$) and θ_{bl} is the angle between them. Both m_b^2 and m_l^2 are neglected, hence, $m_{bl}^2 \simeq 2p^b \cdot p^l$. While the $\cos\theta_l^*$ variable is used commonly to measure the polarisation of W bosons in t quark decays, where θ_l^* is the angle of the lepton momentum with respect to the helicity axis in the W rest frame, it is used for other purposes in this analysis. If a t quark decay is mediated through an H^+ and the H^+ is more massive than the W boson, the b quark usually has a smaller momentum than in the case of a t quark decay mediated through a W boson. Also, a lepton l arising from a τ decay is likely to have a smaller momentum than a lepton arising directly from a real W boson. As a result, the presence of a charged Higgs boson in a leptonic quark decay strongly reduces the invariant product $p^b \cdot p^l$, leading to values of $\cos\theta_l^*$ close to -1.

The event topology considered in this thesis belongs to a class of events in which the presence of undetected particles in the final states prevents full reconstruction of the mass of the particle that is sought after. Often in such cases it is possible to define kinematic variables that are bounded by the unknown mass and, thus, the mass value can be inferred from an edge in the distribution of a variable over many events. These variables generally are referred to as *transverse mass observables*. In this analysis,

transverse mass observables can be used to discriminate between leptons produced in $H^+ \to \tau\nu$ decays and leptons arising from W bosons [73]. Specifically, the charged Higgs boson transverse mass can be used: m_T^H is used for the single lepton events and m_{T2}^H is used for the two lepton events.

2.9.5.1 Single Lepton Events

In single lepton $t\bar{t}$ events in which a W boson decays directly into an electron or muon and one neutrino, the W transverse mass is obtained by constraining the square of the missing mass $\left(p^{missing}\right)^2$ to be zero, making the assumption that it comes only from the massless neutrino associated with the direct W decay (that is, a minimisation of the invariant mass $\left(p^l + p^{missing}\right)^2$ is performed using the longitudinal momentum and the energy of the neutrino):

$$\begin{aligned}\left(m_T^W\right)^2 &= \min_{\left\{\substack{p_z^{\text{missing}}, E^{\text{missing}} \\ \left(p^{\text{missing}}\right)^2 = 0}\right\}} \left[\left(p^l + p^{\text{missing}}\right)^2\right] \\ &= 2p_T^l E_T^{\text{missing}} \left(1 - \cos\phi_{l,\text{missing}}\right),\end{aligned} \tag{2.23}$$

where p_z^{missing} and E^{missing} are the longitudinal momentum and the energy of the neutrino, respectively, and p_T^l and E_T^{missing} are the transverse momenta of the lepton and the neutrino, respectively, with $\phi_{l,\text{missing}}$ being the azimuthal angle between them. In the case of a leptonic τ decay either from a W of charged Higgs boson, this constraint is not valid because the missing momentum arises from three neutrinos, hence, $\left(p^{\text{missing}}\right)^2 \neq 0$. However, if one of the two b quarks can be associated with the leptonically decaying t quark, the *charged Higgs boson transverse mass* can be

determined by performing a maximisation of the invariant mass $\left(p^{l}+p^{\text{missing}}\right)^{2}$ using the longitudinal momentum and the energy of the neutrinos in the single lepton $t\bar{t}$ event:

$$\left(m_{T}^{W}\right)^{2}=\max_{\left\{\substack{p_{z}^{\text{missing}},E^{\text{missing}}\\ \left(p^{\text{missing}+p^{l}+p^{b}}\right)^{2}=m_{t}^{2}}\right\}}\left[\left(p^{l}+p^{\text{missing}}\right)^{2}\right]. \tag{2.24}$$

Thus, the explicit expression for the charged Higgs boson transverse mass is as follows:

$$m_{T}^{H}=\sqrt{\left(\sqrt{m_{\text{t}}^{2}+\left(\vec{p}_{T}^{\,l}+\vec{p}_{T}^{\,b}+\vec{p}_{T}^{\,\text{missing}}\right)^{2}}-p_{T}^{b}\right)^{2}-\left(\vec{p}_{T}^{\,l}+\vec{p}_{T}^{\,\text{missing}}\right)^{2}}. \tag{2.25}$$

2.9.5.2 Two Lepton Events

In two lepton $t\bar{t}$ events, the final state includes two leptons and missing energy on both 'sides' of the event, making its full reconstruction more complicated than the single lepton $t\bar{t}$ events. With one t quark decaying to $\bar{b}W$ and the other decaying to bH^+, there are the following size constraints:

$$\begin{aligned}
\left(p^{H^+} + p^b\right)^2 &= m_t^2, \\
\left(p^{l^-} + p^{\bar{\nu}_l}\right)^2 &= m_W^2, \\
\left(p^{l^-} + p^{\bar{\nu}_l} + p^{\bar{b}}\right)^2 &= m_t^2, \\
\left(p^{\bar{\nu}_l}\right)^2 &= 0 \text{ and} \\
\vec{p}_T^{\,H^+} - \vec{p}_T^{\,l^+} + \vec{p}_T^{\,\bar{\nu}_l} &= \vec{p}_T^{\,\text{missing}}.
\end{aligned} \tag{2.26}$$

where l denotes an e, a μ or a τ and p^{H^+} and $p^{\bar{\nu}_l}$ are the unknown quantities in the event. This system of constraints leaves two free parameters over which the charged Higgs boson mass is maximised in order to obtain the *generalised charged Higgs boson transverse mass*. If one of the free parameters is chosen to be the z component of the charged Higgs boson momentum, the generalised charged Higgs boson transverse mass can be determined by performing a maximisation using the result from the single lepton case:

$$m_{T2}^H = \max_{\{\text{constraints (equation 2.26)}\}} \left[m_T^H \left(\vec{p}_T^{\,H^+} \right) \right], \tag{2.27}$$

where

$$m_T^H\left(\vec{p}_T^{\,H^+}\right) = \sqrt{\left(\sqrt{m_t^2 + \left(\vec{p}_T^{\,H^+} + \vec{p}_T^{\,b}\right)^2} - p_T^b\right)^2 - \left(\vec{p}_T^{\,H^+}\right)^2}. \tag{2.28}$$

The maximisation over the remaining parameter is performed numerically after having assigned each of the two b quarks to its corresponding lepton.

The transverse masses m_T^H and m_{T2}^H are larger than the charged Higgs boson mass m_{H^+} and smaller than the t quark mass m_t used in the constraints. Therefore, they can serve as discriminants between t quark decays mediated by a W and t quark decays mediated by a charged Higgs boson, based on their different masses.

Chapter 3

Statistical Methodology

3.1 Introduction

This chapter offers a brief, practical description of the statistical theory used in the $H^+ \to \tau_{lep.} + \nu$ charged Higgs boson search of this thesis. Initially, the concepts of hypotheses (in a statistical sense), statistical tests etc. are discussed. Then, the profile likelihood ratio and modified frequentist confidence level CL_s statistical tools are described. The Bayesian approach to statistics is outlined and, finally, there is a brief description of software used in the statistical and limit setting aspects of the search.

3.2 A Search as a Statistical Test

The general procedure used to search for some new phenomenon in the context of a frequentist statistical test is outlined in this section. The task is to make a statement about how well observed data stands in agreement with given predicted probabil-

ities, i.e., a *hypothesis*. For the purposes of discovering a new signal process, one defines the null hypothesis, H_0, as describing only known processes, designated here as *background*. This hypothesis is tested against the *alternative* hypothesis, H_1, which includes both the background and the sought after signal. In setting limits, the model consisting of the signal *and* background acts as the null hypothesis, H_0, which is tested against the model consisting of *only* the background, H_1. The outcome of a search such as this quantifies the level of agreement of the observed data with a hypothesis H by computing a p value (i.e., a probability), under the assumption of H, of finding data of equal or greater incompatibility with the predictions of H. The hypothesis is regarded as excluded if its p value is below a specified threshold.

In particle physics, the p value is often converted into an equivalent significance, defined such that a variable with a Gaussian distribution found a certain number of standard deviations above its mean has an upper tail probability equal to p. Following from this, it is often useful to describe the sensitivity of an experiment as the expected (median) significance that can be obtained with a measurement under the assumption of various hypotheses. In ATLAS, a 3σ result conventionally is taken as evidence of a possible discovery and a 5σ result conventionally is taken as a discovery. A detailed analysis would involve consideration of the *look elsewhere effect* (LEE) [74]. Essentially, this effect involves the likelihood of seemingly finding something in an entire probed region being greater than the likelihood of seemingly finding something in a subregion selected especially for the signal; there is a type of 'probability boost' arising from searching in many places. The 'boost factor' arising due to the LEE is approximately the ratio of difference between the lower and upper mass points of the entire mass region to the signal width. Depending on the details of the specific

search, this could result easily in a factor of 10–100. In general, as the search range is increased, the p value increases because more possibilities are opened. The 5σ convention was conceived with effects such as the LEE considered: 5σ is rare enough that, even accounting for the LEE, it is probably something significant.

Consider an experiment in which the values of kinematic variables are measured for each selected event and, thus, the resulting data is represented by histograms. A variable x is measured for each event in the signal sample and these values are used to construct a histogram:

$$\vec{n} = (n_1, \ldots, n_N)\,, \tag{3.1}$$

which is simply the set of values for the number of entries in each of the N bins. The expectation value of n_i can be given as

$$E\left[n_i\right] = \mu s_i + b_i, \tag{3.2}$$

where the mean number of entries in the bin of index i from signal and background are given by the following:

$$s_i = s_{\text{tot.}} \int_{\text{bin}_i} f_s\left(x; \vec{\theta_s}\right) dx; \tag{3.3}$$

$$b_i = b_{\text{tot.}} \int_{\text{bin}_i} f_b\left(x; \vec{\theta_b}\right) dx. \tag{3.4}$$

The parameter μ determines the strength of the signal process; $\mu = 0$ corresponds to the background only hypothesis and $\mu = 1$ corresponds to the nominal signal hypothesis. The functions $f_s\left(x;\vec{\theta_s}\right)$ and $f_b\left(x;\vec{\theta_b}\right)$ are the probability density functions (PDFs) of the variable x for the signal events and background events, respectively, with $\vec{\theta_s}$ and $\vec{\theta_b}$ representing parameters that characterise the shapes of the probability density functions. The quantities $s_{tot.}$ and $b_{tot.}$ are the total mean number of events for the signal and the background respectively. All nuisance parameters are denoted as follows:

$$\vec{\theta} = \left(\vec{\theta_s}, \vec{\theta_b}, b_{tot.}\right). \tag{3.5}$$

The signal normalisation, $s_{tot.}$, is fixed to the value predicted by the nominal signal model (as opposed to being an adjustable parameter).

In addition to the measured histogram, subsidiary measurements can be made in order to help constrain the nuisance parameters. For example, a control sample in which mainly background events are expected may be selected. From these events, a histogram of some chosen kinematic variable could be constructed:

$$\vec{m} = (m_1, \ldots, m_M). \tag{3.6}$$

The expectation value of m_i can be given as

$$E\left[m_i\right] = u_i\left(\vec{\theta}\right), \tag{3.7}$$

where u_i are quantities calculable depending on the parameters $\vec{\theta}$. This measurement is constructed often in order to provide information on the background normalisation factor, $b_{tot.}$, and possibly on the signal and background shape parameters.

3.3 Profile Likelihood Ratio

A likelihood ratio test is a statistical test used to compare the fit of two models, one of which (the null model) is a special case of the other (the alternative model). The test is based on the likelihood ratio, which expresses how many times more likely the data are under one model than the other. This likelihood ratio, or equivalently its logarithm form, can then be used to compute a p value. When the logarithm form of the likelihood ratio is used, the statistic is known as a log likelihood ratio test statistic and the probability distribution of this test statistic, assuming that the null model is true, can be approximated using Wilks' theorem [75]. In the case of distinguishing between two models, each of which has no unknown parameters, use of the likelihood ratio test can be justified by the Neyman-Pearson lemma [76, 77], which demonstrates that such a test has the highest power among all competitors.

The likelihood function is the product of Poisson probabilities for all bins:

$$\mathcal{L}\left(\mu, \vec{\theta}\right) = \prod_{j=1}^{N} \frac{\left(\mu s_j + b_j\right)^{n_j}}{n_j!} e^{-(\mu s_j + b_j)} \prod_{k=1}^{M} \frac{u_k^{m_k}}{m_k!} e^{-u_k} \tag{3.8}$$

In order to test a hypothesised value of μ, the *profile likelihood ratio* is considered:

$$\lambda\left(\mu\right) = \frac{\mathcal{L}\left(\mu, \hat{\hat{\vec{\theta}}}\right)}{\mathcal{L}\left(\hat{\mu}, \hat{\vec{\theta}}\right)}. \tag{3.9}$$

$\hat{\hat{\vec{\theta}}}$ is the value of $\vec{\theta}$ for which $\mathcal{L}$ is maximised for the specified μ; i.e., it is the conditional maximum likelihood estimator of $\vec{\theta}$ and, thus, is a function of μ. The denominator is the maximised (unconditional) likelihood function; i.e., $\hat{\mu}$ and $\hat{\vec{\theta}}$ are the maximum likelihood estimators. The presence of the nuisance parameters broadens the profile likelihood as a function of the μ signal process strength parameter relative to the likelihood if their values were fixed. This corresponds to the loss of information about μ arising from the systematic uncertainties.

In the equation for the profile likelihood ratio (equation 3.9), the values for λ can range from 0 to 1, with a value of λ near 1 implying good agreement between the data and the hypothesised value of μ. Thus, it can be convenient to use the statistic

$$t_\mu = -2 \ln \lambda\left(\mu\right) \tag{3.10}$$

as the basis of a statistical test. For this test statistic, increasing values of t_μ correspond to increasing incompatibility between the data and the hypothesised value of

μ. The level of disagreement can be quantified using the p value:

$$p_\mu = \int_{t_{\mu,\,\text{obs.}}}^{\infty} f\left(t_\mu|\mu\right) dt_\mu, \tag{3.11}$$

where $t_{\mu,\,\text{obs.}}$ is the value of the test statistic t_μ observed from the data and $f\left(t_\mu|\mu\right)$ denotes the PDF of t_μ under the assumption of the signal strength parameter μ. In using the test statistic t_μ, a data set may result in a low p value in two distinct ways: the estimated signal strength $\hat{\mu}$ may be found to be greater than the hypothesised value μ or it may be found to be less than μ. Thus, the μ values rejected because their p values are less than a specified threshold α may lie on either side of those values not rejected, i.e., a two sided confidence interval for μ may be obtained.

Using results by Wilks [75] and Wald [78], a paper by Cowan, Cranmer, Gross and Vitells [79] outlines the derivation of a comprehensive set of asymptotic formulae, based on the profile likelihood, for use in searches for new physics. A technique introduced in the paper is the Asimov dataset, which is, in a sense, the most representative dataset of an ensemble. When it is used to evaluate the estimators for all parameters, it provides the true parameter values. Asimov datasets can be used to simplify the estimation of measurement sensitivities and to compute Jeffrey's prior [77].

Likelihood based statistical approaches enable statistical tests in searches for processes that have been predicted but not yet seen, such as the production of Higgs bosons. The statistical significance of an observed signal can be quantified by means of a p value or its equivalent Gaussian significance. Finding both the significance and the expected significance for a data set can involve extensive Monte Carlo calcu-

lations[1]. The approximate methods reported here allow the calculation of both the significance for given data as well as the full sampling distribution of the significance under the hypothesis of different signal models without the requirement of Monte Carlo calculations [2].

3.4 Modified Frequentist Confidence Level CL_s

3.4.1 Significance Level $1 - \mathrm{CL}_b$

The p value under the assumption of a background only hypothesis can be described as follows:

$$p_b = \int_{-\infty}^{q_{\mathrm{obs.}}} f\left(q|b\right) \mathrm{d}q, \tag{3.12}$$

where $f\left(q|b\right)$ is the probability density function for the log likelihood ratio, q, under the assumption of the background only (null) hypothesis. This p value is known as $1 - \mathrm{CL}_b$.

[1] Monte Carlo methods are stochastic techniques, meaning they are based on the use of random numbers and probability statistics to investigate problems. The use of Monte Carlo methods allows for the modelling of physical problems for which more direct models are computationally unfeasible. With Monte Carlo methods, a large system can be sampled in a number of random configurations and the resulting data can be used to describe the system as a whole.

[2] See section 6.7.6 for the methodological application of the profile likelihood.

3.4.2 Discovery Potential $1 - \mathrm{CL}_{s+b}$

The p value under the assumption of a signal and background hypothesis can be described as follows:

$$p_{s+b} = \int_{q_{\mathrm{obs.}}}^{-\infty} f\left(q|s+b\right) \mathrm{d}q, \tag{3.13}$$

where $f\left(q|s+b\right)$ is the probability density function for the log likelihood ratio, q, under the assumption of a signal and background (alternate) hypothesis. This p value is known as $1 - \mathrm{CL}_{s+b}$. This is a standard frequentist confidence limit. For example, with $\mathrm{CL}_{s+b} \leq 0.05$, the signal and background hypothesis is excluded at the 95% confidence level.

3.4.3 Approximate Confidence CL_s

The standard frequentist confidence limit is acceptable in most cases, however, the spurious downward fluctuation of the background is a possibility that could lead to an invalid exclusion of a certain Higgs mass; that is, an exclusion limit may be computed for a mass at which the experiment is not sensitive, simply due to a spurious downward fluctuation in the background. In order to deal with this possibility, CL_s [80, 81] is defined as the ratio of the confidences CL_{s+b} and CL_b:

$$\mathrm{CL}_s \equiv \frac{\mathrm{CL}_{s+b}}{\mathrm{CL}_b} \equiv \frac{p_{s+b}}{1 - p_0}. \tag{3.14}$$

CL_s, the *modified frequentist confidence level*, allows for consideration of the confidence in the signal alone. While a signal can be said to have been excluded with a confidence level equal to $1 - \alpha$ when $CL_s < \alpha$ (for an exclusion at the 95% confidence level), this value should not be thought of as a confidence level; it is a log likelihood ratio test which uses the CL_s value to imply exclusion or the $1 - CL_b$ value to estimate the significance of a possible discovery. Essentially, $1 - CL_{s+b}$ corresponds to discovery potential, CL_{s+b} corresponds to the false exclusion rate, CL_b corresponds to the exclusion potential and $1 - CL_b$ corresponds to the false discovery rate (which corresponds to significance level). Thus, CL_s may be considered as an approximate confidence in the signal only hypothesis. What is generally wanted is the *exact* confidence in the signal hypothesis, but as long as there is background in the experiment this does not exist. If the signal and background hypothesis is well separated from the background hypothesis, then $CL_s \simeq CL_{s+b}$.

3.5 ATLAS Statistical Methods

ATLAS searches, for the most part, investigate some signal in a sample of events dominated by other background physical sources. The events are the output of the detector, filtered by reconstruction algorithms which construct objects such as electrons and jets. Simulations are used to tune calibrations, characterise the event reconstruction and compare the outcome of an experiment with theoretical models.

A typical simulation consists of a few different steps. Initially, the result of the primary particle interaction is simulated using an *event generator*. Usually, only one specific process of interest is considered (e.g., Higgs boson production with a specific

channel). Different Monte Carlo productions are then organised to obtain a variegate set of processes which can be considered either signal or background depending on the analysis. The next step is to simulate the effects of the passage of the produced particles and decay products through the detector. Finally, the detector response is simulated: for each energy deposition into an active material, another Monte Carlo process produces the electronic signal. This is processed in a way which closely follows the design of the front end electronics, obtaining the simulated detector output in the same format as the data coming from the real detector.

Statistical uncertainties can arise from fluctuations in the energy deposition in the active materials and from electronic noise. Systematic uncertainties due to the limited knowledge of the real detector performance and to the details of the offline reconstruction also contribute to the final uncertainty and need to be addressed individually. Theoretical uncertainties in the physical models need also to be accounted for.

In searches for new phenomena, the p value is interpreted as the probability to observe at least as many events as the outcome of our experiment in the hypothesis of no new physics. Most discovery claims in high energy physics are based on p value calculations. A p value threshold of 0.05 corresponds to the significance $\sim 1.64\sigma$. This is used commonly in high energy physics for setting upper limits with a 95% confidence level [82].

3.6 Bayes' Theorem

3.6.1 Some Formulae from Probability Calculus

Let X and Y be propositions or events.

$$p(\sim X) = 1 - p(X). \tag{3.15}$$

The probability of anything other than X happening is equal to the total probability of anything happening less the probability of X happening.

$$p(X \wedge Y) = p(X)\, p(Y|X) = p(Y)\, p(X|Y). \tag{3.16}$$

In general, the probability of X and Y happening is equal to the probability of X happening multiplied by the probability of Y happening, given that X is happening and is also equal to the probability of Y happening multiplied by the probability of X happening, given that Y is happening.

X and Y are said to be independent if $p(X|Y) = p(X)$ and $p(Y|X) = p(Y)$. Thus, if X and Y are independent,

$$p(X \wedge Y) = p(X)\, p(Y) = p(Y)\, p(X) \text{ and} \tag{3.17}$$

$$p(X \vee Y) = p(X) + p(Y) - p(X \wedge Y). \tag{3.18}$$

The probability of either X or Y happening, but not both together, is simply the probability of X happening added to the probability of Y happening less the probability of both X and Y happening together.

$$p\left(X\right) = p\left(X \wedge Y\right) + p\left(X \wedge {\sim}Y\right) = p\left(Y\right) p\left(X|Y\right) + p\left({\sim}Y\right) p\left(X|{\sim}Y\right). \tag{3.19}$$

The probability of X happening is equal to the probability of X happening *with* Y added to the probability of X happening *without* Y. X and Y are said to be disjoint if they cannot both be true at the same time: $p\left(X \wedge Y\right) = 0$, $p\left(X|Y\right) = 0$ and $p\left(X|Y\right) = 0$.

Let $X_1, \ldots, X_N$ be propositions or events. Then, in general, the probability of all X events happening is given by the following formula:

$$p\left(\bigwedge_{i=1}^{n} X_i\right) = p\left(X_1\right) \prod_{i=2}^{n} p\left(x_i | \bigwedge_{j=1}^{i-1} X_j\right), \tag{3.20}$$

where $\bigwedge$ is defined as the *logical and iterative operator* $\bigwedge_{i=1}^{n} x_i = x_1 \wedge \ldots \wedge x_n$. If the operator has no arguments, then the evaluation is *truth*, $\top$, because truth is the identity for the logical and operation. This may be known as the *empty and*. If X_i are independent of each other, then the probability of all X events happening simplifies to

$$p\left(\bigwedge_{i=1}^{n} X_i\right) = \prod_{i=1}^{n} p\left(X_i\right). \tag{3.21}$$

3.6.2 Bayes' Theorem

Following from the law of conjunction (see equation 3.16),

$$p\left(X|Y\right) = p\left(X\right)\frac{p\left(X|Y\right)}{p\left(Y\right)}. \tag{3.22}$$

This formula, known as Bayes' theorem, is useful for reasoning between causes and effects [83]. Considering burglary as a cause of an alarm, it is natural to think in terms of what proportion of burglaries trigger the alarm. That is $p\left(\text{alarm}|\text{burglary}\right)$. This corresponds to the frequentist approach. However, in practical terms, when the alarm goes off, one is interested in knowing the probability of its cause. That is $p\left(\text{burglary}|\text{alarm}\right)$. For this example, Bayes' theorem may be used in the following manner:

$$p\left(\text{burglary}|\text{alarm}\right) = p\left(\text{burglary}\right)\frac{p\left(\text{alarm}|\text{burglary}\right)}{p\left(\text{alarm}\right)}. \tag{3.23}$$

A variant of Bayes' theorem takes into account background knowledge B. It allows reasoning about the probability of a hypothesis H, given evidence E, all in the presence of background knowledge B:

$$p\left(H|E \wedge B\right) = p\left(H|B\right)\frac{p\left(E|E \wedge B\right)}{p\left(E|B\right)}. \tag{3.24}$$

3.6.3 Discovery

Discovery can have many meanings, from discovery of an anticipated entity such as the Higgs boson, to discovery of unanticipated new physics. Bayesian analysis is relevant to both of these types of discovery, but, here, focus is placed on the discovery of anticipated events because it typically reduces to Bayesian hypothesis testing. The Bayesian approach to discovery is essentially the Bayesian approach to hypothesis testing. A major difficulty in the implementation of Bayesian hypothesis testing is the choice of the needed prior distributions of unknown parameters.

Discovery is taken to mean finding and verifying a rare signal against a noisy background. There are many variants and formulation is critical. Key elements include:

- the reference frame in which signals are defined,
- the statistical properties of the noise,
- the temporal sequence of data collection,
- the statistical character of the signal,
- the frequency of occurrence of signals and
- the multistage character of the search process.

The reference framework may be an ordered set of histogram bins, for example. Typical noise processes are either Gaussian processes or Poisson processes and it can be important to allow for errors in estimating their properties. Observation may be in

one step or by the gradual accretion of frequencies over time. The signal may be a single blip or a set of occurrences at nearby points in the reference frame.

Concerning the presence of signal, there are two main situations to consider: there may be no signal present or just one. In the second situation, there are likely to be a limited nonzero number of signals present and the challenge is to find as many of them as possible with few false results. The first situation generally is more appropriate for current issues in particle physics.

3.7 Software

3.7.1 ROOT

ROOT [84] is an object oriented data analysis framework aimed at solving data analysis challenges in high energy physics. While *ROOT* is simply a name, a possible acronym for the system could be *"Rapid Object-Oriented Technology"* [85]. ROOT was developed in the context of the NA49 experiment at CERN. NA49 generated data of approximately 10 TB per run. This rate of data provided a test environment for the development of ROOT, as the next generation of data analysis. ROOT features *CINT*, a C++ interpreter.

3.7.2 RooFit and RooStats

The RooFit [86] library provides a toolkit for modelling the expected distribution of events in a physics analysis. Models can be used to perform unbinned maximum likelihood fits, produce plots and generate Monte Carlo samples for various studies. The core functionality of RooFit is to enable the modelling of 'event data' distributions, in which each event is a discrete occurrence in time and has one or more measured observables associated with it. Experiments of this nature result in datasets obeying Poisson (or binomial) statistics. The natural modelling language for such distributions is probability density functions that describe the probability density of the distribution of observables x in terms of the function parameter p.

In RooFit, every variable, data point, function and PDF is represented in a C++ object. So, for example, in constructing a RooFit model, the mathematical components of the model map to separate C++ objects. Objects are classified by the data or function type that they represent, not by their respective role in a particular setup. All objects are self documenting.

The full complexity of an individual channel's respective likelihood functions are packaged using RooFit/RooStats [87, 88] *workspaces*. A combined probability model is formed by identifying nuisance parameters associated with common systematic effects. In order to perform a combined search, the results from each of the search channels are brought together and form one overall statistical model of the data. One of the most difficult aspects of this process is the fact that a single source of systematic uncertainty in how a detector works can have an effect on multiple search channels. The treatment of these correlated systematic uncertainties requires some

coördination between the individual search channels. The statistical tools of RooFit and RooStats, in particular, the workspace, are designed to handle this type of complexity. Specifically, accounting simultaneously for systematic effects on various different components is possible using *HistFactory*, a tool used for a coherent treatment of systematics. HistFactory and the workspace are standard statistical software tools in ATLAS.

Chapter 4

Large Hadron Collider

4.1 Large Hadron Collider

The Large Hadron Collider (LHC) is an experimental facility at the European Organisation for Nuclear Research (CERN) near Geneva. The CERN accelerator complex is depicted in figure 4.1.

The LHC is a synchotron particle accelerator built in a $\sim$ 27 km circular tunnel as deep as 175 m below the surface. It produces two counter rotating beams of protons which collide at four points around its circumference. The current centre of mass energy is 8 TeV (an energy of 4 TeV per beam), with future plans for an increase to 14 TeV. The centre of mass energy produced during collisions facilitates the production of heavy particles while the luminosity, a measure of the intensity of the beams, enables a large number of interesting interactions to take place in laboratory conditions. This high energy, high luminosity (with respect to previous experiments) environment will enable the exploration of important questions concerning the origin

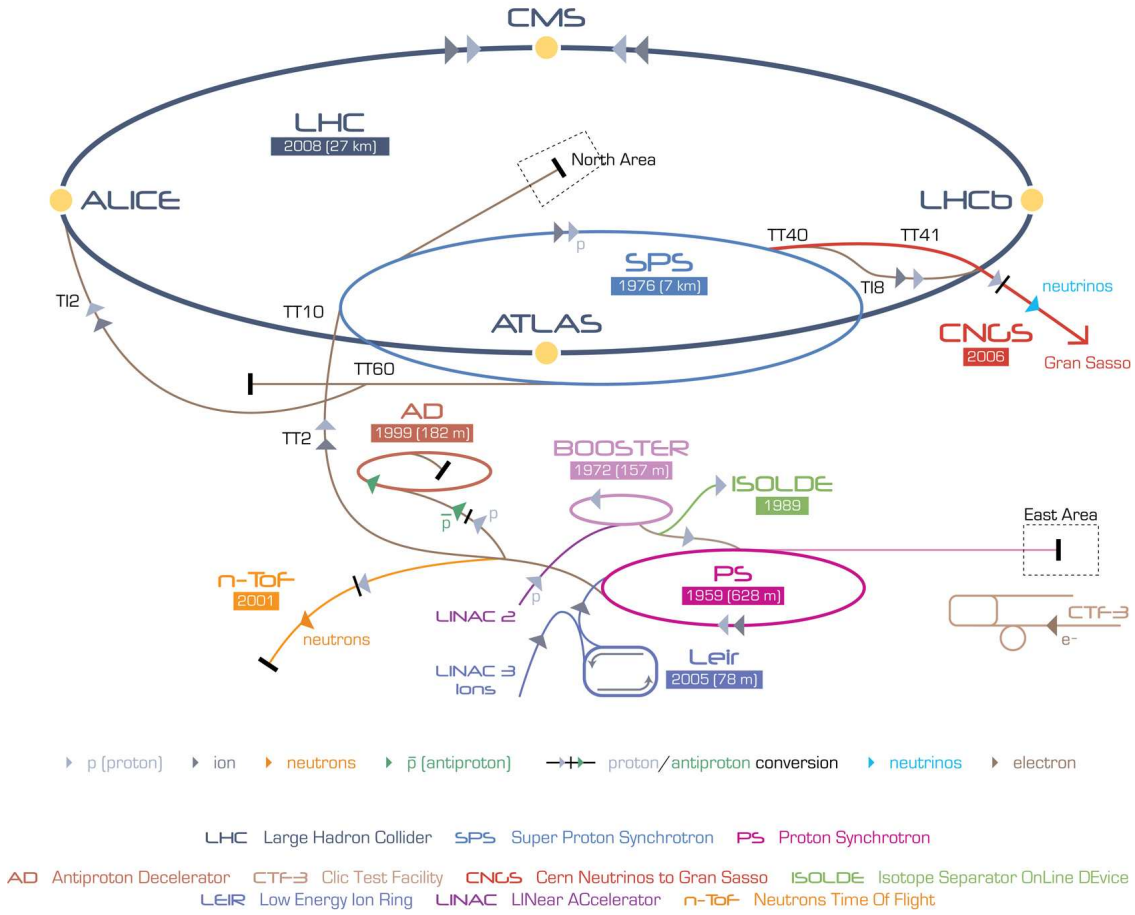

Figure 4.1: CERN accelerator complex

of mass for gauge bosons, the measured predominance of matter over antimatter and more detailed descriptions of mass particles and their interactions.

The LHC utilises many preexisting CERN facilities, including the full range of CERN proton machines serving as the injector chain and the ~ 27 km tunnel previously used by the Large Electron Positron (LEP) collider.

4.1.1 General Description of LHC operation

The journey of the proton particles in the LHC begins with the Linac 2 linear accelerator, which accelerates protons from the proton source to an energy of 50 MeV. The protons then proceed to the Proton Synchrotron Booster (PSB), the first and smallest circular proton accelerator in the accelerator chain of the LHC. The PSB accelerates the protons from 50 MeV to 1.4 GeV. Protons are injected then into the Proton Synchotron (PS), which is the first major particle accelerator at CERN (originally built as a 28 GeV proton accelerator). The PS accelerates the protons to 25 GeV, before the protons are injected into the Super Proton Synchotron (SPS). The SPS has been used to accelerate protons and antiprotons, electrons and positrons (for use in the LEP) and heavy ions. As a proton-antiproton collider, it supplied accelerated particles for the UA1 and UA2 experiments which resulted in the discovery of the mediator bosons of the weak interaction, the W and Z bosons. The SPS is used in the CERN Neutrinos to Gran Sasso (CNGS) experiment to produce a neutrino stream for the Gran Sasso laboratory, where neutrinos are detected promptly by the detector of the Oscillation Project with Emulsion Racking Apparatus (OPERA) experiment. The SPS is the final injector for the LHC (as it was for the LEP) and accelerates the

protons to 450 GeV. Once inside the LHC, the protons are guided and accelerated by the LHC dipole magnets and radio frequency (RF) cavities to energies of several TeV. The LHC beam pipe is stored in a cryostat, at a temperature of 1.9 K, facilitating the function of the superconducting magnets to direct the proton beams around the ring of the LHC. The RF cavities, which are also superconducting, ensure that the $\sim 10^{11}$ protons in each bunch in the beam occur every 50 ns[1]. At the LHC full design luminosity, there should be twenty-three interactions in every bunch crossing. The effect of multiple collisions in a crossing is known as pileup and adds complexity to analyses. A cross section of the LHC beam pipe is shown in figure 4.2, while a three dimensional representation of a cryodipole is shown in figure 4.3

4.1.2 Luminosity

In an experiment, the number of events observed in a certain time is given by the product of the cross section of the process under observation (the effective area which governs the probability of some scattering or absorption event) and the instantaneous luminosity;

$$N_{events} = L\sigma_{event}, \tag{4.1}$$

where σ_{event} is the cross section and L is the luminosity. Luminosity is a measurement of the number of collisions that can be produced in a detector per centimetre squared per second. The luminosity can be obtained semiqualitatively from

[1]It is planned for the bunch spacing to decrease to 25 ns in the future.

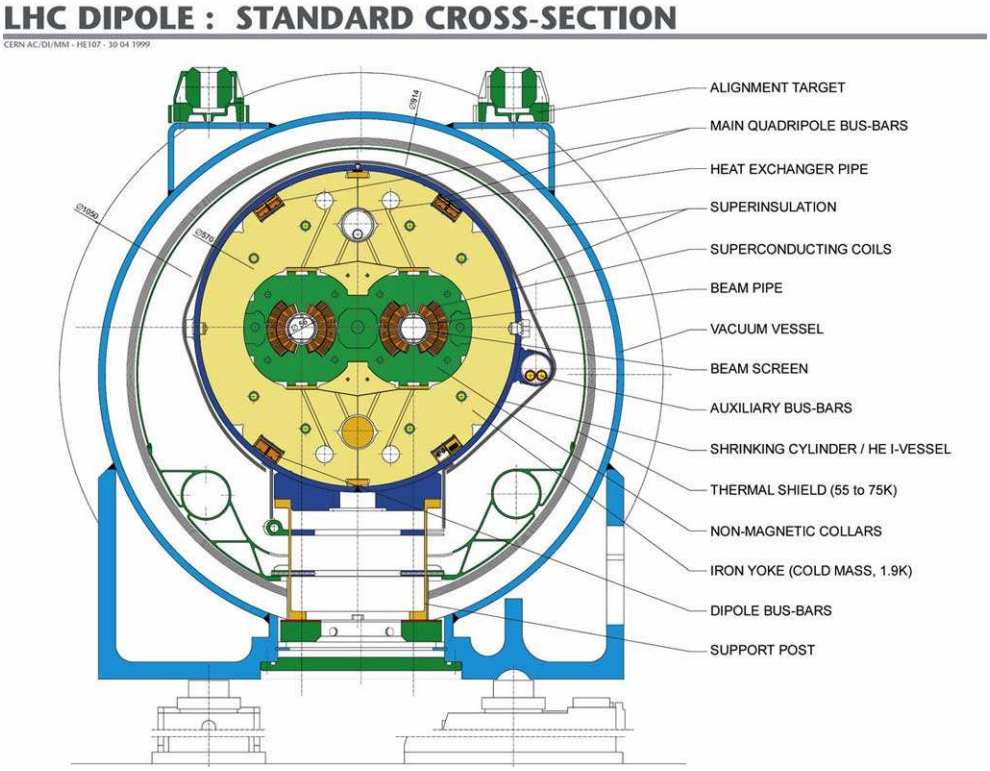

Figure 4.2: Cross section of LHC superconducting cryodipole

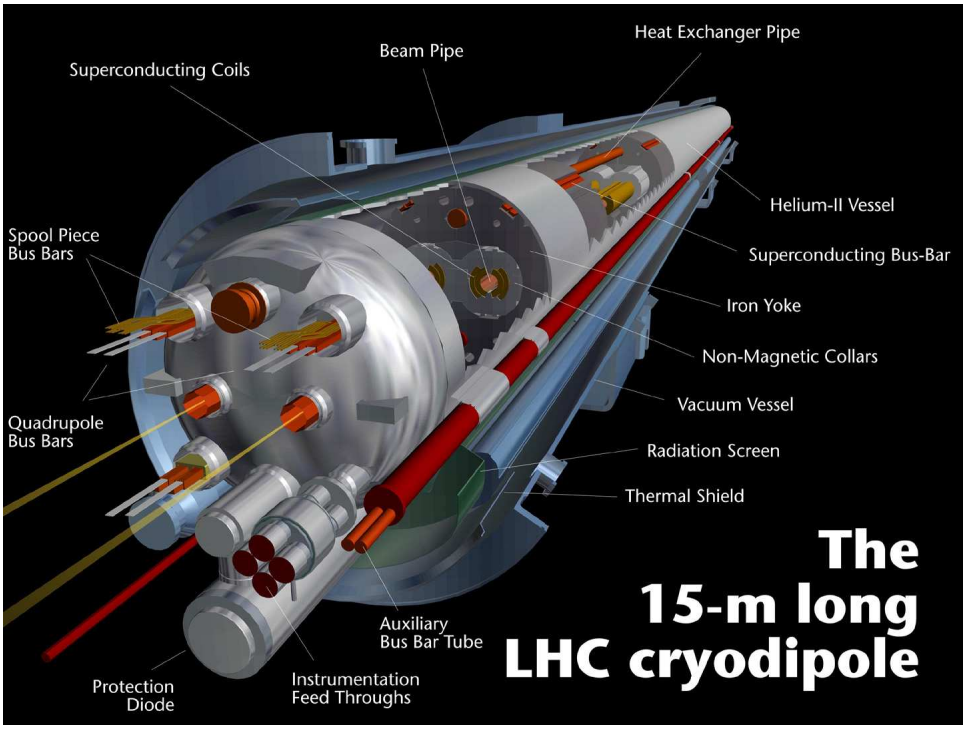

Figure 4.3: Three dimensional representation of LHC superconducting cryodipole

- the number of protons (N^2, because each particle in a bunch may collide with any particle in the opposing bunch),
- the time between bunches, t, and
- the section effective of collision, $s_{eff.}$, that depends on the cross section of the bunch (effective because the profile of the beam does not have a sharp edge).

The section effective of collision can be given as follows:

$$s_{eff.} = 4\pi\sigma^2, \tag{4.2}$$

where σ is the transverse size of the bunch at the interaction point. Consideration can be given also to the geometric luminosity reduction factor, F, due to the crossing angle at the interaction point, however, for the LHC, this factor is very near unity, so

$$L \simeq \frac{N^2}{ts_{eff.}} \tag{4.3}$$

The beam size can be expressed in terms of two quantities, one termed the transverse emittance, ϵ, and the other termed the amplitude function, β.

The transverse emittance is a beam quality parameter reflecting the process of bunch preparation, extending all through the injector chain to the source of hadrons. A low emittance particle beam is a beam in which the particles are confined to a small distance and have similar momenta. In a colliding beam accelerator, keeping the

emittance small, keeps the likelihood of particle interactions high, resulting in higher luminosity. Emittance could be thought of as the smallest aperture a beam could fit through and also thought of as a measurement of the parallelism of a beam. Emittance is measured in units of length, but is considered usually as a length multiplied by an angle. The emittance measured in the spatial dimension parallel to the motion of a particle is called the longitudinal emittance while the emittance measured in perpendicular dimensions are referred to as the transverse emittances. The emittance changes as a function of beam momentum; increasing the beam energy reduces the emittance.

The amplitude function is determined by the accelerator magnet configuration (the quadrupole magnet arrangement) and the powering. Expressed in terms of the cross sectional size of the bunch, σ, and the transverse emittance, the amplitude function is

$$\beta = \frac{\pi\sigma^2}{\epsilon} \tag{4.4}$$

So, the amplitude function is approximately the width of the beam squared divided by the emittance. Of particular significance is the value of the amplitude function at the interaction point, β^*. In order to increase the number of collisions at the interaction point, it is desirable to minimise the value of the amplitude function at the interaction point.

Using the bunch crossing frequency, f, the luminosity can be expressed as

$$L \simeq \frac{fN^2}{4\pi\sigma^2} \tag{4.5}$$

and considering different numbers of protons per crossing bunches, and x and y components of σ separately, it can be expressed as

$$L \simeq \frac{fN_1N_2}{4\pi\sigma_x\sigma_y}. \tag{4.6}$$

From equations 4.4 and 4.5, the luminosity can be expressed in terms of the emittance and amplitude function in the following way:

$$L \simeq \frac{fN^2}{4\epsilon\beta^*} \tag{4.7}$$

There can be further considerations of the luminosity (involving, for example, the relativistic Lorentz factor γ), but, essentially, in order to achieve high luminosity, high population bunches of low emittance should be made to collide at high frequency at locations where the beam optics provides the the lowest possible values of the amplitude function. The nominal luminosity of the LHC is 1×10^{34} cm^{2}s^{-1}. A sample of LHC nominal beam parameters is given in table 4.1.

Table 4.1: LHC nominal beam parameters

parameter	value
LHC circumference	26.66 km
beam energy	7 TeV
dipole magnetic field strength	8.33 T
dipole magnet temperature	1.9 K
particles per bunch	1.15×10^{11}
bunches per beam	2808
bunch crossing frequency	40 MHz
bunch length (σ_z)	7.5 cm
bunch width (σ_x)	15.9 μm
luminosity	1×10^{34} cm^{-2}s^{-1}

The integrated luminosity is a number used to determine the total luminosity (or, equivalently, the number of events) detected over a certain time:

$$\mathcal{L} = \int L.dt. \tag{4.8}$$

4.1.3 LHC Experiments

Four main experiments are located around the ring of the LHC: A Large Toroidal LHC Apparatus (ATLAS) and the Compact Muon Solenoid (CMS) are general purpose detectors, A Large Ion Collider Experiment (ALICE) is a heavy ion detector designed to exploit the lead-lead runs of the LHC and the Large Hadron Collider Beauty experiment (LHCb) is an experiment designed to investigate CP violation using b quarks.

4.1.3.1 A Large Ion Collider Experiment (ALICE)

ALICE is an experiment designed to study heavy ion collisions at the LHC. Periodically, the LHC accelerates and collides lead ions. The main aim of the ALICE Collaboration is to study the quark-gluon plasma (a state of matter consisting of asymptotically free quarks and gluons) produced in these collisions, in effect, studying conditions similar to those before the Hadron epoch in the early universe.

4.1.3.2 A Large Toroidal LHC Apparatus (ATLAS)

ATLAS is described in detail in chapter 5.

4.1.3.3 Compact Muon Solenoid (CMS)

The CMS is a general purpose detector build to complement and compete with ATLAS. Some of the main goals include exploration of physics at the TeV scale, discovery or exclusion of Higgs bosons and the search for evidence of physics beyond the standard model, such as supersymmetry and extra dimensions. The CMS detector electromagnetic calorimeter is made of lead tungstate crystals which are ideal for high precision measurements in the $H \to \gamma\gamma$ decay channel.

4.1.3.4 Large Hadron Collider Beauty (LHCb)

LHCb is a layered detector, built with subdetectors stacked behind one another. Some of the main goals of the LHCb Collaboration are the study of CP violation (which is possibly the primary cause of the matter-antimatter asymmetry observed in the universe) and the study of rare decays in the b and c sector.

Chapter 5

A Large Toroidal LHC Apparatus

5.1 ATLAS

5.1.1 General Description of ATLAS Operation

ATLAS [89, 90] (depicted in figure 5.1) is a general purpose detector designed to exploit the full potential of the LHC proton-proton collision programme. Some of the unexplored aspects of the Standard Model within the scope of ATLAS are the mechanism of spontaneous symmetry breaking (which manifests Higgs bosons), the decay modes of the t quark and precise determination of its mass and CP violation, which may be observable in many decays involving the b quark. Many models beyond the standard model (BSM) are open for study using data from ATLAS, including supersymmetry, extra dimensions, quantum gravity, technicolour, little Higgs, no Higgs, grand unified theory, hidden valleys, leptoquarks, compositeness, heavy neutrino, and fourth generation particle models.

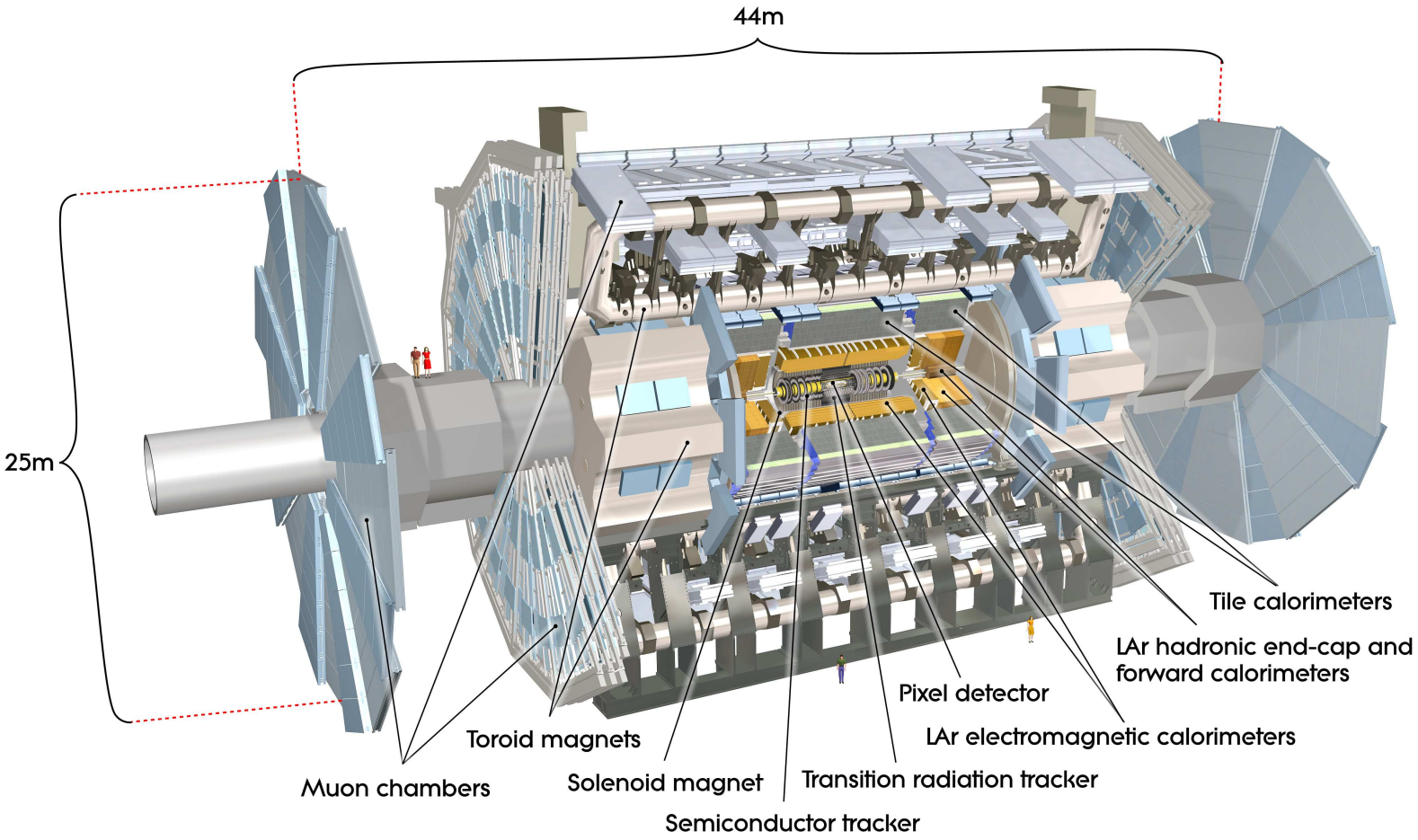

Figure 5.1: ATLAS detector

ATLAS is also designed to probe for the more general framework of *supersymmetry*. Two predictions of supersymmtery are

- the existence of at least five different Higgs bosons, often within the mass range accessible to ATLAS and
- a large number of new particles produced at a mass scale that ATLAS can often establish and measure with high precision.

The discovery of the W^+, W^- and Z^0 particles of the electroweak interactions was a large advancement in the description of fundamental interactions. ATLAS is capable of discovering and measuring particles with similar properties but with masses up to ~ 50 times greater than those of the W^+, W^- and Z^0 particles.

ATLAS is designed for a large discovery potential and for precision measurements [90]. An experiment with these ambitions should detect clean signals and perform accurate measurements of

- charged leptons,
- largely hidden particles[1],
- hadronic jets,
- b quarks and
- photons.

[1]These largely hidden particles, such as neutrinos, may be detected through missing energy measurements.

In addition, ATLAS should provide reconstruction of complete final states, such as the decay products of B hadrons at low luminosity. The general design concept to achieve these goals includes three main detector systems: a *tracker*, a *calorimeter* and a *muon spectrometer*.

- The *tracker* consists of semiconductor pixel and strip detectors for high accuracy measurements of charged particle trajectories, followed by a straw tube detector producing images of events and independent identification of electrons. A thin superconducting solenoid coil provides a 2 T magnetic field for the tracker.

- The *calorimeter* consists of an electromagnetic calorimeter in liquid argon technology (for high resolution, calibration precision and stability), followed by a hadronic calorimeter consisting of steel with scintillating tiles.

- The high precision *muon spectrometer* surrounds the calorimeter. A superconducting air core toroidal magnet system provides the magnetic field for the muon spectrometer.

All detection systems of ATLAS have large solid angle coverage in order to optimise the efficiency for detection of low rate signals from multiparticle decays.

The initial flow of information from the detectors is reduced by a dedicated selection system, the *trigger*. It is based on hierarchical decision making, where the lowest level is based on coarse calorimeter and muon spectrometer information and higher levels use data from the full experimental apparatus. A *data acquisition system* merges the information from the different systems and stores it for further processing and analysis. *Software* is used to reconstruct stored detector signals in order to access the physical properties of detected particles. It also simulates ATLAS in detail

in order to correct for small distortions in measurements induced by the apparatus and to estimate the expected background levels.

The detector systems of ATLAS are controlled by the Detector Control System (DCS) [91]. By monitoring detector hardware, it is capable of flagging unusual behaviour in ATLAS subsystems and of applying corrective measures in some instances. The Detector Control System also handles communications between the LHC, CERN technology services, the magnet systems of ATLAS and the detector safety system.

5.1.2 ATLAS Detector

5.1.2.1 ATLAS Coördinate System

The origin of the coördinate system is defined as the centre of the detector at the nominal interaction point. The z axis is oriented parallel to the beam line with the positive sense in the anticlockwise direction. The positive sense of the x axis points from the origin to the centre of the LHC accelerator ring and the positive sense of the y axis points upwards (perpendicular to the x and z axes). The detector has an approximate cylindrical geometry, most frequently described using the (R, ϕ, z) coördinates. The polar angle θ is defined as the angle measured from the beam axis in the xz plane and the azimuthal angle ϕ is defined as the angle measured in the xy plane around the z axis (clockwise when viewing in the positive sense of the z axis). The polar angle θ is used in the Lorentz invariant measure of position in the detector known as *pseudorapidity*, η.

Rapidity is defined relative to a beam axis as

$$\varphi = \frac{1}{2} \ln \frac{E + p_z c}{E - p_z c}, \tag{5.1}$$

where E is energy, c is the maximum speed in special relativity and p_z is the component of momentum along the beam axis. Rapidity, in the context of special relativity, is essentially a hyperbolic angle that differentiates a moving frame of reference from a fixed frame of reference associated with distance and time coördinates.

For a particle with a speed close to c, the rapidity is approximated by the pseudorapidity, η, which is defined as

$$\eta = \ln \tan \left(\frac{\theta}{2} \right), \tag{5.2}$$

where θ is the angle between the particle momentum and the beam axis.

Generally, the transverse energy E_T, momentum p_T and missing transverse energy $\not{E}_T$ are defined in the xy plane. Often it is useful to consider the distance between objects in the detector in the $\eta\phi$ plane. This distance is defined as

$$\Delta R = \sqrt{\Delta\eta^2 + \Delta\phi^2}, \tag{5.3}$$

where $\Delta\eta$ is the difference in pseudorapidity and $\Delta\phi$ is the difference in azimuthal angles of two objects under consideration.

5.1.2.2 Inner Detector

The Inner Detector (ID) of ATLAS (shown in figure 5.2) begins a few centimetres from the beam axis and extends to a radius of 1.15 m, providing full tracking over a region of $|\eta| < 2.5$. It has a length of 7 m and is contained within a magnetic field of strength 2 T. It is composed of three mechanically separate components, a barrel section that occupies ± 80 cm along the beam axis and two endcaps. In the barrel region, the high precision detectors are mounted on concentric layers around the beam axis.

The Inner Detector consists of three distinct subsystems (shown in figure 5.3), together designed to perform tracking. Specifically, precision measurements of particle momentum above 0.5 GeV for charged tracks between the beam pipe and the electromagnetic calorimeter are provided. Secondary vertex identification using reconstructed tracks and information on impact parameters can be used to indicate the presence of short lived particles such as τ leptons and b quarks.

Interactions at 14 TeV would require excellent pattern recognition of ionising particle trails; high granularity is required this close to the beam pipe as this is where track density is greatest. The Pixel Detector (PD) and Semiconductor Tracker (SCT) are precision tracking detectors designed for this purpose. They are arranged in concentric cylinders around the beam axis in the barrel region of the detector. In the endcaps, they are arranged in discs perpendicular to the beam axis (which can be seen in figure 5.2).

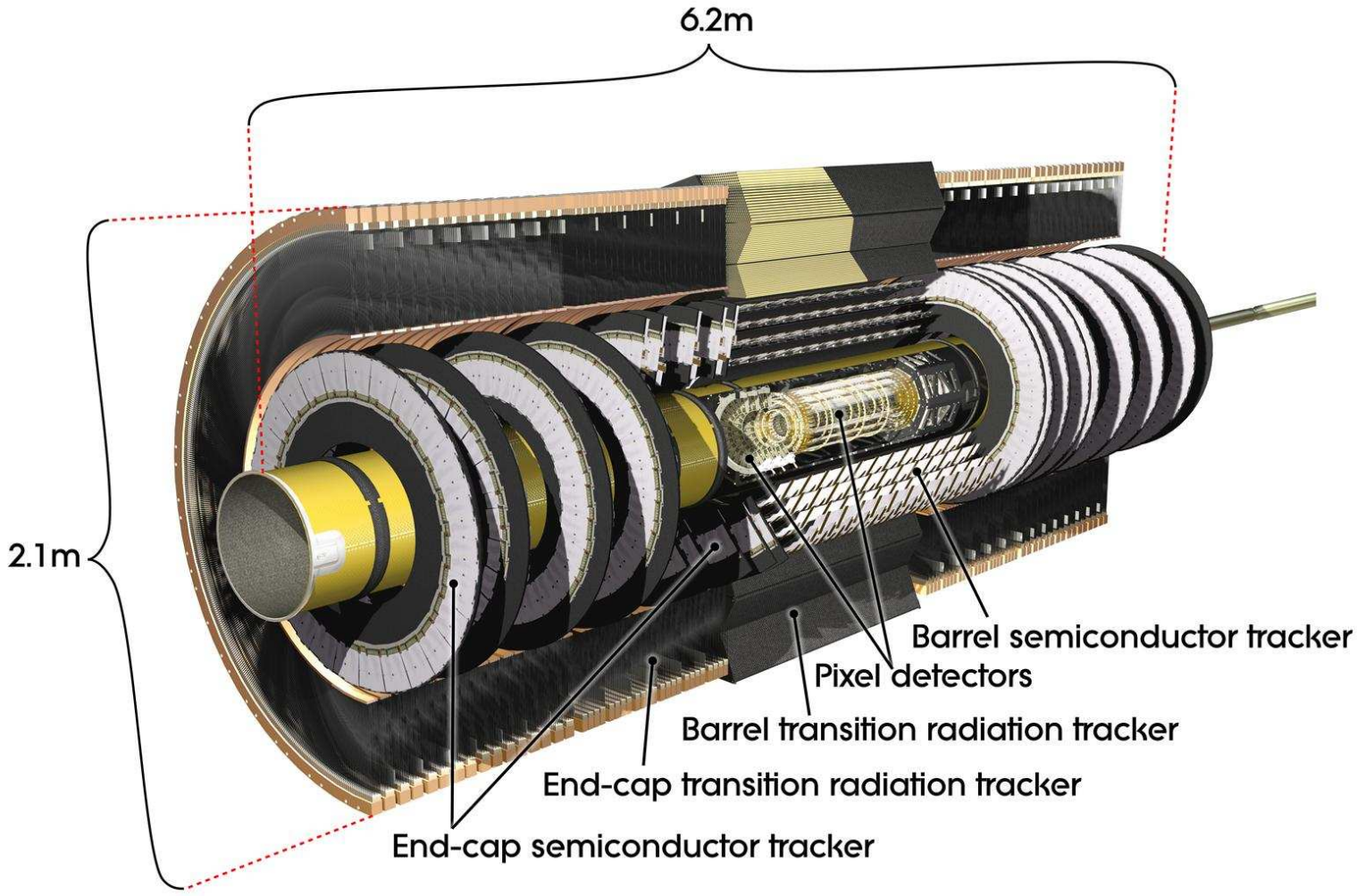

Figure 5.2: ATLAS Inner Detector

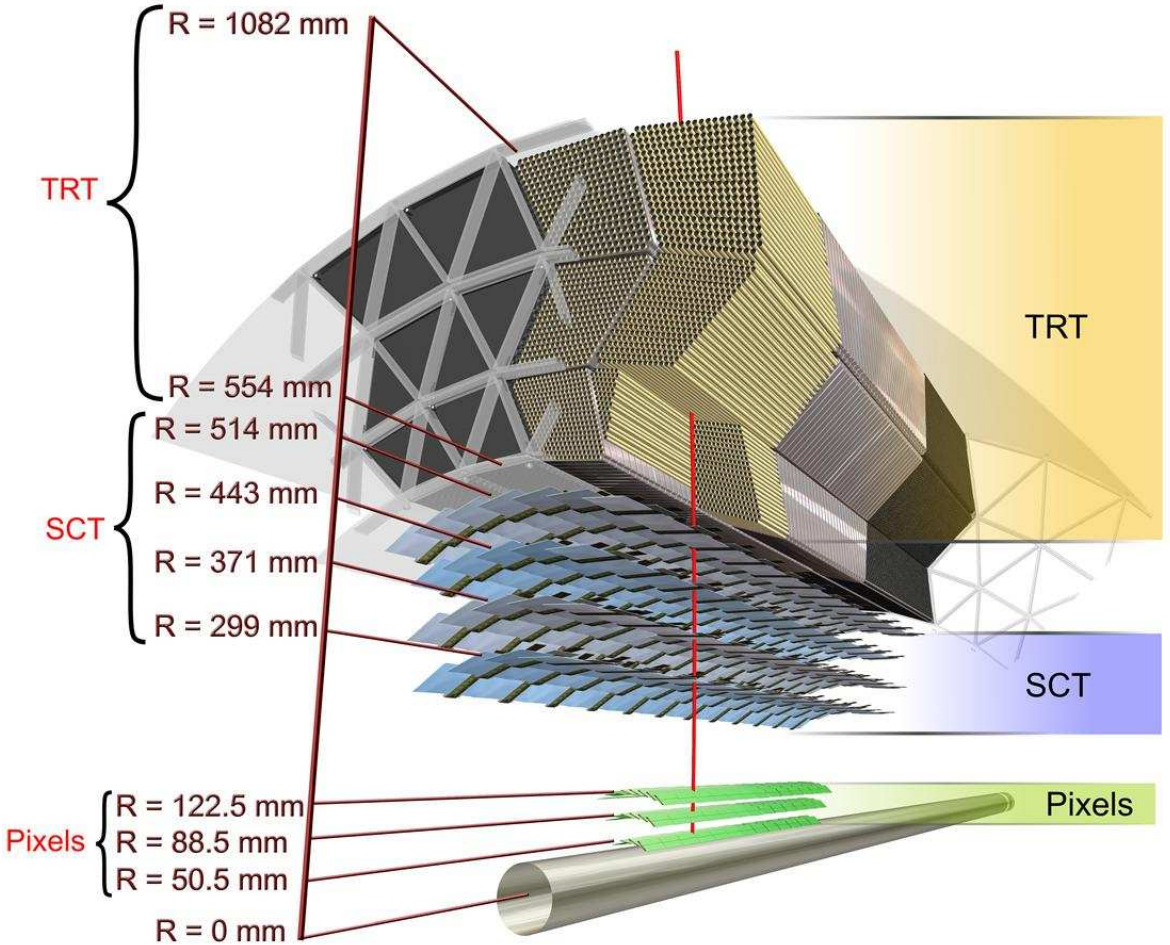

Figure 5.3: Cross section of ATLAS Inner Detector

5.1.2.3 Pixel Detector

The Pixel Detector is the innermost part of the inner detector and provides precise tracking close to the interaction point. Each track transits approximately three pixel layers, segmented in $R-\phi$ and z space. This provides three points in space for reconstruction of the track. The first layer of the Pixel Detector is the vertexing layer, which serves to resolve the secondary vertices of short lived particles.

5.1.2.4 Semiconductor Tracker

The Semiconductor Tracker is the middle component of the Inner Detector and is similar in concept and function to the Pixel Detector but with silicon microstrips instead of silicon pixels. The Semiconductor Tracker is critical for providing basic tracking in the plane perpendicular to the beam axis.

5.1.2.5 Transition Radiation Tracker

The Transition Radiation Tracker (TRT) is the outermost component of the Inner Detector and is a combination of a straw tracker and a transition radiation detector. The detecting elements are drift tubes (straw tube detectors). Straw tube detectors are intrinsically radiation hard and can operate at very high rates due to their small diameter and the isolation of the sense wires within individual gas volumes. The Transition Radiation Tracker covers naturally a larger volume than the Pixel Detector and the Semiconductor Tracker and is capable of detecting transition radiation. Transition radiation is emitted when particles traverse the boundary between media with different dielectric properties. Each straw is filled with a gas that can become

ionised when a charged particle transits it. The probability of a photon of transition radiation being emitted at a particular boundary is small so the straw tube detectors are surrounded by materials designed to contain many such transitions. Since the quantity of transition radiation is greatest for highly relativistic particles and particles of a particular energy have a greater speed the less massive they are, particle paths with many strong signals can be identified as belonging to the lightest observed charged particles, electrons. Basically, the radiated energy increases with the Lorentz factor of the particle rather than the velocity. Particles with a sufficiently high Lorentz factor, such as electrons, produce high threshold hits with reasonable efficiency, thereby providing a high electron identification efficiency.

5.1.2.6 Calorimetry

While tracking detectors are designed to measure position while minimising the effect this measurement has on the particle, calorimeters are designed to measure the energy of the incident particle through total absorption. Using alternating layers of material and detectors, particles traversing a calorimeter create showers and deposit energy which can be used in measurement.

When a high energy electron or photon is incident upon matter, predominantly it interacts through pair production and bremsstrahlung, producing a cascade of secondary electrons and photons. As the shower develops, the number of secondary particles increases and the average energy decreases. Such showers are characterised longitudinally by the radiation length X_0 and have a narrow transverse profile.

High energy hadrons interact predominantly through a succession of inelastic hadron-nucleus collisions resulting in the production of secondary hadrons. Such

showers have a lateral spread and nuclear interaction length λ that is approximately an order of magnitude greater than the radiation length X_0, depending on the material.

Information such as the width of the shower and its depth in the detector is used to determine whether the incident object is a jet or a lepton. To aid in this determination, the calorimetry in ATLAS is accomplished using two main calorimetry systems, the Electromagnetic Calorimeter (EMCAL) and the Hadronic Calorimeter (HCAL). See figure 5.4 for a depiction of the calorimetry systems of ATLAS.

Together, the Electromagnetic Calorimeter and the Hadronic Calorimeter cover out to $|\eta| \leq 4.9$.

5.1.2.7 Electromagnetic Calorimeter

The Electromagnetic Calorimeter is a high granularity sampling calorimeter covering out to $|\eta| \leq 2.5$. It consists of alternating layers of lead, for production of showers, and liquid argon, for particle detection. These layers are arranged in an accordion geometry (see figure 5.5), providing continuous azimuthal (ϕ) coverage with minimal density variations.

Essentially, the Electromagnetic Calorimeter absorbs energy from particles that interact electromagnetically, which include charged particles and photons.

5.1.2.8 Hadronic Calorimeter

The barrel region of the Hadronic Calorimeter (often referred to as the Tile Calorimeter) consists of steel with scintillating tiles that sample the energy deposited. The Hadronic Endcap Calorimeter (HEC) consists of liquid argon and copper.

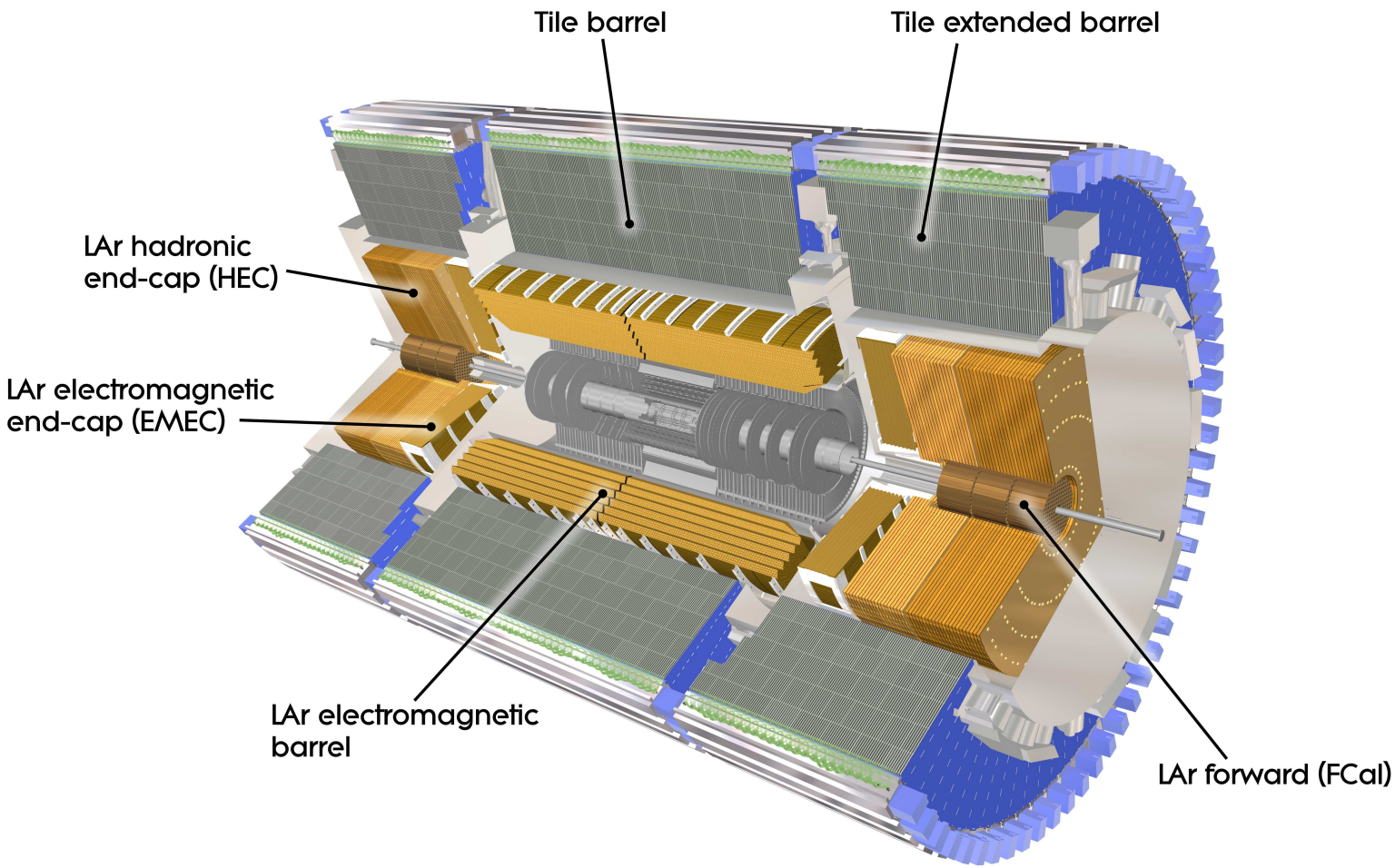

Figure 5.4: Calorimetry in ATLAS

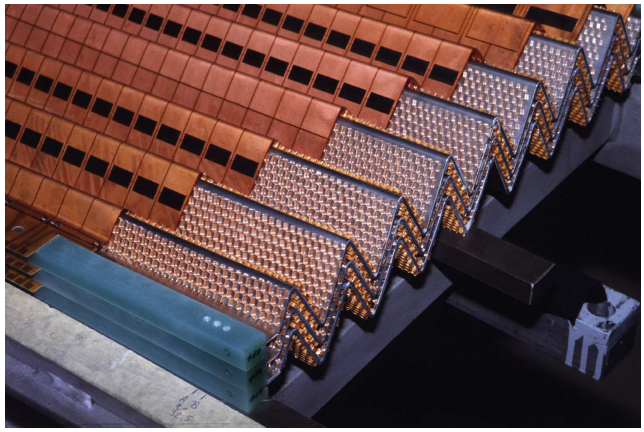

Figure 5.5: ATLAS liquid argon Electromagnetic Calorimeter

Essentially, the Hadronic Calorimeter absorbs energy from particles that pass through the Electromagnetic Calorimeter and interact strongly. These particles are mostly hadrons.

5.1.2.9 Muon Spectrometer

With no strong interactions and large mass, muons lose energy primarily in ionisation. With minimal energy loss, they pass through the calorimeters to the Muon Spectrometer (shown in figure 5.6) for identification and momentum measurement.

The paths of muons in the detector are deflected in the magnetic field of the superconducting air core toroid magnets and detected in the muon chambers. In the barrel region of the muon detectors, the muon chambers are arranged in three cylindrical layers around the beam axis, out to $|\eta| \leq 1.4$. The deflection in the barrel region of the muon detector is provided by the barrel toroid. In the endcap region of the muon detectors, in the range $1.4 \leq |\eta| \leq 2.7$, the deflection is provided by two smaller magnets housed in the barrel toroid cryostat, aligned with the central

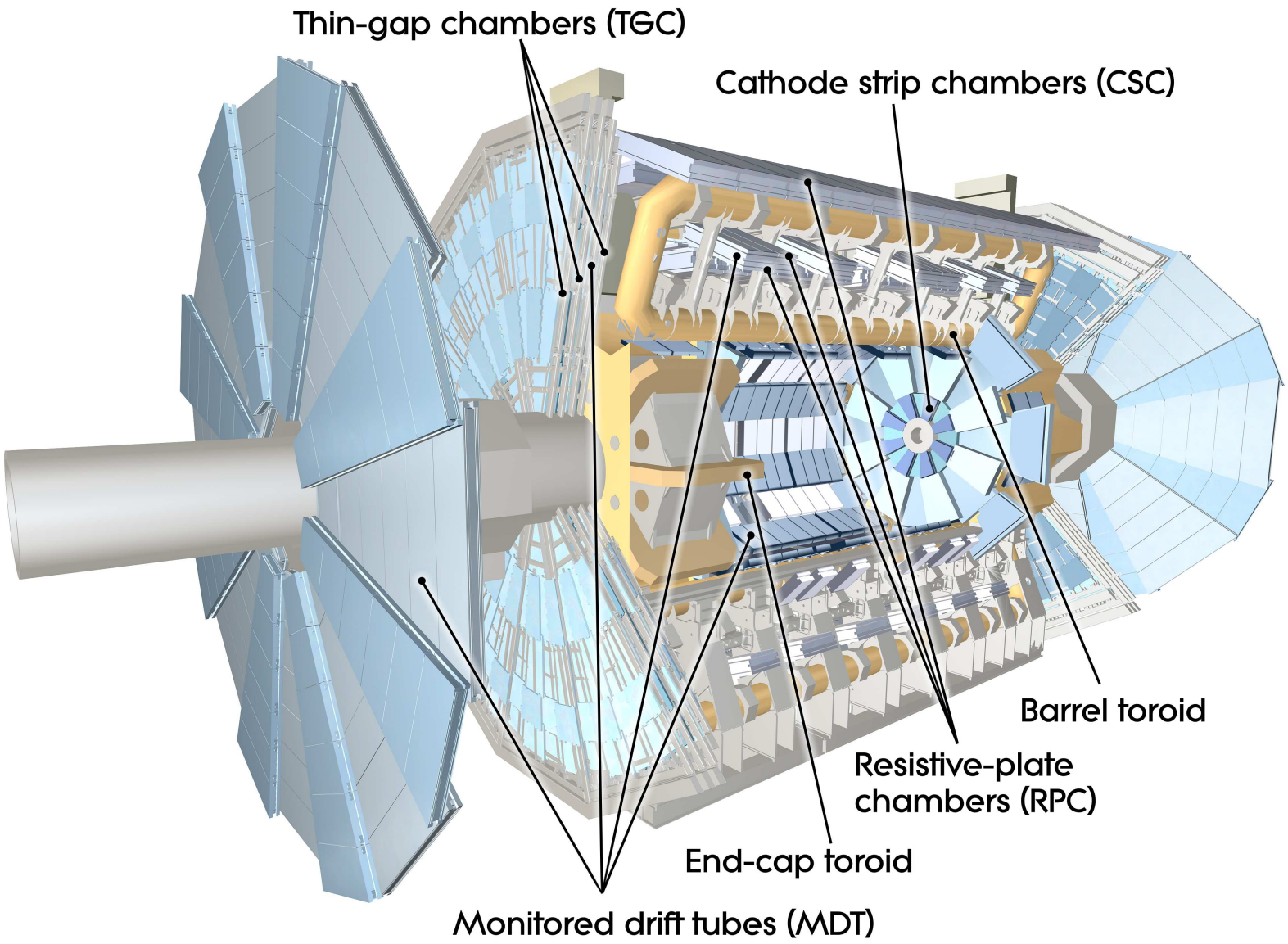

Figure 5.6: Muon Spectrometer

solenoid. The chambers in the endcap region of the muon detectors are perpendicular to the beam axis, also arranged in three layers.

The Muon Spectrometer is composed of two types of muon detector, the Monitored Drift Chambers (MDTs) and the Cathode Strip Chambers (CSCs). The Monitored Drift Chambers provide coverage over most of the pseudorapidity range of the muon detectors and provide precision measurement of track coördinates from the mechanically isolated sense wires in the detector. The Cathode Strip Chambers provide measurement of the pseudorapidity of the muons in the first layer of the muon spectrometer.

5.1.2.10 Magnet System

ATLAS uses two large superconducting magnet systems to deflect charged particles for the purpose of momentum measurement. Deflection is described by the Lorentz force which is proportional to velocity. The particles from LHC collisions will be travelling at close to c generally and, thus, the Lorentz force imparted on particles of different momenta approximately is uniform. Hence, particles with high momentum curve little and particles with low momentum curve significantly. The curvature of the deflection can be measured and the particle momentum can be determined from this curvature.

The inner solenoid produces a magnetic field of strength 2 T surrounding the Inner Detector. The outer toroidal magnetic field is produced by eight air core superconducting barrel loops and two endcaps, all located outside the calorimeters and within the muon system.

5.1.2.11 Forward Detectors

Three additional detectors are located in the very forward region of ATLAS, far from the interaction point, in the LHC tunnel.

Luminosity measurement using Cherenkov Integrating Detector (LUCID), located at ± 17 m from the interaction point (one detector in each endcap region of ATLAS), measures inelastic *pp* scattering at very small angles in order to measure the integrated luminosity and to provide online monitoring of the instantaneous luminosity and beam conditions. The detectors are at a radial distance of approximately 10 cm from the beam line.

Absolute Luminosity For ATLAS (ALFA), located at ± 240 m from the interaction point, is a scintillating fibre tracker detector inside *Roman pots*. Roman pots are devices located very close to the beam line (inserted directly into the beam vacuum pipe) in order to capture particles which scatter by very small angles. The ALFA detector is as close as 1 mm to the beam. The purpose of the ALFA detector is the measurement of elastic *pp* scattering and small angles in the coulomb nuclear interference (CNI) region.

The Zero Degree Calorimeter (ZDC), located at ± 140 m from the interaction point, detects forward neutrons and photons with $|\eta| > 8.3$ in both *pp* and heavy ion collisions. Neutral particles can be measured by the alternating layers of quartz rods and tungsten layers in the Zero Degree Calorimeter. The Zero Degree Calorimeter aids in determining the centrality of heavy ion collisions, which is strongly correlated with the number of very forward (spectator) neutrons.

5.1.2.12 Triggers and Data Acquisition

Data produced by the detectors of ATLAS are processed directly by the Triggers and Data Acquisition (TDAQ) system. The system is comprised of subsystems that correspond typically to subdetectors of ATLAS. The trigger consists of three levels, Level 1 (L1), High Level and Event Filter (EF). Each level of the trigger reduces the event rate recorded using decisions made about detected events.

The trigger Level 1, is based on electronics on the detector and the trigger High Level and Event Filter run primarily on a computer cluster near ATLAS. After Level 1, about 100,000 events per second are selected. After the Event Filter, a few hundred events per second remain. These events are stored for analysis.

After this event selection, event reconstruction is performed on the stored events, constructing objects for physics analysis such as jets, photons and leptons.

5.1.2.13 Resolution

Table 5.1 shows the resolution performance goals [92] of the various subdetector components, with E and p_T measured in GeV.

Table 5.1: ATLAS subdetector performance goals

detector component	required resolution
tracking	$\frac{\sigma_{P_T}}{P_T} = 0.05\%\ p_T \oplus 1\%$
electromagnetic calorimetry	$\frac{\sigma_E}{E} = \frac{10\%}{\sqrt{E}} \oplus 0.7\%$
hadronic calorimetry in barrel and endcaps	$\frac{\sigma_E}{E} = \frac{50\%}{\sqrt{E}} \oplus 3\%$
hadronic calorimetry forward	$\frac{\sigma_E}{E} = \frac{100\%}{\sqrt{E}} \oplus 10\%$
muon spectrometer	$\frac{\sigma_{p_T}}{p_T} = 10\%$ at $p_T = 1$ TeV

Chapter 6

Search for Charged Higgs Bosons Decaying via $H^+ \to \tau_{lep.} + \nu$ in $t\bar{t}$ Events

6.1 Introduction

This chapter describes the approach to the search for charged Higgs bosons in $H^+ \to \tau_{lep.} + \nu$. The theoretical basis of the search is described in section 2.9.5.

Initially, the Monte Carlo and data samples used are described. Then, the reconstruction of physics objects is outlined. The data-driven approach used to derive the contribution of background containing misidentified (fake) leptons is presented next. Then, the measurements of $\cos\theta_l^*$ and the transverse mass m_T^H are presented for an analysis of $H^+ \to \tau_{lep.} + \nu$ events with a single lepton in the final state and for an analysis of $H^+ \to \tau_{lep.} + \nu$ events with two leptons in the final state. With

the assumption of the branching fraction $\mathcal{B}(H^+ \to \tau\nu) = 1$, the results of the analyses are presented as upper limits on the branching fraction $\mathcal{B}(t \to bH^+)$ at the 95% confidence level. These results are then discussed. Finally, a brief outline of recent developments and comment on future searches is given.

6.2 Monte Carlo and Data Samples

This section describes briefly the Monte Carlo and data samples used in the analyses. For greater detail, the ATLAS Conference Note [93] for this analysis should be consulted.

Background processes considered in this analysis include $t\bar{t} \to b\bar{b}W^+W^-$ production, single t quark events, production of $Z/\gamma^* + \text{jets}$ and $W + \text{jets}$, diboson events and QCD multijet events with fake leptons. Monte Carlo samples for $t\bar{t}$ and single t quark events are generated using the MC@NLO [94] generator. The parton shower is simulated by HERWIG [95] and the underlying event is simulated by JIMMY [96]. Single vector boson production is simulated using ALPGEN [97] interfaced to HERWIG and JIMMY for the underlying event model. Diboson events (WW, WZ and Z) are generated and hadronised using HERWIG. For these events, inclusive decays are used for both gauge bosons and a generator level filter is applied, requiring at least one electron or muon with $p_T > 10$ GeV and pseudorapidity $|\eta| < 2.8$. The Standard Model samples used are summarised in table 6.1.

Table 6.1: Standard Model background Monte Carlo samples

process	generator	cross section (pb)
$t\bar{t}$ with at least one lepton (e, μ, τ)	MC@NLO	89.7
single t quark W_t channel (inclusive)	MC@NLO	14.6
single t quark t channel with lepton	MC@NLO	21.3
single t quark s channel with lepton	MC@NLO	1.4
$W \to lv + \text{jets}$	ALPGEN	3.1×10^4
$Z/\gamma^* \to ll + \text{jets}$, $m(ll) < 10$ GeV	ALPGEN	1.5×10^4
WW	HERWIG	17.0
ZZ	HERWIG	1.3
WZ	HERWIG	5.5

Three types of signal samples are produced with PYTHIA [98] for m_{H^+} between 90 GeV and 160 GeV:

- $t\bar{t} \to b\bar{b}H^+W^-$,
- $t\bar{t} \to b\bar{b}H^-W^+$ and
- $t\bar{t} \to b\bar{b}H^+H^-$.

The charged Higgs boson decay mode is always $H^+ \to \tau\nu$. When a t quark decays into Wb, the W boson subsequently decays inclusively. For τ decays, TAUOLA [99] is used and for photon radiation from charged leptons, PHOTOS [100] is used. Event generators are tuned to describe ATLAS data: the parameter sets AMBT1 (ATLAS Minimum Bias Tune 1) [101] and AUET1 (ATLAS Underlying Event Tune 1) [102] are used respectively for the hadronised events with PYTHIA and HERWIG/JIMMY.

All Monte Carlo events are propagated through a GEANT4 (Geometry and Tracking 4) [103] simulation [104] of ATLAS and are then reconstructed using the same algorithms as the sample data. Only data taken with all ATLAS subsystems fully operational are used. This results in a data sample of 1.03 ± 0.04 fb^{-1} for a subset of

the data from the 2011 data-taking period of pp collisions at 7 TeV in stable beam conditions.

In order to account for pileup (overlapping signals in the detector from other neighbouring bunch crossings), minimum bias events are added to the hard process in each Monte Carlo sample. Prior to the analysis, simulated events are reweighted to a given data sample using the average number of pileup interactions (~ 6 for the data subset used).

6.3 Object Reconstruction

6.3.1 Electron and Muon Triggers

The events used in this analysis pass a single lepton (electron or muon) trigger. In order to ensure that electrons with a transverse energy greater than 25 GeV and muons with a transverse momentum greater than 20 GeV are in the plateau region of the trigger efficiency curve, the electron trigger has a transverse momentum threshold of 20 GeV and the muon trigger has a transverse momentum threshold of 18 GeV.

6.3.2 Event Cleaning

Further event cleaning is performed by requiring that no jet be consistent with having originated from detector effects, such as spikes in the endcap Hadronic Calorimeter, coherent noise in the Electromagnetic Calorimeter or various backgrounds not caused by collision events. Further cleaning of backgrounds not caused by collision events is accomplished by considering only events with a reconstructed primary vertex with at

least five associated tracks.

6.3.3 Electron Reconstruction

Electrons are reconstructed by matching clustered deposits of energy in the Electromagnetic Calorimeter to tracks reconstructed in the Inner Detector. They are required to meet quality prescriptions based on the expected shower shape of electrons [105]. Electrons are required to have a transverse energy greater than 15 GeV and to be *isolated*. Electrons are considered *isolated* when they have less than 3.5 GeV of transverse energy, after corrections for pileup and leakage, in a cone of $\Delta R = 0.2$ around the electron (see equation 5.3), excluding the energy deposit from the electron itself. Electrons are required to be in the fiducial volume of the detector, with $|\eta| < 2.47$ (the transition region between the barrel and endcap calorimeters is excluded).

6.3.4 Muon Reconstruction

Muons are reconstructed by matching a track reconstructed in the Muon Spectrometer to tracks reconstructed in the Inner Detector [106]. They are required to have a transverse momentum greater than 15 GeV, $|\eta| < 2.5$ and to be isolated. Muons are considered isolated when the both the transverse energy deposited in the calorimeters and the transverse momentum of all Inner Detector tracks amount to less than 4 GeV in a cone of $\Delta R = 0.3$, excluding the energy deposit from the muon itself. Muons are rejected if they are found within $\Delta R < 0.4$ of any jet with a transverse momentum greater than 20 GeV.

6.3.5 Jet Reconstruction

Jets are reconstructed using the anti-k_t jet clustering algorithm [107] with the size parameter value $R = 0.4$. This jet finding algorithm uses three dimensional noise suppressed clusters in the calorimeters, reconstructed at the electromagnetic energy scale. The jets are then calibrated at the hadronic energy scale with correction factors based on Monte Carlo simulations [108] dependent on the transverse momentum and the pseudorapidity of the jets. In order to avoid overlap between electrons and jets, jets with an axis within $\Delta R < 0.2$ or the direction of an electron are rejected.

Jets containing b hadrons (jets initiated by b quarks) are identified using a high performance b tagging algorithm [109] combining impact parameter information with the explicit determination of an inclusive secondary vertex. The cut point is determined to give a nominal efficiency of approximately 70% for b jets with a transverse momentum of greater than 20 GeV in $t\bar{t}$ events. The b tagging algorithm relies on information from the Inner Tracker, so the pseudorapidity acceptance region is $|\eta| < 2.5$.

6.3.6 Missing Transverse Energy Reconstruction

Missing transverse energy [110] is reconstructed using three dimensional noise suppressed clusters in the calorimeters, calibrated at the electromagnetic energy scale, and using muons reconstructed in the Muon Spectrometer. Clusters belonging to jets with a transverse momentum greater than 20 GeV are then calibrated to the hadronic energy scale. Calorimeter cells *not associated with any object* are also taken into account and calibrated at the electromagnetic energy scale. Muons reconstructed in the Inner Detector are used to recover muons in regions not covered by the Muon

Spectrometer. The muon contribution to the missing transverse energy calculated differently for isolated and non-isolated muons in order to deal appropriately with the energy deposited by muons in the calorimeters.

6.4 Data Driven Estimation of Backgrounds with Misidentified Leptons

While the lepton identification of ATLAS is largely reliable, there is a non-negligible contribution from non-isolated leptons. These leptons (which arise from such processes as the semileptonic decay of a b or c hadron, from the decay-in-flight of a $\pi^{\pm}$ or K meson and, in the case of fake electron objects, from the reconstruction of a π^0, photon conversion and shower fluctuations) are called *fake* leptons, as opposed to isolated leptons (which arise from such processes as the decays of W and Z bosons), which are called *real* leptons.

Two data samples are defined: the *tight* sample, which contains mostly events with real leptons, and the *loose* sample, which contains mostly events with fake leptons. The data samples arise simply from different lepton identification criteria, specifically, the loose sample arises by loosening the isolation requirement for the leptons.

In the single lepton events, QCD multijet events, in which a jet is misidentified as a lepton, may constitute a non-negligible background. The number of events containing one loose or one tight lepton can be given as follows:

$$N^L = N_f^L + N_r^L, \tag{6.1}$$

$$N^T = N_f^T + N_r^T, \tag{6.2}$$

where N_r and N_f respectively are the numbers of events containing real and fake leptons passing either a loose (L) or a tight (T) selection. The rates for a real or fake lepton to be identified as a tight lepton can be given as follows:

$$r = \frac{N_r^T}{N_r^L}, \tag{6.3}$$

$$f = \frac{N_f^T}{N_f^L}. \tag{6.4}$$

Then, the number of fake leptons passing the tight selection can be given as follows:

$$N_f^T = \frac{f}{r-f}\left(rN^L - N^T\right). \tag{6.5}$$

This is the total fake lepton contribution in the single lepton events.

In the two lepton events, fake leptons can originate from QCD multijet events and from $W\,(\rightarrow l\nu_l) + \text{jets}$. Due to the presence of two leptons in the event, one of the leptons is required to pass the tight selection criteria while the other lepton is required to pass either the loose selection criteria in the loose sample (which corresponds to

the number of events N^{TL}) or the tight selection criteria in the tight sample (which corresponds to the number of events N^{TT}). Derived in a similar manner as for the case of the single lepton events, the total fake lepton contribution in the two lepton events can be given as follows:

$$N_f^{TT} = \frac{f}{r-f}\left(rN^{TL} - N^{TT}\right). \tag{6.6}$$

Thus, the main pieces of information used for the data driven method of estimation of the fake lepton contributions are the efficiencies for a true lepton to be identified as a real lepton (r) and for a fake lepton to be identified as a real lepton (f).

The lepton identification efficiency r is measured using a tag and probe method in $Z \to l^+l^-$ events with a dilepton invariant mass in the range 86 – 96 GeV (in which one lepton is required to pass the tight selection criteria). The rate at which the other lepton passes the same tight selection criteria defines r. On the other hand, a control sample with fake leptons is selected by considering data events with exactly one lepton passing the loose selection criteria. In order to select events dominated by QCD processes, missing transverse energy is required to be in the range 5 – 20 GeV. Following the removal of other Standard Model processes with leptons identified as true, the rate at which a loose lepton passes the tight selection criteria defines f.

Any significant dependence on kinematic or topological observables such as the transverse momentum and pseudorapidity of the lepton, the jet multiplicity, the number of b tagged jets etc. are taken into account in the final parameterisation of the r and f efficiencies.

6.5 Search with Single Lepton Events

6.5.1 Event Selection

In order to select single lepton (monoleptonic) $t\bar{t}$ events for the search, the following cuts are applied to the data and Monte Carlo samples:

- Exactly one trigger matched lepton is required with
  - $E_T > 25$ GeV for an electron and
  - $p_T > 20$ GeV for a muon.
- At least four jets with $p_T > 20$ GeV and $|\eta| < 2.5$, including exactly two b tagged jets are required.
- In order to select events with a large missing transverse energy while rejecting those in which the large missing transverse energy arises from badly reconstructed leptons (where the asimuthal angle $\phi_{l,\text{missing}}$ between the lepton and the missing transverse energy is small), the following is required:
  - $\not\!\!E_T > 40$ GeV if $|\phi_{l,\text{missing}}| \geq \frac{\pi}{6}$ and
  - $\not\!\!E_T \times |\sin(\phi_{l,\text{missing}})| > 40$ GeV if $|\phi_{l,\text{missing}}| < \frac{\pi}{6}$.

6.5.2 Jet Identification

Having selected single lepton events, the jets must be assigned correctly (in particular, the b jet of the leptonic side of the event). In order to do this, the combination of one b jet and two light quark jets (j) that minimises the test statistic of a χ^2 test is found by iterating over all selected jets:

$$\chi^2 = \frac{(m_{jjb} - m_{\mathrm{t}})^2}{\sigma_{\mathrm{t}}^2} + \frac{(m_{jj} - m_W)^2}{\sigma_W^2}, \tag{6.7}$$

where σ_{t} and σ_W are respectively the assumed widths of the reconstructed t quark and W boson, as estimated from correctly identified combinations in $t\bar{t}$ events. The corresponding assignment efficiency is 74%. At this stage, events are removed if $\chi^2 > 5$. Events having a second lepton with $E_T > 15$ GeV (electron) or $p_T > 15$ GeV (muon) are discarded.

6.5.3 Control Region

In the presence of a charged Higgs boson, the predicted cross section of 165 pb for $t\bar{t}$ for $t\bar{t} \to b\bar{b}W^+W^-$ cannot be relied on. A control region enriched with Standard Model-like $t\bar{t}$ events is defined based on the discriminating variable $\cos\theta_l^*$, where a fiducial cross section, σ_{bbWW}, can be measured for the $t\bar{t} \to b\bar{b}W^+W^-$ process. Events from the $t\bar{t} \to b\bar{b}H^{\pm}W^{\mp}$ and $t\bar{t} \to b\bar{b}H^+H^-$ processes may be found in the control region also, so the σ_{bbWW} cross section is considered as a free parameter when the upper limits on the branching fraction $\mathcal{B}(t \to bH^+)$ are calculated. With $B \equiv \mathcal{B}(t \to bH^+)$, the σ_{bbHW} and σ_{bbHH} cross sections for $t\bar{t} \to b\bar{b}H^{\pm}W^{\mp}$ and $t\bar{t} \to b\bar{b}H^+H^-$ respectively

then are given by the following:

$$\sigma_{bbHW} = \sigma_{bbWW} \times \frac{2B}{1-B}, \tag{6.8}$$

$$\sigma_{bbHH} = \sigma_{bbWW} \times \frac{B^2}{(1-B)^2}. \tag{6.9}$$

Table 6.2 shows how the event selection affects the Standard Model processes and $t\bar{t}$ events with at least one decay $t \to bH^+$, assuming $m_{H^+} = 130$ GeV and a cross section of 38.7 pb, compared with 1.03 fb^{-1} of ATLAS data. A fitted value of 165.1 pb is used for σ_{bbWW} (as obtained when setting the exclusion limit for that mass) and $\mathcal{B}(t \to bH^+) = 10\%$. Events passing the selection cuts are dominantly single lepton $t\bar{t}$ events.

Table 6.2: Events for simulated processes in the single lepton channel

process	events
$t\bar{t}$ $(bbWW)$	3081
single t quark	88
W + jets	85
Z + jets	5.2
diboson	2.0
QCD	56
$\sum$ SM	3317
data	3421
130 GeV H^+, $\mathcal{B}(t \to bH^+) = 10\%$	190

6.5.4 Reconstruction of Discriminating Variables

The discriminating variable $\cos\theta_l^*$ can be calculated on the leptonic 'side' of the event by using the charged lepton and the associated b jet. The $\cos\theta_l^*$ distribution obtained in ATLAS data and Monte Carlo simulations is shown in figure 6.1 [93]. The control region enriched with $t\bar{t} \to b\bar{b}W^+W^-$ events is defined as $0.2 < \cos\theta_l^* < 1$. In order to select a signal region enriched with $t\bar{t} \to b\bar{b}H^\pm W^\mp$ and $t\bar{t} \to b\bar{b}H^+H^-$ events, $\cos\theta_l^* < -0.6$ is required, as indicated by the arrow. In order to enhance decays of charged W or Higgs bosons via $\tau \to l\nu_l\nu_\tau$, $m_T^H < 60$ GeV is required.

For events in the signal region, m_T^H is used as a discriminating variable to search for charged Higgs bosons, as shown in figure 6.2 [93].

ATLAS data is found to agree well with the Standard Model expectations and neither an excess of events (with respect to the prediction for $t\bar{t} \to b\bar{b}W^+W^-$ events) nor a significant deformation of the m_T^H distribution is observed.

6.6 Search with Two Lepton Events

6.6.1 Event Selection

In order to select two lepton (dileptonic) $t\bar{t}$ events for the search, the following cuts are applied to the data and Monte Carlo samples:

- Exactly two trigger matched leptons, including at least one matched to the single lepton trigger, are required with
  - $E_T > 25$ GeV for an electron and

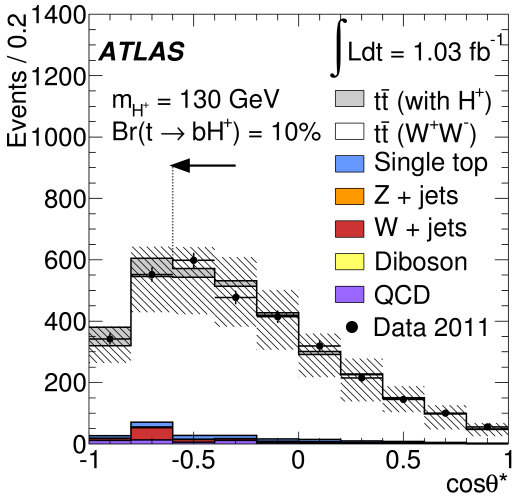

Figure 6.1: Reconstruction of $\cos\theta_l^*$ on the leptonic side of the single lepton events

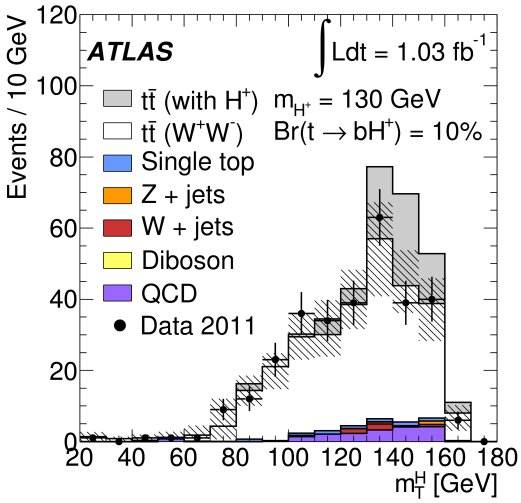

Figure 6.2: Reconstruction of m_T^H on the leptonic side of the single lepton events

- $p_T > 20$ GeV for a muon.

- At least two jets with $p_T > 20$ GeV and $|\eta| < 2.5$, including exactly two b tagged jets are required.

- For ee and $\mu\mu$ events, the dilepton invariant mass m_{ll} must be greater than 15 GeV and must satisfy $|m_{ll} - m_Z| > 10$ GeV together with $\not{E}_T > 40$ GeV.

- For $e\mu$ events, the scalar sum of the transverse energies of the two leptons and all selected jets must satisify $\sum E_T > 130$ GeV.

6.6.2 Jet Identification

There is a four fold ambiguity in assigning the two leptons and the two b jets to their parents. Only those events which have incorrect pairing that is easy to find are selected in an attempt to determine the correct l - b pairing. These are identified as having $\cos\theta_l^* > 1$ for either of the two l - b pairs. For such events with a clear incorrect pairing, the other l - b combinations are chosen, provided that they have $cos\theta_l^* < 1$. For events with $cos\theta_l^* < 1$ for all pairings, the two l - b pairs that minimise the sum of the distances $\Delta R\,(l,b)_{\text{pair 1}} + \Delta R\,(l,b)_{\text{pair 2}}$ in the $\eta\phi$ plane are chosen. In simulated $t\bar{t}$ events, this assignment efficiency is 66%. The particles of the l-b pair with the smallest value for $\cos\theta_l^*$ are assigned to the H^+ 'side' and its partner pair to the W 'side'. In simulated events with $m_{H^+} = 130$ GeV, this assignment efficiency is 62%. The events for which the numerical computation of m_{T2}^H does not converge are discarded.

6.6.3 Control Region

Again, as the predicted cross section of 165 pb for $t\bar{t} \to b\bar{b}W^+W^-$ can not be relied on, a control region enriched with Standard Model-like events is defined based on the discriminating variable $\cos\theta_l^*$, where a fiducial cross section σ_{bbWW} can be measured for the $t\bar{t} \to b\bar{b}W^+W^-$ process when the upper limits on $\mathcal{B}(t \to bH^+)$ are derived. In the two lepton channel, a downward fluctuation of data in the control region yields fitted values of σ_{bbWW} lower than the Standard Model prediction.

Table 6.3 shows how the event selection affects the Standard Model processes and the $t\bar{t}$ events, compared with 1.03 fb^{-1} of ATLAS data. The expected number of events for a Monte Carlo $t\bar{t}$ sample with at least one decay $t \to bH^+$ is also shown in the last column, assuming $m_{H^+} = 130$ GeV and a cross section of 35.3 pb. It corresponds to a fitted value of 150.4 pb for σ_{bbWW} (as obtained when setting the exclusion limit for that mass) and $\mathcal{B}(t \to bH^+) = 10\%$. Events passing the selection cuts are dominantly two lepton $t\bar{t}$ events.

Table 6.3: Events for simulated processes in the two lepton channel

process	events
$t\bar{t}$ $(bbWW)$	864
single t quark	18
Z + jets	1.5
diboson	0.3
QCD and W + jets	40
$\sum$ SM	924
data	992
130 GeV H^+, $\mathcal{B}(t \to bH^+) = 10\%$	115

6.6.4 Reconstruction of Discriminating Variables

The distribution of the discriminating variable $\cos\theta_l^*$ calculated on the H^+ 'side' of the event in ATLAS data and Monte Carlo simulations is shown in figure 6.3 [93]. The control region enriched with $t\bar{t} \to b\bar{b}W^+W^-$ events is defined as $-0.4 < \cos\theta_l^* < 1$. In order to select a signal region enriched with $t\bar{t} \to b\bar{b}H^\pm W^\mp$ and $t\bar{t} \to b\bar{b}H^+H^-$ events, $\cos\theta_l^* < -0.6$ is required, as indicated by the arrow.

For events in the signal region, the generalised transverse mass m_{T2}^H is used as a discriminating variable to search for charged Higgs bosons, as shown in figure 6.4 [93].

Neither an excess of events (with respect to the prediction for $t\bar{t} \to b\bar{b}W^+W^-$ events) nor a significant deformation of the m_{T2}^H distribution is observed.

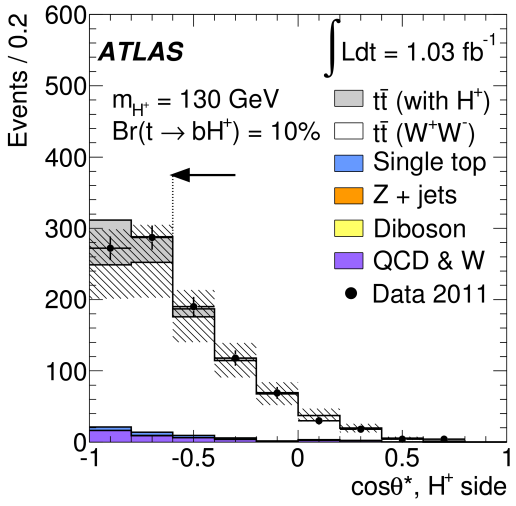

Figure 6.3: Reconstruction of $\cos\theta_l^*$ on the leptonic side of the two lepton events

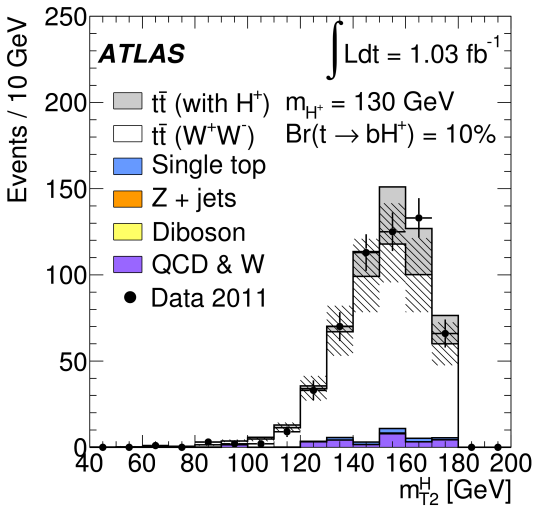

Figure 6.4: Reconstruction of m_T^H on the leptonic side of the two lepton events

6.7 Limits on the Branching Fraction of $t \to bH^+$

6.7.1 Systematic Uncertainties

Systematic uncertainties arising from the measurement of the integrated luminosity [111] and the object reconstruction are considered. The uncertainties mostly are related to trigger, reconstruction and identification efficiencies, as well as the energy and momentum resolution and scale of various objects under consideration.

In order to examine the impact of most sources of systematic uncertainty on analysis results, the selection cuts for each analysis are reapplied after shifting a particular parameter by ± 1 standard deviation of its uncertainty.

The systematic uncertainty arising from the generation of $t\bar{t}$ events and the parton shower model is estimated, the acceptance is computed for $t\bar{t}$ events produced

with MC@NLO interfaced to HERWIG/JIMMY, or POWHEG [112] interfaced to PYTHIA. For the signal samples, which are generated with PYTHIA (i.e., at the leading order only), no alternative generator is available. Instead, the systematic uncertainty for the signal samples is set to the relative difference in acceptance between $t\bar{t}$ events generated with MC@NLO interfaced to HERWIG/JIMMY or AcerMC [113] (which is also at the leading order only) interfaced to PYTHIA. The systematic uncertainties arising from initial and final state radiation are computed using $t\bar{t}$ samples generated with AcerMC and PYTHIA, where initial and final state radiation parameters are set to a range of values not excluded by the experimental data. The greatest relative differences with respect to the reference sample in the signal region are used as the systematic uncertainties.

In the single lepton channel, a factor 2 up/down normalisation uncertainty is assigned to the Monte Carlo W + jets background sample, with an associated log normal constraint because the W + jets background is not predicted precisely, especially after the b tagging requirement.

In the data driven methods used to identify events containing fake leptons, the main systematic uncertainties arise from the sample dependence (the fake efficiencies are calculated in a control region dominated by gluon initiated events, but are used later in a data sample with a higher fraction of quark initiated events) and from Monte Carlo samples used for the removal of real leptons in the determination of the fake efficiencies, which are sensitive to the dominant instrumental systematic uncertainties.

A summary of the systematic uncertainties considered in this study and their treatment in the analysis are given in table 6.4.

Table 6.4: Main systematic uncertainties considered in this analysis

source of uncertainty	treatment in analysis
integrated luminosity	$\pm 3.7\%$
electron trigger efficiency	$\pm$ (0.4%–1.0%), depending on η
electron reconstruction efficiency	$\pm$ (0.7%–1.8%), depending on η
electron identification efficiency	$\pm$ (2.2%–3.8%), depending on E_T and η
electron energy scale	$\pm$ (0.3%–1.8%), additional constant term, depending on p_T and η
electron energy resolution	$\pm$ (0.5%–2.4%), depending on p_T and η
muon trigger efficiency	$\pm$ (0.5%–7.9%), depending on p_T, η, ϕ and the data taking period
muon reconstruction efficiency	$\pm$ (0.4%–0.8%), depending on E, η and ϕ
muon identification efficiency	scale factor $= 1.0008 \pm 0.0004$
muon momentum scale and resolution	up to $\pm 1\%$, depending on p_T and η
jet energy resolution (JER)	$\pm$ (10%–30%), depending on p_T and η
jet energy scale (JES)	$\pm$ (2.5%–14%), depending on p_T and η + pileup term (2%–7%) in quadrature
jet reconstruction efficiency	randomly drop jets (2%) from events and symmetrise
b tagging efficiency	$\pm$ (0.4%–1.0%), depending on η
b tagging mistag rate	$\pm$ (0.4%–1.0%), depending on η
b jet jet energy scale	$\pm$ (0.4%–1.0%), depending on η
missing transverse energy	uncertainties from object scale and resolution + 10% flat pileup contribution
event generation and parton shower	single lepton analysis: 5.1% for $t\bar{t}$, 9.1% for the signal (in SR) two lepton analysis: 6.2% for $t\bar{t}$, 3.9% for the signal (in SR)
initial and final state radiation	single lepton analysis: 7.9% two lepton analysis: 7.7%
$W +$ jets (single lepton channel)	factor 2 up/down with an associated log normal constraint
data driven methods used to identify events with fake leptons	single lepton analysis: 32% two lepton analysis: 28%

6.7.2 Methodology

With the assumption of $\mathcal{B}(H^+ \to \tau\nu) = 1$, upper limits on the branching fraction $B \equiv \mathcal{B}(t \to bH^+)$ are extracted as a function of the charged Higgs boson mass. Since the signal and the $t\bar{t}$ background are correlated, the event rate of the $t\bar{t} \to b\bar{b}W^+W^-$ background is derived from the measurement in the control region (CR). In the single lepton analysis, the region is $-0.2 < \cos\theta_l^* < 1$ (with the $m_T^H < 60$ GeV cut) and in the two lepton analysis, the region is $-0.4 < \cos\theta_l^* < 1$.

For any branching fraction B, the expected number of $t\bar{t} \to b\bar{b}H^{\pm}W^{\mp}$ events, μ_H, is given by the following:

$$\mu_H = \mu_W \times \frac{2B}{1-B}, \tag{6.10}$$

where μ_W is the expected number of Standard Model-like $t\bar{t} \to b\bar{b}W^+W^-$ background events and μ_{others} is the expected number of background events from other Standard Model processes.

Other searches [114] suggest that t quarks decay into bH^+ in less than 10% of the cases, hence the contribution from $t\bar{t} \to b\bar{b}H^+H^-$ is small. Given the small contribution of the process, it is not considered in the limit setting calculations. By not considering the $t\bar{t} \to b\bar{b}H^+H^-$ events, the estimation of the upper limit on $\mathcal{B}(t \to bH^+)$ is somewhat conservative.

6.7.3 Expected Events in the Control Region

The expected number of events in the control region of the $\cos\theta_l^*$ distribution is given by the following:

$$\mu^{CR} = \mu_W \epsilon_W + \mu_H \epsilon_H + \mu_{\text{others}}^{CR} = \mu_W \left(\epsilon_W + \frac{2B}{1-B} \epsilon_H \right) + \mu_{\text{others}}^{CR}, \tag{6.11}$$

where ϵ_W and ϵ_H are the corresponding acceptances of the Standard Model-like $t\bar{t} \to b\bar{b}W^+W^-$ events and of the signal $t\bar{t} \to b\bar{b}H^\pm W^\mp$ events (derived from Monte Carlo simulations).

6.7.4 Expected Events in the Signal Region

The expected number of events in the signal region is given by the following:

$$\mu^{SR} = \mu_W \epsilon_W \delta_W + \mu_H \epsilon_H \delta_H + \mu_{\text{others}}^{SR} = \mu_W \left(\epsilon_W \delta_W + \frac{2B}{1-B} \epsilon_H \delta_H \right) + \mu_{\text{others}}^{SR}, \tag{6.12}$$

where δ_W and δ_H are scaling factors from the control region to the signal region (also derived from Monte Carlo simulations).

6.7.5 Observed Events in the Control and Signal Regions

Let m and n be the number of observed events in the control and signal regions of the $\cos\theta_l^*$ distribution, respectively. In the signal region, the simulated (generalised) transverse mass distributions are described using a probability density func-

tion $f_i\left(m_T\right)$. Thus, the expected and observed number of events in each bin i (of the discriminating transverse mass variable distribution) are $\mu_i^{SR} = \mu^{SR} f_I\left(m_T\right)$ and n_i, respectively. The likelihood is given as follows:

$$\mathcal{L}\left(B\right) = \text{Poisson}\left(m|\mu^{CR}\right) \prod_i \text{Poisson}\left(m_i|\mu_i^{SR}\right) \prod_j p\left(\tilde{\theta}_j|\theta_j\right), \tag{6.13}$$

where nuisance parameters are represented by θ. Nuisance parameters are used to describe the effect of systematic uncertainties and $p\left(\tilde{\theta}_j|\theta_j\right)$ are the Gaussian constraints relating each parameter to its nominal estimate $\tilde{\theta}_j$.

6.7.6 Profile Likelihood Statistical Analysis

A profile likelihood statistical analysis is performed with the branching fraction B as one parameter of interest and μ_W as an additional nuisance parameter that is constrained only by data in the control and signal regions. The profile likelihood test statistic is as follows [79]:

$$q_B = -2\log\frac{\mathcal{L}\left(B, \hat{\hat{\theta}}_B, \hat{\hat{\mu}}_{W,B}\right)}{\hat{B}, \hat{\theta}, \hat{\mu}_W}, 0 \leq \hat{B} \leq B, \tag{6.14}$$

where $\hat{\hat{\theta}}_B$ and $\hat{\hat{\mu}}_{W,B}$ are the maximum likelihood estimators of the nuisance parameters for a fixed branching fraction B and $\hat{\theta}$, $\hat{\mu}_W$ and $\hat{B}$ are the global maximum likelihood estimators of θ, μ_W and B, respectively. The limit is derived using the CL_s criteria based on a fully frequentist ensemble in which n_I, m and $\hat{\theta}_j$ are randomised.

6.8 Results

6.8.1 Single Lepton Analysis

The upper limits on the branching fraction $\mathcal{B}(t \to bH^+)$ at the 95% confidence level, obtained for an integrated luminosity of 1.03 fb^{-1}, with the assumption of $\mathcal{B}(H^+ \to \tau\mu) = 1$, is shown for the single lepton channel in figure 6.5 with all systematic uncertainties included.

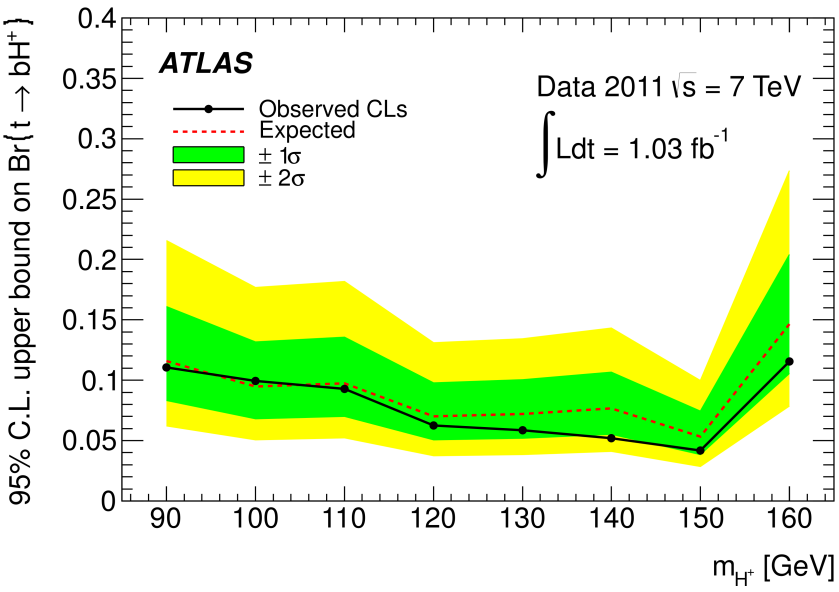

Figure 6.5: Upper limits on $\mathcal{B}(t \to bH^+)$ at the 95% confidence level in the single lepton channel, as a function of charged Higgs boson mass, with the assumption of $\mathcal{B}(H^+ \to \tau\mu) = 1$

Solid lines denote the observed upper limits at the 95% confidence level and dashed lines represent the expected upper limits at the 95% confidence level. The outer edges of the green and yellow regions denote the 1σ and 2σ uncertainty bands, respectively.

The fitted values of μ_W (the expected number of Standard Model-like $t\bar{t} \to b\bar{b}W^+W^-$ background events) lies between 0.99 and 1.03 times the Standard Model prediction, with uncertainties in the range 2% – 3%.

6.8.2 Two Lepton Analysis

The upper limits on the branching fraction $\mathcal{B}(t \to bH^+)$ at the 95% confidence level, obtained for an integrated luminosity of 1.03 fb^{-1}, with the assumption of $\mathcal{B}(H^+ \to \tau\mu) = 1$, is shown for the two lepton channel in figure 6.6 with all systematic uncertainties included.

A downward fluctuation of data in the control region yields fitted values of μ_W between 0.78 and 1.06 times the Standard Model prediction, with uncertainties in the range 5% – 25%. For a charged Higgs boson mass of 160 GeV, the b jets from $t \to bH^+$ are usually so soft that they are not likely to pass the transverse momentum cut at 20 GeV, leading to a significant loss of sensitivity at that mass.

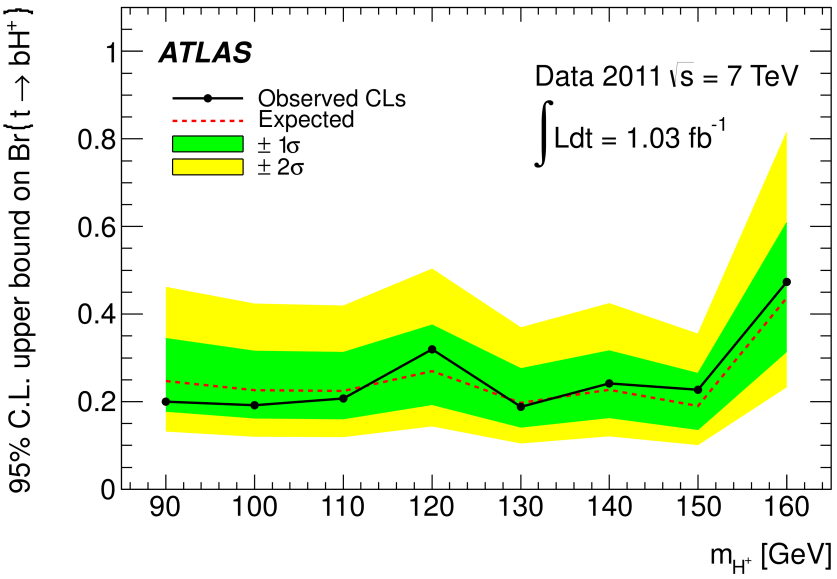

Figure 6.6: Upper limits on $\mathcal{B}(t \to bH^+)$ at the 95% confidence level in the two lepton channel, as a function of charged Higgs boson mass, with the assumption of $\mathcal{B}(H^+ \to \tau\mu) = 1$

6.8.3 Combination

Since the two channels considered in this study are orthogonal, a combined exclusion limit can be computed. For the purposes of this combination, the systematic uncertainties for both channels are assumed to be 100% correlated. The combined exclusion limit on the branching fraction $\mathcal{B}(t \to bH^+)$ is shown in figure 6.7 and a comparison between the upper limits on $\mathcal{B}(t \to bH^+)$ for the single lepton channel, the two lepton channel and the combination of both channels is shown in table 6.5.

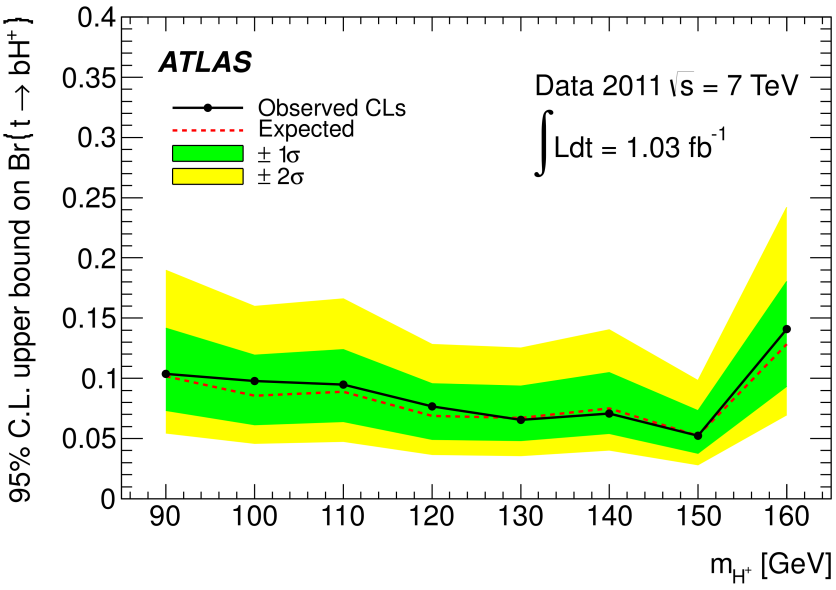

Figure 6.7: Upper limits on $\mathcal{B}(t \to bH^+)$ at the 95% confidence level in the combination of the single lepton channel and the two lepton channel, as a function of charged Higgs boson mass, with the assumption of $\mathcal{B}(H^+ \to \tau\mu) = 1$

Table 6.5: Observed and expected upper limits on $\mathcal{B}(t \to bH^+)$ at the 95% confidence level for the single lepton channel, the two lepton channel and the combination of both channels

		m_{H^+} (GeV)	90	100	110	120	130	140	150	160
upper limit on $\mathcal{B}(t \to bH^+)$ at the 95% confidence level	single lepton channel	expected	11.1%	9.9%	9.3%	6.3%	5.8%	5.2%	4.2%	11.6%
		observed	11.6%	9.5%	9.7%	7.0%	7.2%	7.7%	5.3%	14.6%
	two lepton channel	expected	20.0%	19.2%	20.7%	32.0%	18.8%	24.2%	22.7%	47.3%
		observed	24.7%	22.6%	22.4%	26.9%	19.8%	22.6%	19.0%	43.7%
	combination	expected	10.4%	9.8%	9.5%	7.7%	6.6%	7.1%	5.2%	14.1%
		observed	10.2%	8.5%	8.9%	6.9%	6.7%	7.5%	5.2%	12.9%

While the expected upper limit improves after the combination, the observed combined upper limit on $\mathcal{B}(t \to bH^+)$ is slightly worst than that for the single lepton analysis alone. The single lepton analysis is more sensitive than the two lepton analysis, thus, the combined upper limit is very close to the single lepton upper limit. The compatibility with background is measured by p_0 values, which range between 26% and 50%. Hence, no indication of a H^+-like excess is found.

6.8.4 Results in the Context of the MSSM

The upper limits in the context of the $m_h^{\text{max.}}$ scenario of the MSSM [115] in the $m_{H^+}, \tan\beta$ plane are shown in figure 6.8. Since the assumption $\mathcal{B}(H^+ \to \tau\mu) = 1$ significantly is not fulfilled at low values of $\tan\beta$, upper limits are not calculated in the region associated with low values of $\tan\beta$ (exclusion limits are not shown above 140 GeV). The blue dashed lines indicate the theoretical uncertainties. The relative uncertainties on the branching fraction $\mathcal{B}(t \to bH^+)$ considered and added linearly [72] are outlined in table 6.6.

6.9 Conclusions

6.9.1 Discussion on Results

This thesis presented the results of a search for charged Higgs bosons decaying via $H^+ \to \tau_{lep.} + \nu$ in $t\bar{t}$ events based on 1.03 fb^{-1} of ATLAS proton-proton collision data at a central of mass energy $\sqrt{s} = 7$ TeV using the single lepton and two lepton channels in $t\bar{t}$ decays with a leptonically decaying τ in the final state.

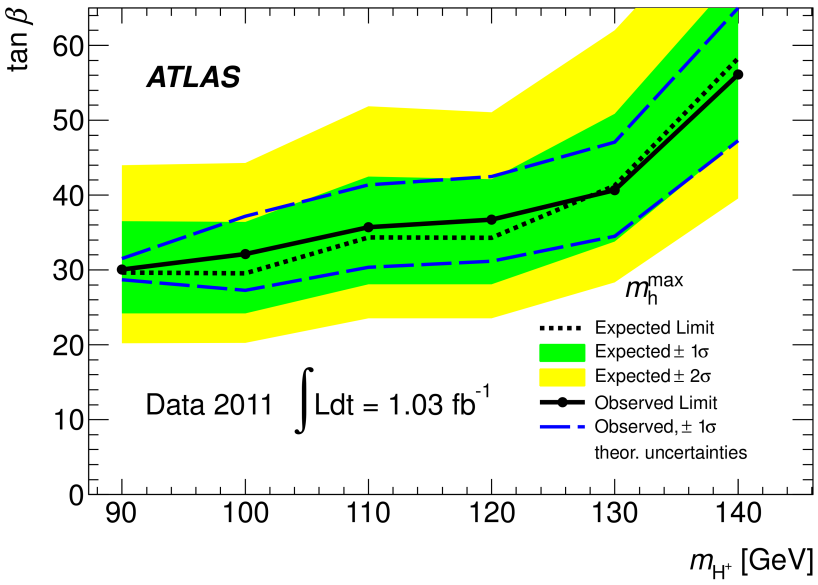

Figure 6.8: Limits for charged Higgs boson production from t quark decays in the context of the $m_h^{\text{max.}}$ scenario of the MSSM, with the assumption of $\mathcal{B}\left(H^+ \to \tau\mu\right) = 1$

Table 6.6: Relative uncertainties on $\mathcal{B}(t \to bH^+)$ in the context of the $m_h^{\text{max.}}$ scenario of the MSSM

source of uncertainty	treatment in analysis
one loop electroweak corrections missing in calculations	5%
missing two loop QCD corrections	2%
Δ_b-induced uncertainties, where Δ_b is a correction factor to the running b quark mass [116]	$\sim 1\%$ (depending on $\tan\beta$)

Discriminating variables were identified in order to distinguish between leptons produced in τ decays and leptons arising directly from W boson decays. In both the single lepton and two lepton channels, the data agree well with the Standard Model expectation. Assuming $\mathcal{B}(H^+ \to \tau\mu) = 1$, the upper limits on the branching fraction $\mathcal{B}(t \to bH^+)$ at the 95% confidence level are between 5.2% and 14.1% for charged Higgs boson masses in the range 90 GeV $\leq m_{H^+} \leq$ 160 GeV.

6.9.1.1 Comparison with Previous Results

The results obtained in this search constitute an improvement over upper limits provided by Tevatron experiments [117]. Except for the 160 GeV mass, the exclusion limits are comparable to (or somewhat higher than) results presented by the CMS Collaboration [118] and by the ATLAS Collaboration [114].

The observed and expected upper limits on $\mathcal{B}(t \to bH^+)$ at the 95% confidence level for the single lepton channel, the two lepton channel and the combination for the search described in this thesis are compared with recent CMS results [118] in table 6.7 while the observed and expected upper limits on $\mathcal{B}(t \to H^+b) \times \mathcal{B}(H^+ \to \tau^+\nu)$ at the 95% confidence level for charged Higgs bosons produced in t quark decays are shown for recent ATLAS results [114] in figure 6.9 together with the best limit provided by the Tevatron experiments [117].

In the context of the $m_h^{\text{max.}}$ scenario of the MSSM, values of $\tan\beta$ greater than 30–56 are excluded in the mass range 90 GeV $\leq m_{H^+} \leq$ 140 GeV. In recent ATLAS results [114], values of $\tan\beta$ greater than 22–30 were excluded in the mass range 90 GeV $\leq m_{H^+} \leq$ 140 GeV; the upper limits are shown in the context of the $m_h^{\text{max.}}$ scenario of the MSSM in the $m_{H^+}, \tan\beta$ plane in figure 6.10.

Table 6.7: Observed and expected upper limits on $\mathcal{B}(t \to bH^+)$ at the 95% confidence level for the single lepton channel, the two lepton channel and the combination of both channels of the search of this thesis and for recent CMS results

		m_{H^+} (GeV)	80	90	100	110	120	130	140	150	155	160
upper limit on $\mathcal{B}(t \to bH^+)$ at the 95% confidence level	single lepton	expected		11.1%	9.9%	9.3%	6.3%	5.8%	5.2%	4.2%		11.6%
		observed		11.6%	9.5%	9.7%	7.0%	7.2%	7.7%	5.3%		14.6%
	two lepton	expected		20.0%	19.2%	20.7%	32.0%	18.8%	24.2%	22.7%		47.3%
		observed		24.7%	22.6%	22.4%	26.9%	19.8%	22.6%	19.0%		43.7%
	combination	expected		10.4%	9.8%	9.5%	7.7%	6.6%	7.1%	5.2%		14.1%
		observed		10.2%	8.5%	8.9%	6.9%	6.7%	7.5%	5.2%		12.9%
	CMS [118]	expected	4.2%		3.8%		4.1%		4.1%	4.0%	4.0%	4.2%
		observed	3.9%		3.5%		4.1%		4.5%	4.6%	4.9%	4.8%

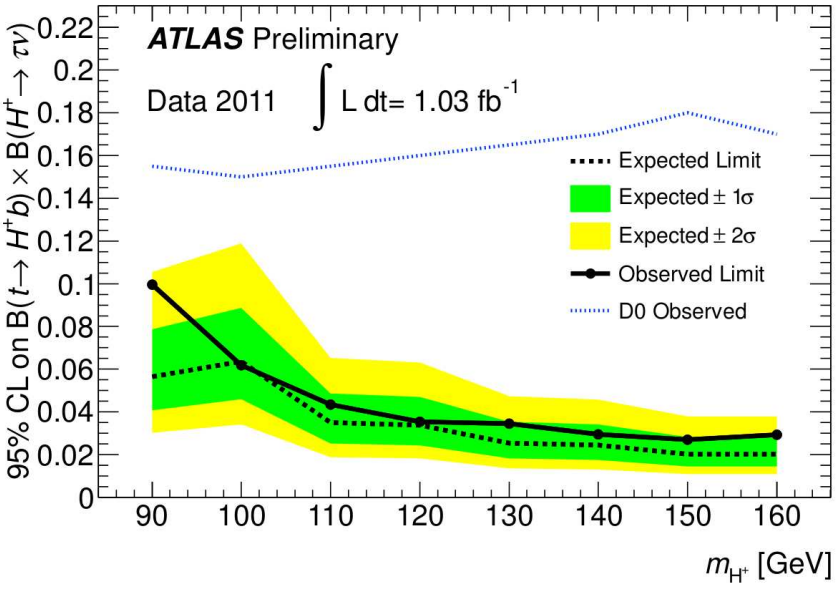

Figure 6.9: Exclusion limits on $\mathcal{B}(t \to H^+b) \times \mathcal{B}(H^+ \to \tau^+\nu)$ at the 95% confidence level as a function of charged Higgs boson mass in recent ATLAS results, shown with the best limit provided by the Tevatron experiments

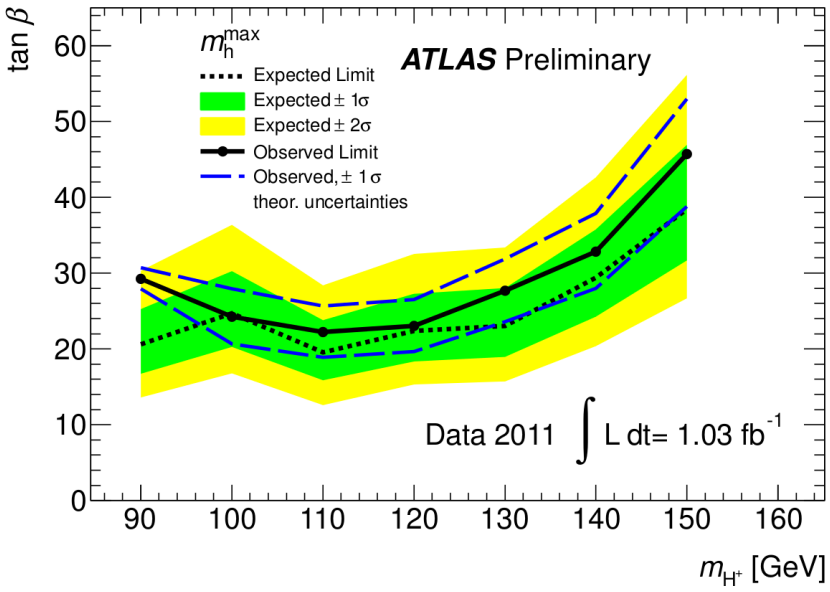

Figure 6.10: Limits for charged Higgs boson production from t quark decays in the context of the $m_h^{\text{max.}}$ scenario of the MSSM in recent ATLAS results

6.9.2 Recent Developments and Future Searches

In this search, no evidence was found for charged Higgs bosons. Things change quickly in physics and the search presented in this thesis has been updated recently with 4.6 fb^{-1} of pp collision data [119]. The search shall continue with greater amounts of data. Recently, the LHC centre of mass beam energy has been increased to 8 TeV. This is likely to lead to interesting discoveries in the very near future.

Chapter 7

Epilogue

7.1 Discovery of a Neutral Boson

On July 4, 2012, the discovery of a neutral boson consistent with the Standard Model Higgs boson hypothesis was announced by the ATLAS and CMS collaborations. The particle is identified as a neutral boson by its decays to pairs of vector bosons whose net electric charge is zero and the observation in the diphoton channel disfavours the spin 1 hypothesis. While the results are compatible with the Standard Model Higgs boson, more data are needed to assess its nature in detail. Recently, the ATLAS and CMS results were published formally [120, 121].

7.2 Consideration of the Mass of the Neutral Boson in the Context of Asymptotic Safety of Gravity

The Standard Model does not include gravity. General relativity may be viewed as a low energy, large scale (compared to the Planck length) approximation of a more fundamental quantum description of gravity. *Asymptotic safety* [122, 123] is a mathematical method that allows gravity to be incorporated into quantum field theory.

Asymptotic safety is an important consideration because if it is understood how to incorporate gravity into the quantum field theories and if the masses of all of the Standard Model particles except one have been measured, then the mass that the remaining particle must be in order for the physics to remain accurate at all energies can be predicted; requiring the universe to be stable constrains the last free parameter, the mass of the Higgs boson, to be one value. If the mass appears to be that value, it may be indicative that, if asymptotic safety is a valid idea, there are no new particles in the universe that couple to the Standard Model. That is, there would be no new particles to be found using colliders all up to Planck energies.

A mass of 126 GeV, with an uncertainty of a few GeV, was predicted in the context of asymptotic safety of gravity in a paper by Shaposhnikov and Wetterich in 2009 [124]. This mass corresponds to the mass of the neutral boson recently discovered at the LHC in the ATLAS and CMS experiments [120, 121].

So, if the asymptotic safety of gravity is valid and the newly discovered particle is

the Higgs boson, it may be that the Higgs boson is the last unfound particle reasonably accessible to particle colliders.

7.3 Current Studies and the Future

The LHC physics programme is planned to continue for the near future, with a planned upgrade raising the centre of mass energies to 14 TeV and future possible particle collider experiments currently are under consideration. Measurements of the properties of the newly discovered particle currently are underway and it is likely that a reasonably conclusive description of the particle's properties shall be possible in the very near future and, in the progress of physics, today's sensation is tomorrow's calibration.

References

[1] J. F. Gunion, H. E. Haber, G. L. Kane and S. Dawson, *The Higgs Hunter's Guide*, Frontiers in Physics, Perseus Publishing (June 2000)

[2] V. Barger, J. L. Hewett and R. J. N. Phillips, *New constraints on the charged Higgs sector in two-Higgs-doublet models*, Physics Review D, 41 (11), 3421–3441 (June 1990)

[3] G. N. Lewis, *The Conservation of Photons*, Nature, 118, 874–875 (December 1926)

[4] B. Franklin, *The Papers of Benjamin Franklin Volume 1 January 6, 1706 Through December 31, 1734*, Yale University Press (September 1959)

[5] ATLAS Collaboration, *Search for down-type fourth generation quarks with the ATLAS detector in events with one lepton and high transverse momentum hadronically decaying W bosons in $\sqrt{s} = 7$ TeV pp collisions*, CERN-PH-EP-2011-230 (July 2012)

[6] E. C. G. Stückelberg, *La mécanique du point matériel en théorie de relativité et en théorie des quanta*, Helvetica Physica Acta, 15, 23–37 (1942)

[7] R. P. Feynman, *A Relativistic Cut-Off for Classical Electrodynamics*, Physical Review, 74 (8), 939–946 (October 1948)

[8] R. P. Feynman, *The Theory of Positrons*, Physical Review, 76 (6), 749–759 (September 1949)

[9] R. P. Feynman, *Space-Time Approach to Quantum Electrodynamics*, Physical Review, 76 (6), 769–789 (September 1949)

[10] CDF Collaboration, *Precise measurement of the W-boson mass with the CDF II detector*, FERMILAB-PUB-12-061-E (March 2012)

[11] K. Nakamura et al., *Review of Particle Physics*, Journal of Physics G: Nuclear and Particle Physics, 37 (2010)

[12] D. Stoler, *Photon Antibunching and Possible Ways to Observe It*, Physical Review Letters, 33 (23), 1397–1400 (October 1974)

[13] R. P. Feynman, *Space-Time Approach to Non-Relativistic Quantum Mechanics*, Reviews of Modern Physics, 20 (2), 367–387 (April 1948)

[14] R. P. Feynman, *Mathematical Formulation of the Quantum Theory of Electromagnetic Interaction*, Physical Review, 80 (3), 440–457 (November 1950)

[15] C. N. Yang and R. L. Mills, *Conservation of Isotopic Spin and Isotopic Gauge Invariance*, Physical Review, 96 (1), 191–195 (October 1954)

[16] M. Gell-Mann and F. E. Low, *Quantum Electrodynamics at Small Distances*, Physical Review, 95 (5), 1300–1312 (September 1954)

[17] Z. Bern, L. Dixon, D. C. Dunbar and D. A. Kosower, *One-Loop n-Point Gauge Theory Amplitudes, Unitarity and Collinear Limits*, Nuclear Physics B, 425, 217–260 (August 1994)

[18] D. J. Gross and F. Wilczek, *Asymptotically Free Gauge Theories. I*, Physical Review D, 8 (10), 3633–3652 (November 1973)

[19] D. J. Gross and F. Wilczek, *Ultraviolet Behavior of Non-Abelian Gauge Theories*, Physical Review Letters, 30 (26), 1343–1346 (June 1973)

[20] F. Wilczek, *Nobel Lecture: Asymptotic freedom: From paradox to paradigm*, Reviews of Modern Physics, 77 (3), 857–870 (September 2005)

[21] Y. Nambu, *Quasi-Particles and Gauge Invariance in the Theory of Superconductivity*, Physical Review, 117 (3), 648–663 (February 1960)

[22] J. Goldstone, *Field Theories with "Superconductor" Solutions*, Nuovo Cimento, 19, 154–164 (1961)

[23] B. W. Lee, *Renormalization of the σ-model*, Nuclear Physics B, 9 (5), 649–672 (March 1969)

[24] P. W. Anderson, *Plasmons, Gauge Invariance, and Mass*, Physical Review, 130 (1), 439–442 (April 1963)

[25] A. Klein and B. W. Lee, *Does Spontaneous Breakdown of Symmetry Imply Zero-Mass Particles?*, Physical Review Letters, 12 (10), 266–268 (March 1964)

[26] W. Gilbert, *Broken Symmetries and Massless Particles*, Physical Review Letters, 12 (25), 713–714 (June 1964)

[27] F. Englert and R. Brout, *Broken Symmetry and the Mass of Gauge Vector Mesons*, Physical Review Letters, 13 (9), 321–323 (August 1964)

[28] P. W. Higgs, *Broken Symmetries, Massless Particles and Gauge Fields*, Physics Letters, 12, 132–133 (September 1964)

[29] P. W. Higgs, *Broken Symmetries and the Masses of Gauge Bosons*, Physical Review Letters, 13 (16), 508–509 (October 1964)

[30] G. S. Guralnik, C. R. Hagen and T. W. B. Kibble, *Global Conservation Laws and Massless Particles*, Physical Review Letters, 13 (20), 585–587 (November 1964)

[31] S. Weinberg, *A Model of Leptons*, Physical Review Letters, 19 (21), 1264–1266 (November 1967)

[32] A. Salam, *Gauge Unification of Fundamental Forces*, Reviews of Modern Physics, 52, 525–538 (December 1980)

[33] G. 't Hooft, *Renormalization of massless Yang-Mills fields*, Nuclear Physics B, 33 (1), 173–199 (October 1971)

[34] G. 't Hooft and M. Veltman, *Regularization and Renormalization of Gauge Fields*, Nuclear Physics B, 44 (1), 189–213 (1972)

[35] S. L. Glashow, *Partial Symmetries of Weak Interactions*, Nuclear Physics, 22, 579–588 (February 1961)

[36] J. R. Ellis, M. K. Gaillard and D. V. Nanopoulos, *A Phenomenological Profile of the Higgs Boson*, Nuclear Physics B, 106, CERN-TH-2093 (1976)

[37] S. Weinberg, *Implications of dynamical symmetry breaking*, Physical Review D, 13 (4), 974–996 (February 1976)

[38] S. Weinberg, *Implications of dynamical symmetry breaking: An addendum*, Physical Review D, 19 (4), 1277–1280 (February 1979)

[39] E. Gildener, *Gauge-symmetry hierarchies*, Physical Review D, 14 (6), 1667–1672 (September 1976)

[40] L. Susskind, *Dynamics of spontaneous symmetry breaking in the Weinberg-Salam theory*, Physical Review D, 20 (10), 2619–2625 (November 1979)

[41] H. Miyazawa, *Baryon Number Changing Currents*, Progress of Theoretical Physics, 36 (6), 1266–1276 (August 1966)

[42] H. Miyazawa, *Spinor Currents and Symmetries of Baryons and Mesons*, Physical Review, 170 (5), 1586–1590 (June 1968)

[43] F. Zwicky, *Die Rotverschiebung von extragalaktischen Nebeln*, Helvetica Physica Acta, 6, 110–127 (February 1933)

[44] F. Zwicky, *On the Masses of Nebulae and of Clusters of Nebulae*, The Astrophysical Journal, 86 (3), 217–246 (October 1937)

[45] J. Dietrich P. et al., *A filament of dark matter between two clusters*, Nature, 487 (7406), 202–204 (July 2012)

[46] S. Dimopoulos and H. Georgi, *Softly broken supersymmetry and SU(5)*, Nuclear Physics B, 193 (1), 150–162 (December 1981)

[47] S. Dimopoulos, S. Raby and F. Wilczek, *Supersymmetry and the scale of unification*, Physical Review D, 24 (6), 1681–1683 (Sep 1981)

[48] L. Randall and R. Sundrum, *Out of this world supersymmetry breaking*, Nuclear Physics B, 557, 79–118 (September 1999)

[49] Y. Bai, V. Barger, L. L. Everett and G. Shaughnessy, *The 2HDM-X and Large Hadron Collider Data*, arXiv:1210.4922 (October 2012)

[50] K. Sato and H. Sato, *Primordial Higgs Mesons and Cosmic Background Radiations*, Progress of Theoretical Physics, 54 (3), 912–913 (May 1975)

[51] K. Sato and H. Sato, *Higgs Meson Emission from a Star and a Constraint on its Mass*, Progress of Theoretical Physics, 54 (5), 1564–1565 (July 1975)

[52] J. Rafelski, G. S. B. Müller and W. Greiner, *Critical Discussion of the Vacuum Polarization Measurements in Muonic Atoms*, Annalen der Physik, 88, 419–453 (December 1974)

[53] S. L. Adler, R. F. Dashen and S. B. Treiman, *Comments on proposed explanations for the muonic-atom x-ray discrepancy*, Physical Review D, 10 (11), 3728–3735 (December 1974)

[54] R. Barbieri and T. E. O. Ericson, *Evidence against the existence of a low mass scalar boson from neutron-nucleus scattering*, Physics Letters B, 57 (3), 270–272 (July 1975)

[55] D. Kohler, B. A. Watson and J. A. Becker, *Experimental Search for a Low-Mass Scalar Boson*, Physical Review Letters, 33 (27), 1628–1631 (December 1974)

[56] L. L. Camilleri et al., *Physics with Very High-Energy e^+ e^- Colliding Beams*, CERN, Geneva, CERN-76-18 (November 1976)

[57] B. W. Lee, C. Quigg and H. Thacker, *Weak Interactions at Very High-Energies: The Role of the Higgs Boson Mass*, Physical Review D, 16, 1519–1531 (September 1977)

[58] J. D. Bjorken, *Weak Interactions*, invited talk presented at 13$^{\text{th}}$ Rencontre de Moriond, Les Arcs, France (12–24 March 1978)

[59] J. Ellis, G. L. Fogli and E. Lisi, *The Higgs boson mass from precision electroweak data*, Zeitschrift für Physik C: Particles and Fields, 69 (4), 627–633, CERN-TH-95-202 (1996)

[60] LEP Working Group for Higgs boson searches, ALEPH Collaboration, DELPHI Collaboration, L3 Collaboration and OPAL Collaboration, *Search for the standard model Higgs boson at LEP*, Physics Letters B, 565, 61–75, CERN-EP-2003-011 (July 2003)

[61] TEVNPH (Tevatron New Phenomena and Higgs) Working Group, *Combined CDF and D0 Upper Limits on Standard Model Higgs Boson Production with up to* 8.6 fb^{-1} *of Data*, FERMILAB-CONF-11-354-E (July 2011)

[62] H. M. Georgi, S. L. Glashow, M. E. Machacek and D. V. Nanopoulos, *Higgs Bosons from Two-Gluon Annihilation in Proton-Proton Collisions*, Physical Review Letters, 40 (11), 692–694 (March 1978)

[63] R. Cahn and S. Dawson, *Production of very massive Higgs bosons*, Physics Letters B, 136 (3), 196–200 (March 1984)

[64] S. L. Glashow, D. V. Nanopoulos and A. Yildiz, *Associated production of Higgs bosons and Z particles*, Physical Review D, 18 (5), 1724–1727 (September 1978)

[65] ATLAS Collaboration, *An update to the combined search for the Standard Model Higgs boson with the ATLAS detector at the LHC using up to* 4.9 fb^{-1} *of pp collision data at* $\sqrt{s} = 7$ *TeV*, ATLAS-CONF-2012-019 (March 2012)

[66] ATLAS Collaboration, *Combined search for the Standard Model Higgs boson using up to* 4.9 fb^{-1} *of pp collision data at* $\sqrt{s} = 7$ *TeV with the ATLAS detector at the LHC*, Physics Letters B, 710, 49–66, CERN-PH-EP-2012-019 (February 2012)

[67] ATLAS Collaboration, *Search for the Standard Model Higgs boson in the diphoton decay channel with* 4.9 fb^{-1} *of pp collisions at* $\sqrt{s} = 7$ *TeV with ATLAS*, Physical Review Letters, 108, CERN-PH-EP-2012-013 (February 2012)

[68] ATLAS Collaboration, *Search for the Standard Model Higgs boson in the decay channel* $H \to ZZ^{(*)} \to 4l$ *with* 4.8 fb^{-1} *of pp collision data at* $\sqrt{s} = 7$ *TeV with ATLAS*, Physics Letters B, 710, 383–402, CERN-PH-EP-2012-014 (February 2012)

[69] CMS Collaboration, *Search for the standard model Higgs boson decaying to bottom quarks in pp collisions at* $\sqrt{s} = 7$ *TeV*, Physics Letters B, 710 (2), 284–306 (April 2012)

[70] CMS Collaboration, *Search for a Higgs boson in the decay channel* $H \to ZZ^{(*)} \to q\bar{q}l^{-}l^{+}$ *in pp collisions at* $\sqrt{s} = 7\ TeV$, CMS-HIG-11-027 (February 2012)

[71] CMS Collaboration, *Search for the standard model Higgs boson in the decay channel* $H \to ZZ \to 4l$ *in pp collisions at* $\sqrt{s} = 7\ TeV$, CMS-HIG-11-025 (February 2012)

[72] S. Dittmaier et al., *Handbook of LHC Higgs Cross Sections: 1. Inclusive Observables*, CERN, Geneva (February 2011)

[73] E. Gross and O. Vitells, *Transverse mass observables for charged Higgs boson searches at hadron colliders*, Physical Review D, 81 (2010)

[74] E. Gross and O. Vitells, *Trial factors for the look elsewhere effect in high energy physics*, The European Physical Journal C, 70, 525–530 (November 2010)

[75] S. S. Wilks, *The Large-Sample Distribution of the Likelihood Ratio for Testing Composite Hypotheses*, The Annals of Mathematical Statistics, 9 (1), 60–62 (March 1938)

[76] J. Neyman and E. S. Pearson, *On the Problem of the most Efficient Tests of Statistical Hypotheses*, Philosophical Transactions of the Royal Society of London, 231, 289–337 (January 1933)

[77] H. Jeffreys, *An invariant form for the prior probability in estimation problems*, Proceedings of the Royal Society of London A, 186 (1007), 453–461 (September 1946)

[78] A. Wald, *Tests of Statistical Hypotheses Concerning Several Parameters When the Number of Observations is Large*, Transactions of the American Mathematical Society, 54 (3), 426–482 (November 1943)

[79] G. Cowan, K. Cranmer, E. Gross and O. Vitells, *Asymptotic formulae for likelihood-based tests of new physics*, The European Physical Journal C, 71 (February 2011)

[80] A. L. Read, *Modified frequentist analysis of search results (the CL_s method)*, CERN-OPEN-2000-205 (January 2000)

[81] A. L. Read, *Presentation of search results: the CL_s technique*, Journal of Physics G: Nuclear and Particle Physics, 28 (10), 2693 (2002)

[82] C. Röver, C. Messenger and R. Prix, *Bayesian versus frequentist upper limits*, Proceedings of the PHYSTAT 2011 Workshop on Statistical Issues Related to Discovery Claims in Search Experiments and Unfolding, CERN, Geneva, Switzerland, 17–20 January 2011, CERN-2011-006 (September 2011)

[83] W. Edwards, H. Lindman and L. J. Savage, *Bayesian Statistical Inference for Psychological Research*, Psychological Review, 70 (3), 193–242 (May 1963)

[84] *ROOT: A Data Analysis Framework*, URL `http://root.cern.ch` (November 2012)

[85] R. Brun, *Re: What does ROOT stand for?*, RootTalk, URL `http://root.cern.ch/root/roottalk/roottalk98/0718.html` (May 1998)

[86] W. Verkerke and D. Kirkby, *The RooFit toolkit for data modeling*, physics/0306116 (June 2003)

[87] L. Moneta et al., *The RooStats Project*, PoS, ACAT2010 (September 2010)

[88] G. Schott, *RooStats for Searches*, contributed to PHYSTAT 2011 Workshop on Statistical Issues Related to Discovery Claims in Search Experiments and Unfolding (March 2012)

[89] ATLAS Collaboration, *ATLAS: Letter of Intent for a General-Purpose pp Experiment at the Large Hadron Collider at CERN*, Letter of Intent, CERN, Geneva (October 1992)

[90] ATLAS Collaboration, *Expected Performance of the ATLAS Experiment: Detector, Trigger and Physics*, CERN, Geneva, cERN-OPEN-2008-020 (December 2008)

[91] A. Barriuso Poy et al., *The detector control system of the ATLAS experiment*, Journal of Instrumentation, 3 (May 2008)

[92] ATLAS Collaboration, *The ATLAS Experiment at the CERN Large Hadron Collider*, Journal of Instrumentation, 3 (8) (August 2008)

[93] ATLAS Collaboration, *Search for a charged Higgs boson decaying via* $H^+ \to \tau_{lep.} + \nu$ *in* $t\bar{t}$ *events with one or two light leptons in the final state using* 1.03 fb^{-1} *of pp collision data recorded at* $\sqrt{s} = 7$ *TeV with the ATLAS detector*, ATLAS-CONF-2011-151 (November 2011)

[94] S. Frixione et al., *The MC@NLO 4.0 Event Generator.*, CERN-PH-TH-2010-216 (October 2010)

[95] G. Corcella et al., *HERWIG 6.5: an event generator for Hadron Emission Reactions With Interfering Gluons (including supersymmetric processes)*, Journal of High Energy Physics, 01 (January 2001)

[96] J. M. Butterworth, J. R. Forshaw and M. H. Seymour, *Multiparton Interactions in Photoproduction at HERA*, Zeitschrift für Physik C: Particles and Fields, 72, 637–646 (February 1996)

[97] M. L. Mangano et al., *ALPGEN, a generator for hard multiparton processes in hadronic collisions.*, Journal of High Energy Physics, 07, CERN-TH-2002-129 (June 2002)

[98] T. Sjostrand, S. Mrenna and P. Z. Skands, *PYTHIA 6.4 Physics and Manual*, Journal of High Energy Physics, 05 (May 2006)

[99] Z. Wąs and P. Golonka, *TAUOLA as tau Monte Carlo for future applications*, Nuclear Physics B - Proceedings Supplements, 144, 88–94, TAU 2004: Proceedings of the Eighth International Workshop on Tau Lepton Physics (July 2005)

[100] E. Barberio, B. van Eijk and Z. Wąs, *Photos – a universal Monte Carlo for QED radiative corrections in decays*, Computer Physics Communications, 66 (1), 115–128 (July 1991)

[101] ATLAS Collaboration, *Charged particle multiplicities in pp interactions at* $\sqrt{s} = 0.9$ *and* 7 *TeV in a diffractive limited phase space measured with the ATLAS detector at the LHC and new PYTHIA6 tune*, ATLAS-CONF-2010-031 (July 2010)

[102] ATLAS Collaboration, *First tuning of HERWIG/JIMMY to ATLAS data*, ATL-PHYS-PUB-2010-014 (October 2010)

[103] S. Agostinelli et al., *GEANT4–a simulation toolkit*, Nuclear Instruments and Methods in Physics Research Section A: Accelerators, Spectrometers, Detectors and Associated Equipment, 506 (3), 250–303 (2003)

[104] ATLAS Collaboration, *The ATLAS Simulation Infrastructure*, The European Physical Journal C, 70, 823–874, CERN-PH-EP-2010-044 (May 2010)

[105] ATLAS Collaboration, *Electron performance measurements with the ATLAS detector using the 2010 LHC proton-proton collision data*, CERN-PH-EP-2011-117 (October 2011)

[106] ATLAS Collaboration, *Muon reconstruction efficiency in reprocessed 2010 LHC proton-proton collision data recorded with the ATLAS detector*, ATLAS-CONF-2011-063 (April 2011)

[107] M. Cacciari, G. P. Salam and G. Soyez, *The anti-k_t jet clustering algorithm*, Journal of High Energy Physics, 2008 (04) (April 2008)

[108] ATLAS Collaboration, *Jet energy scale and its systematic uncertainty in proton-proton collisions at* $\sqrt{s} = 7$ *TeV in ATLAS 2010 data*, ATLAS-CONF-2011-032 (March 2011)

[109] ATLAS Collaboration, *Commissioning of the ATLAS high-performance b-tagging algorithms in the* 7 *TeV collision data*, ATLAS-CONF-2011-102 (July 2011)

[110] ATLAS Collaboration, *Performance of Missing Transverse Momentum Reconstruction in Proton-Proton Collisions at* $\sqrt{s} = 7$ *TeV with ATLAS*, The European Physical Journal C, 72, CERN-PH-EP-2011-114 (September 2011)

[111] ATLAS Collaboration, *Luminosity Determination in pp Collisions at* $\sqrt{s} = 7$ *TeV using the ATLAS Detector in* 2011, ATLAS-CONF-2011-116 (August 2011)

[112] S. Frixione, P. Nason and C. Oleari, *Matching NLO QCD computations with parton shower simulations: the POWHEG method*, Journal of High Energy Physics, 2007 (11) (November 2007)

[113] J. Sidman and A. V. Tuyl, *Multigraded regularity: syzygies and fat points*, Beiträge zur Algebra und Geometrie, 47 (2) (2004)

[114] ATLAS Collaboration, *Search for Charged Higgs Bosons in the* τ + *jets Final State in* $t\bar{t}$ *Decays with* 1.03 fb^{-1} *of pp Collision Data Recorded at* $\sqrt{s} = 7$ *TeV with the ATLAS Experiment*, ATLAS-CONF-2011-138 (September 2011)

[115] M. S. Carena, S. Heinemeyer, C. E. M. Wagner and G. Weiglein, *Suggestions for Benchmark Scenarios for MSSM Higgs Boson Searches at Hadron Colliders*, The European Physical Journal C, 26, 601–607, ANL-HEP-CP-2002-017 (February 2002)

[116] M. S. Carena, D. Garca, U. Nierste and C. E. M. Wagner, *Effective lagrangian for the $\bar{t}bH^+$ interaction in the MSSM and charged Higgs phenomenology*, Nuclear Physics B, 577, 88–20, CERN-TH-2000-009 (December 1999)

[117] D0 Collaboration, *Search for charged Higgs bosons in top quark decays*, FERMILAB-PUB-09-393-E (August 2009)

[118] CMS Collaboration, *Search for the charged Higgs boson with $H^+ \to \tau\nu$ decay mode in top quark decays*, CMS-PAS-HIG-11-008 (July 2011)

[119] *Search for charged Higgs bosons decaying via $H^\pm \to \tau\nu$ in $t\bar{t}$ events using 4.6 fb^{-1} of pp collision data at $\sqrt{s} = 7$ TeV with the ATLAS detector*, ATLAS-CONF-2012-011 (March 2012)

[120] ATLAS Collaboration, *Observation of a new particle in the search for the Standard Model Higgs boson with the ATLAS detector at the LHC*, Physics Letters B, 716 (1), 1–29 (2012)

[121] CMS Collaboration, *Observation of a new boson at a mass of 125 GeV with the CMS experiment at the LHC*, Physics Letters B, 716 (1), 30–61 (2012)

[122] S. Weinberg, *Ultraviolet divergences in quantum theories of gravitation*, General Relativity: An Einstein Centenary Survey, 790–831 (1979)

[123] R. Percacci, *Asymptotic Safety*, arXiv:0709.3851 (September 2007)

[124] M. Shaposhnikov and C. Wetterich, *Asymptotic safety of gravity and the Higgs boson mass*, Physics Letters B, 683, 196–200 (2010)